minerals

MDPI

Review

Advances in Analysis of the Fe-Ni-Co Alloy and Iron-Bearing Minerals in Meteorites by Mössbauer Spectroscopy with a High Velocity Resolution

Michael V. Goryunov [1], Alevtina A. Maksimova [1,2] and Michael I. Oshtrakh [1,*]

[1] Department of Experimental Physics, Institute of Physics and Technology, Ural Federal University, Ekaterinburg 620002, Russia; goryunov_asd@mail.ru (M.V.G.); alia55@bk.ru (A.A.M.)
[2] The Zavaritsky Institute of Geology and Geochemistry of the Ural Branch of the Russian Academy of Sciences, Ekaterinburg 620016, Russia
* Correspondence: oshtrakh@gmail.com; Tel.: +7-912-283-73-37

Abstract: Meteorites are the space messengers bringing us the unique information about the Solar System formation and evolution as well as about the effects of various extreme space conditions on meteorites and their parent bodies. The main iron-bearing compounds in meteorites are Fe-Ni-Co alloy, olivine $(Fe, Mg)_2SiO_4$, orthopyroxene $(Fe, Mg)SiO_3$, clinopyroxene $(Ca, Fe, Mg)SiO_3$, troilite FeS, chromite $FeCr_2O_4$, hercynite $FeAl_2O_4$, ilmenite $FeTiO_3$, daubréelite $FeCr_2S_4$, schreibersite $(Fe, Ni)_3P$ and some other compounds. Therefore, ^{57}Fe Mössbauer spectroscopy was successfully applied for the analyses of various meteorites for about 60 years of experience. The development of Mössbauer spectrometers with a high velocity resolution, i.e., with a high discretization of the velocity reference signal up to 2^{12}, provides much better adjustment to resonance and significantly increases the spectra quality and analytical possibilities of Mössbauer spectroscopy. In fact, this permits us to decompose the complex Mössbauer spectra of meteorites using the larger number of spectral components related to reliable compounds in comparison with the results obtained using conventional Mössbauer spectrometers with discretization of the velocity reference signal up to 2^9. In the present review we consider the results and advances of various meteorites analyses by means of Mössbauer spectroscopy with a high velocity resolution.

Keywords: Mössbauer spectroscopy; extraterrestrial materials; iron-bearing alloys and compounds; magnetic properties

Citation: Goryunov, M.V.; Maksimova, A.A.; Oshtrakh, M.I. Advances in Analysis of the Fe-Ni-Co Alloy and Iron-Bearing Minerals in Meteorites by Mössbauer Spectroscopy with a High Velocity Resolution. *Minerals* **2023**, *13*, 1126. https://doi.org/10.3390/min13091126

Academic Editor: Elizabeth B. Rampe

Received: 20 June 2023
Revised: 25 July 2023
Accepted: 2 August 2023
Published: 25 August 2023

1. Introduction

Meteorites as the space messengers reaching the Earth every day carry important information about formation and evolution of the Solar System, metamorphism of the matter in space and the effect of extreme space factors [1]. For example, the heated or molten matter in space was cooled with a speed of 1–15° per million years that led to formation of specific phases and phase compositions which cannot be reproduced in the terrestrial conditions. Therefore, meteorites are the subjects of various investigations which can help us to understand various processes of the Solar System formation and development. The majority of meteoritical minerals/phases contains iron. These iron-bearing compounds have been studied using ^{57}Fe Mössbauer spectroscopy since the Mössbauer effect was discovered and the method of γ-resonance spectroscopy was developed (see for review [2,3]). Further development of this technique provides new possibilities in the study of meteorites, e.g., conversion electron Mössbauer spectroscopy (CEMS) and other backscattering Mössbauer techniques permit the surface investigation (e.g., [4,5]), synchrotron Mössbauer spectroscopy allows one to study the areas with high spatial resolution (e.g., [6,7]), and Mössbauer spectroscopy with a high velocity resolution allows for the detailed study of complex materials which represent various meteorites (see [8–12]). In the latter case, a

high velocity resolution means a high discretization of the velocity reference signal formed by the digital-analog converter (2^{12} or 4096 steps) [13–16], while conventional Mössbauer spectrometers usually use discretization of 2^8 or 2^9. The high discretization of the velocity reference signal provides much better and more precise adjustment to resonance, and significantly increases the quality of the spectra and analytical possibilities of Mössbauer spectroscopy but increases the measurement time. This requires a higher level of precision, stability, and sensitivity of the velocity driving system than those in conventional spectrometers. The results and advances of the investigation of meteoritical iron-bearing minerals by Mössbauer spectroscopy with a high velocity resolution will be focused on and discussed in this review.

2. Meteorites

All meteorites are divided into three main types: stony, stony-iron and iron meteorites on the basis of their mineralogical and chemical compositions. Meteorites contain iron-free and iron-bearing phases/compounds. The latter compounds are important for Mössbauer spectroscopy of meteorite matter. The main iron-bearing phases/compounds in meteorites are: Fe-Ni-Co alloy, olivine $(Fe, Mg)_2SiO_4$, orthopyroxene $(Fe, Mg)SiO_3$, Ca-poor and Ca-rich clinopyroxene $(Ca, Fe, Mg)SiO_3$, stoichiometric troilite FeS and pyrrhotite $Fe_{1-x}S$ (probably nonstoichiometric or near stoichiometric troilite with $0.00 < x \leq 0.05$), chromite $FeCr_2O_4$, hercynite $FeAl_2O_4$, ilmenite $FeTiO_3$, schreibersite and its prismatic idiomorphic microcrystals named rhabdites $(Fe, Ni)_3P$, daubréelite $FeCr_2S_4$, etc. (see, e.g., [1,17,18]). The main fractions of stony meteorites are iron-magnesian silicate crystals and some other non-metallic minerals with metal grains and troilite inclusions. Stony-iron meteorites consist of approximately equal contents of silicate minerals and Fe-Ni-Co alloy. The main part of iron meteorites is Fe-Ni-Co alloy with some inclusions and accessory compounds. Fe-Ni-Co alloy in meteorites demonstrates the presence of the α-Fe(Ni, Co), α_2-Fe(Ni, Co), γ-Fe(Ni, Co) and γ-FeNi(Co) phases (i.e., minerals: kamacite, martensite, taenite and tetrataenite, respectively). These phases may be in the forms of: (i) pure one phase, (ii) several phases with boundaries between them and (iii) their fine-grained mixture (plessite structure) α-Fe(Ni, Co)/α_2-Fe(Ni, Co) + γ-Fe(Ni, Co). The content of Ni in these phases varies as follows: up to 7 at.% for α-Fe(Ni, Co), ~9–25 at.% for α_2-Fe(Ni,Co), ~26–48 at.% for γ-Fe(Ni, Co) and ~48–52 at.% for γ-FeNi(Co).

There are several approaches to meteorites classification. One of the most widely used modern classifications suggested in [19] considers undifferentiated and differentiated meteorites and three major divisions (chondrites, primitive achondrites and achondrites) (Figure 1). Undifferentiated meteorites, named chondrites (stony meteorites), are the most primitive meteorites, which were formed along with the Solar System from nebula. The name "chondrites" came from "chondrules", the spherical millimeter-sized silicate aggregates found in the meteorite matrix. Chondrites are divided into three classes: carbonaceous chondrites, ordinary chondrites, and enstatite chondrites. Carbonaceous chondrites are divided in several groups marked CI, CK, CH, CB, etc. Enstatite chondrites clan consists of two groups marked EH (high iron) and EL (low iron). Chondrites also contain two groups R and K which were not related to other classes. Ordinary chondrites are the meteorites which most frequently reach the Earth. They represent about 80% of all meteorites which have fallen and been found until now. Ordinary chondrites are divided into unequilibrated and equilibrated based on the order of their metamorphism: unequilibrated ordinary chondrites have petrologic types 3.0–3.9 while equilibrated ordinary chondrites have petrologic types 4–7. Based on the iron content, these meteorites are divided into the H, L and LL groups: H is high iron content, L is low iron content and LL is low iron and low metallic iron alloy contents (see, e.g., [17]). Ordinary chondrites contain: (i) 25–28 wt.% of total iron and 15–19 wt.% of iron in alloy (the H group), (ii) 20–25 wt.% of total iron and 4–10 wt.% of iron in alloy (the L group) and (iii) 19–22 wt.% of total iron and 1–3 wt.% of iron in alloy (the LL group) (see, e.g., [20,21]).

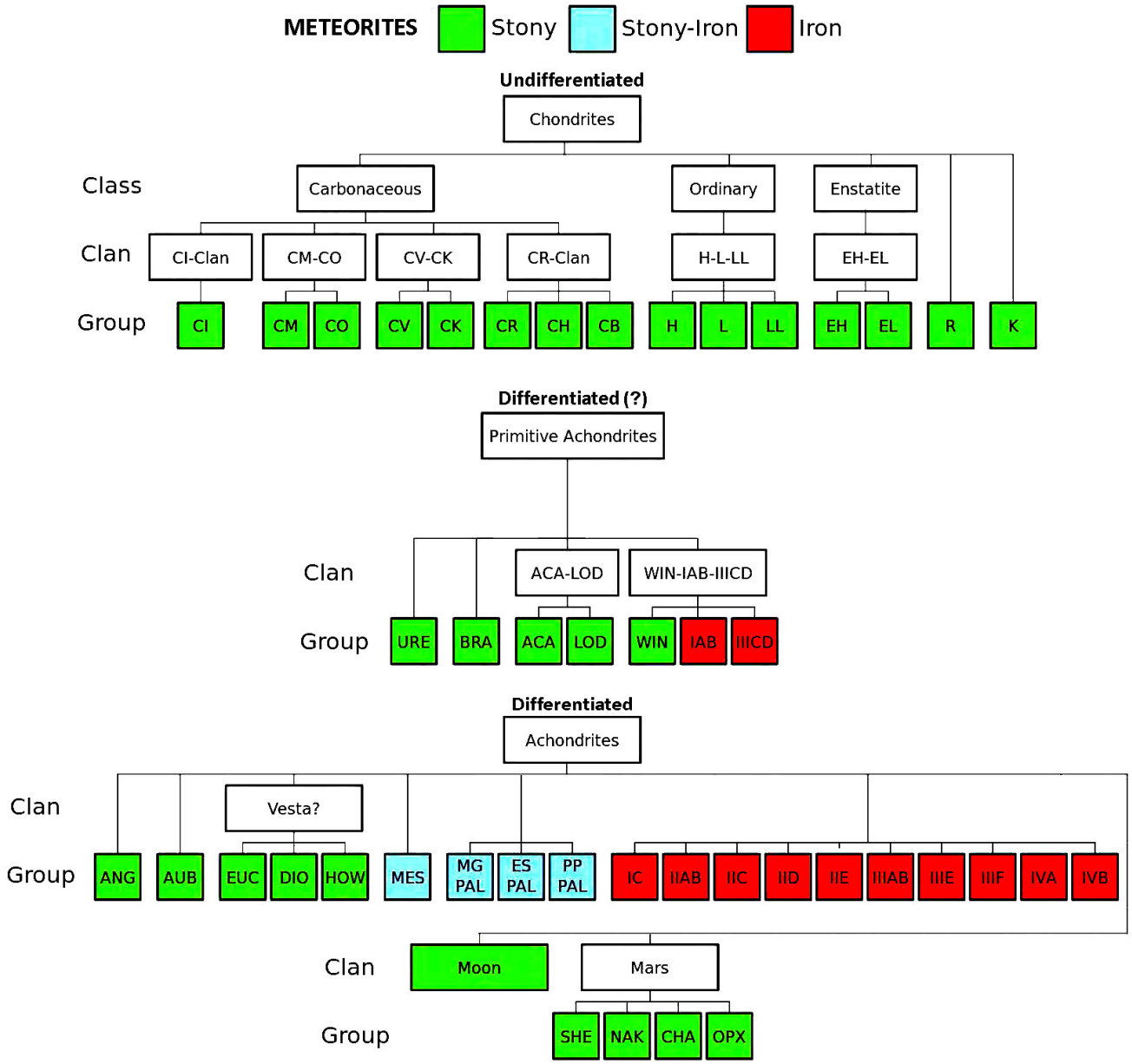

Figure 1. Classification of meteorites demonstrating the major divisions, classes, clans and groups as well as relationships among meteorite groups. URE is ureilite, ACA is acapulcoite, LOD is lodranite, ANG is angrite, AUB is aubrite, BRA is brachinite, WIN is winonaite, EUC is eucrite, DIO is diogenite, HOW is howardite, MES is mesosiderite, MG PAL is main-group pallasite, ES PAL is Eagle Station pallasite, PP PAL is pyroxene pallasite, SHE is shergottite, NAK is nakhlite, CHA is chassignite, and OPX is orthopyroxenite. Adapted from Ref. [19].

Differentiated meteorites were formed in their parent bodies, asteroids and protoplanets, resulting from the thermal metamorphism of the material with further differentiation. Primitive achondrites may be a result of a low-degree partial melting of chondritic material (therefore, this division was marked as "Differentiated (?)") while achondrites resulted from a high degree of chondrites melting [19]. As the result, various groups of stony meteorites, stony-iron meteorites and iron meteorites were formed. Primitive achondrites division includes several groups of stony meteorites such as ureilites, brachinites, acapulcoites and lodranites, and two groups of iron meteorites: IAB and IIICD (these iron meteorites contain silicate inclusions). Achondrites division includes several groups of (i) stony meteorites with angrites and aubrites groups, the howardites-eucrites-diogenites or HED clan, whose

parent body is considered to be asteroid (4) Vesta [22], and Lunar and Martian meteorites, which are rocks ejected by impacts from the Moon and Mars surface, respectively, and later fell to the Earth as meteorites, (ii) stony-iron meteorites consisted of mesosiderites group and three groups of pallasites (the main group pallasites PMG, Eagle Station pallasites and pyroxene pallasites) and (iii) thirteen groups of iron meteorites: IC, IIAB, IIC, IID, etc., as well as some ungrouped and anomalous iron meteorites, with structural classes such as octahedrites, hexahedrites and ataxites.

When meteorites enter the Earth atmosphere with a high velocity, a combustion of the rock surface leads to the formation of ferric oxides in addition to the molten or heated bulk matter. After the velocity decreases and fast cooling starts, the molten surface is solidified with mainly glass-like fusion crust formation. Due to ablation of the molten matter from the surface, the remaining fusion crust is very thin. On the other hand, meteorites on the Earth are affected by water and various other chemical factors leading to terrestrial weathering with the formation of various ferric oxides and oxyhydroxides.

Photographs of fragments of some meteorites from different groups considered in this review are shown in Figure 2. Further, the results of the studies of these and other meteorites by means of Mössbauer spectroscopy with a high velocity resolution and some complementary techniques will be discussed. All meteorite names and groups are in accordance with the Meteoritical Bulletin Database (https://www.lpi.usra.edu/meteor/ (accessed on 15 August 2023)).

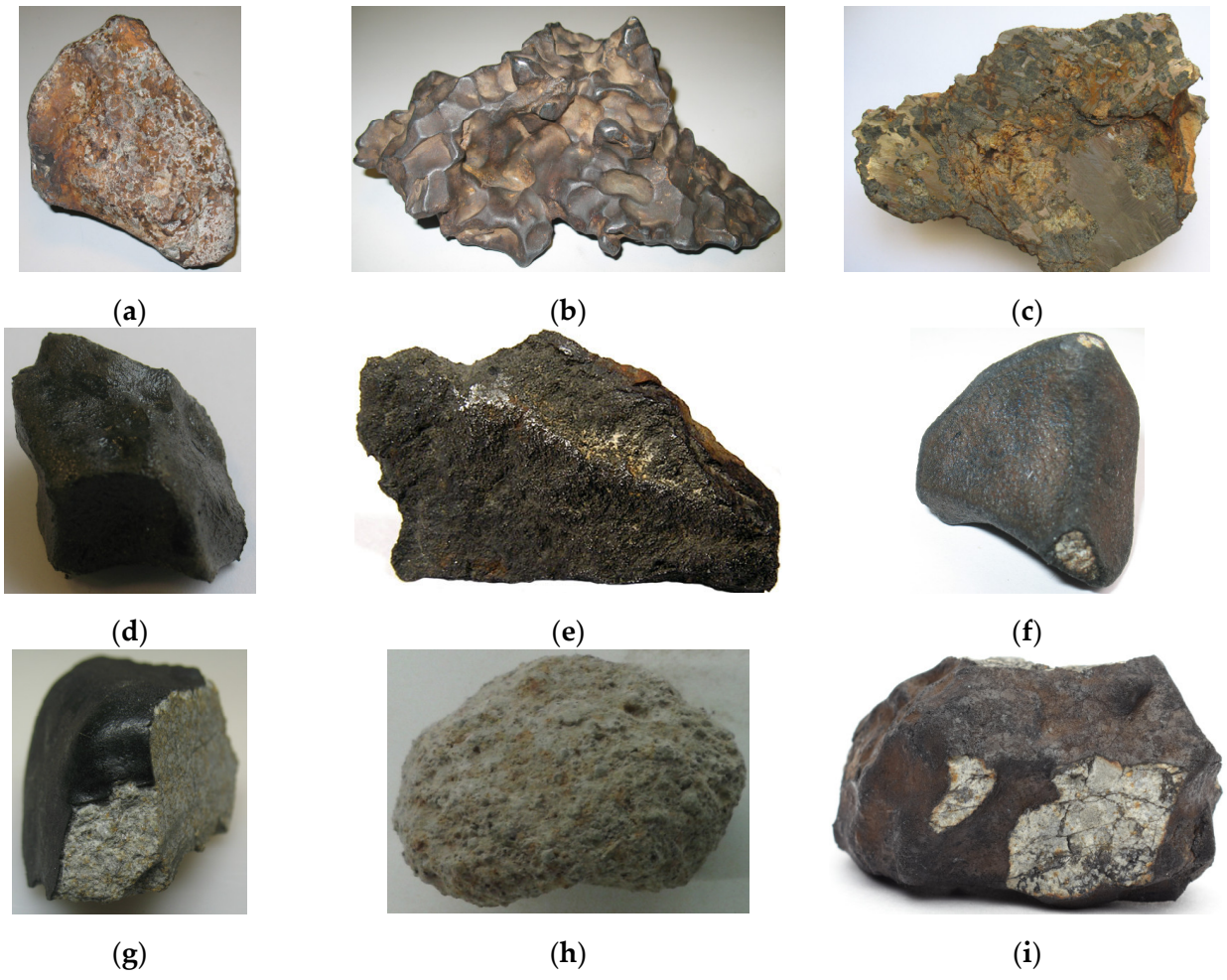

Figure 2. Selected photographs of meteorite fragments: Chinga iron ungrouped (**a**), Sikhote-Alin IIAB iron (**b**), Seymchan main group pallasite (**c**), Sariçiçek howardite (**d**), Isheyevo CH/CBb carbonaceous chondrite (**e**), Annama H5 (**f**), Ozerki L6 (**g**), Bjurböle L/LL4 (**h**) and Chelyabinsk LL5 (**i**) ordinary chondrites. Some fragments contain the fusion crust (**d**,**f**,**g**,**i**).

3. Sample Preparation and Measurements

Samples of bulk meteorite fragments were prepared in the form of powder and very rare as a foil or fine shaving. Powdered samples were taken from the sections of meteorite fragments and then glued on iron-free aluminum foil with a diameter of ~20 mm with a sample thickness in the range of ~8–10 mg Fe/cm^2. The glue which was utilized was medical glue BF-6, a solution of polyvinyl butyral $(C_8H_{14}O_2)_n$ with ethanol. Additionally, polished sections of meteorite fragments were prepared for optical microscopy and scanning electron microscopy (SEM) with energy dispersive spectroscopy (EDS) while the rests of the powdered samples were used for X-ray diffraction (XRD) and magnetization measurements.

All Mössbauer data considered below were obtained using an automated precision Mössbauer spectrometric system based on two SM-2201 spectrometers and a temperature variable liquid nitrogen cryostat (295–90 K) with a moving absorber (see details in [13–16] and references therein). The saw-tooth velocity reference signals in the spectrometers were formed by digital-analog converters with discretization of 2^{12}. All measurements were done in transmission geometry with moving absorbers and spectra registration in 4096 channels. Then, for the spectra fit, some of the measured spectra with poor signal-to-noise ratio for the minor components were converted into the 2048- or 1024-channel spectra by consequent summation of two or four neighboring channels, respectively. ^{57}Co(Rh) sources (Ritverc GmbH, St. Petersburg, Russia) with initial activity of 1.8×10^9 Bq were used at room temperature. Mössbauer spectra of the reference absorbers of α-Fe foils and of the meteorite samples were computer fitted with the least square procedure using UNIVEM-MS program with a Lorentzian line shape. In some cases, the MossWinn code [23] was used for the spectra fits. Spectral parameters such as: isomer shift, δ, quadrupole splitting, Δ (quadrupole shift, ε, for magnetically split spectra, $2\varepsilon = \Delta$), magnetic hyperfine field, H_{eff}, line width, Γ, relative subspectrum (component) area, A, and normalized statistical quality of the fit, χ^2, were determined. The line shapes of the Mössbauer spectra of the reference absorbers of α-Fe foils with thicknesses of 10 and 7 μm were pure Lorentzian with narrow line widths. It should be noted that the δ and ε values for the α-Fe reference absorbers as well as for b.c.c. and f.c.c. Fe-Ni-Co alloys are not exactly zero due to deviations from the ideal cubic structure and much more precise measurements. The instrumental (systematic) error for each spectral point was equivalent to ±0.5 channel (in the velocity scale), while that for the hyperfine parameters was taken equivalent to ±1 channel (in mm/s or kOe) (see [15,16]). If calculated (fitting) error for these parameters exceeded the instrumental (systematic) error, the larger error was used instead. The estimated relative error for A usually did not exceed 10%. The values of δ are given relative to α-Fe at 295 K.

4. Extraterrestrial Fe-Ni-Co Alloys

4.1. Iron Meteorites

Chinga iron ungrouped (iron-ung) meteorite (ataxite) contains ~16.8 at.% of Ni and ~0.5 at.% of Co. Three samples of Chinga metal with different preparations from one fragment were studied first [24]. Three samples were prepared: metal foil with a thickness of 20 μm, fine shaving, and powder. SEM with EDS were used to demonstrate the complex phase composition which is shown in Figure 3a. The Mössbauer spectra of these three samples of Chinga Fe-Ni-Co alloy measured at 295 K in 4096 channels are presented in Figure 3b–d. SEM image shows the presence of the α-Fe(Ni, Co), γ-Fe(Ni, Co) and γ-FeNi phases as well as plessite structure. The Mössbauer spectra reflect this complexity and demonstrate asymmetrical six-line patterns which were better decomposed using six magnetic sextets (in the spectrum of fine shaving an additional small quadrupole doublet with parameters corresponding to Fe^{3+} was revealed). In the case of a smaller number of sextets, e.g., four sextets (the spectrum of Chinga foil presented in 512 channels was fitted using three magnetic sextets only [24]), the misfits at the differential spectra indicated an incomplete fitting model as shown in Figure 3b (see insets). The six obtained magnetic sextets were assigned to the corresponding phases based on the ^{57}Fe hyperfine parameters (hereinafter, we reconsider earlier assignments to some phases).

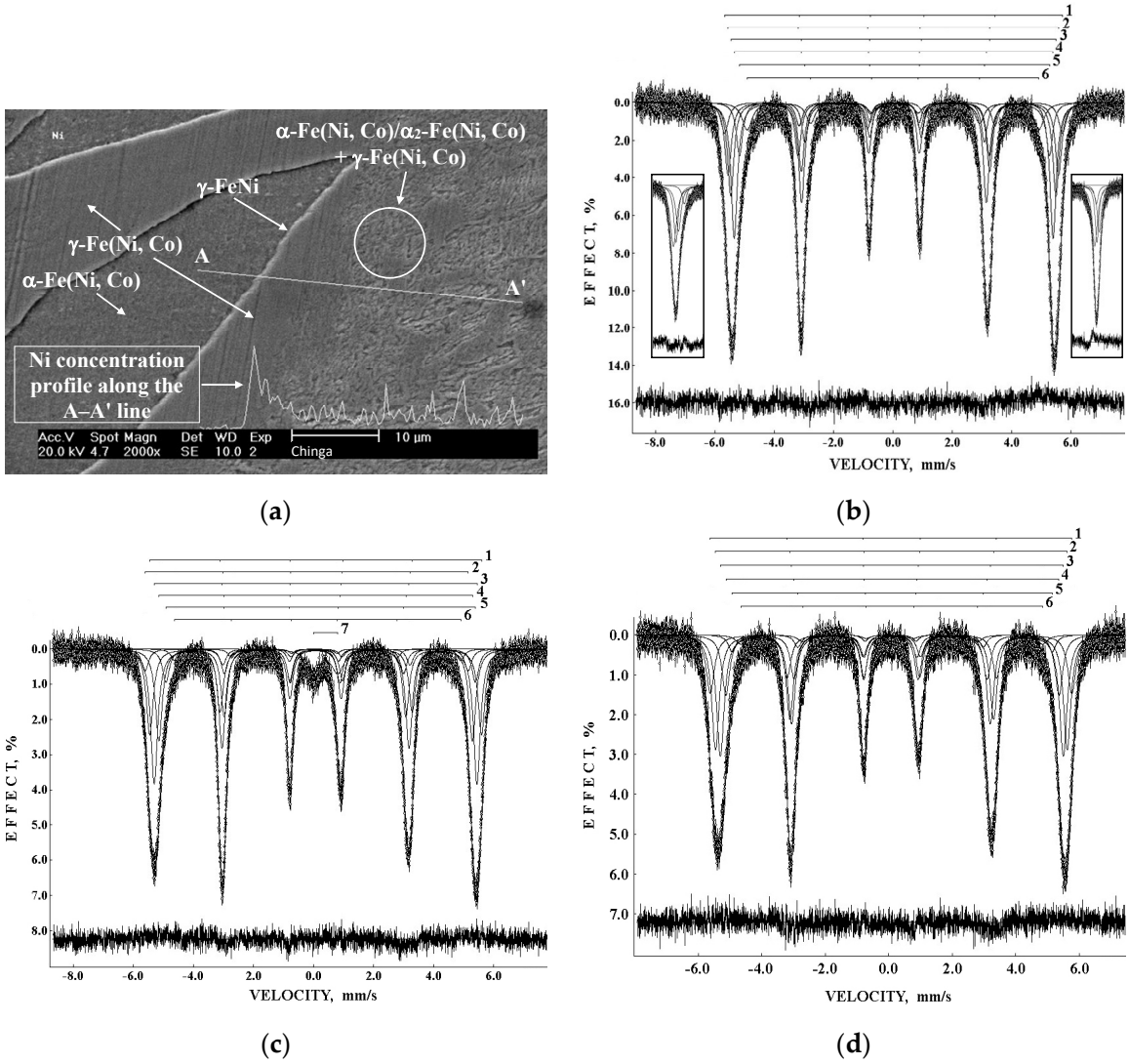

Figure 3. Chinga iron-ung meteorite: scanning electron microscopy image with energy dispersive spectroscopy for chemical analysis indicating the phase composition and Ni variation along the **A–A′** line (**a**) and the 4096-channel Mössbauer spectra of metal foil (**b**), fine shaving (**c**) and powder (**d**). Indicated components 1–7 are the results of the best spectra fits. The differential spectra are shown at the bottom. Insets in (**b**) demonstrate misfits at the differential spectrum for the 1st and the 6th peaks in the fit using 4 sextets only. Adapted from Ref. [24].

The differences in the phase compositions for the three samples (relative areas *A* versus magnetic hyperfine fields H_{eff} for corresponding phases) are shown in Figure 4a–c. Four Fe-Ni-Co phases were revealed: α-Fe(Ni, Co), α_2-Fe(Ni, Co), γ-Fe(Ni, Co) and γ-FeNi phases, i.e., kamacite, martensite, taenite and tetrataenite, respectively. The α_2-Fe(Ni, Co) phase was supposed for the foil and powdered samples (H_{eff} = ~354 kOe) while the γ-FeNi phase was associated with magnetic sextets with H_{eff} = ~296 kOe for the fine shaving and powdered samples. An additional minor paramagnetic component found in the fine shaving sample results of the partial metal oxidation. These results demonstrate that different sample preparations led to some changes in the phase compositions in the Fe-Ni-Co alloy due to mechanical and thermal effects. Therefore, only powdered Fe-Ni-Co alloy samples prepared in the same manner were used further.

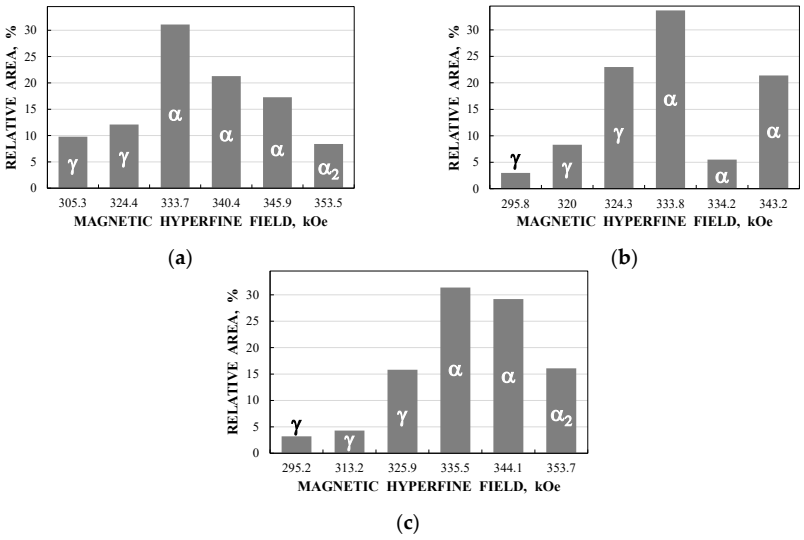

Figure 4. Differences in the relative areas of magnetic sextets revealed in the Mössbauer spectra of Chinga iron-ung meteorite: metal foil (**a**), fine shaving (**b**) and powder (**c**). Magnetic sextets were assigned to indicated phases (γ-, α- and α_2-phases). Data were taken from Ref. [24].

Further, a new Chinga fragment was found with five visually different areas observed in its saw-cut surface (Figure 5a). To investigate the reason of these areas, SEM with EDS, XRD and Mössbauer spectroscopy with a high velocity resolution were applied [25]. The powdered samples were obtained from areas 1, 2, 3 and 5 (area 4 was very thin for sample preparation). SEM images of areas 1, 2, 3 and 5 are shown in Figure 5b–e. Some morphological differences in these areas can clearly be seen. Chemical analysis with EDS indicated ~17.5–18.0 at.% of Ni in all areas. XRD indicated the presence of the α_2-Fe(Ni, Co) phase in all areas as well as slightly different content of the γ-Fe(Ni, Co) phase in these areas: 2.6% (area 1), 1.5% (area 2), 1.8% (area 3) and 2.3% (area 5) in addition to the α-Fe(Ni, Co) phase. The Mössbauer spectra of these area samples measured at 295 K are shown in Figure 6a–d. These Mössbauer spectra were measured with better signal-to-noise ratios than the spectra shown in Figure 3 from [24].

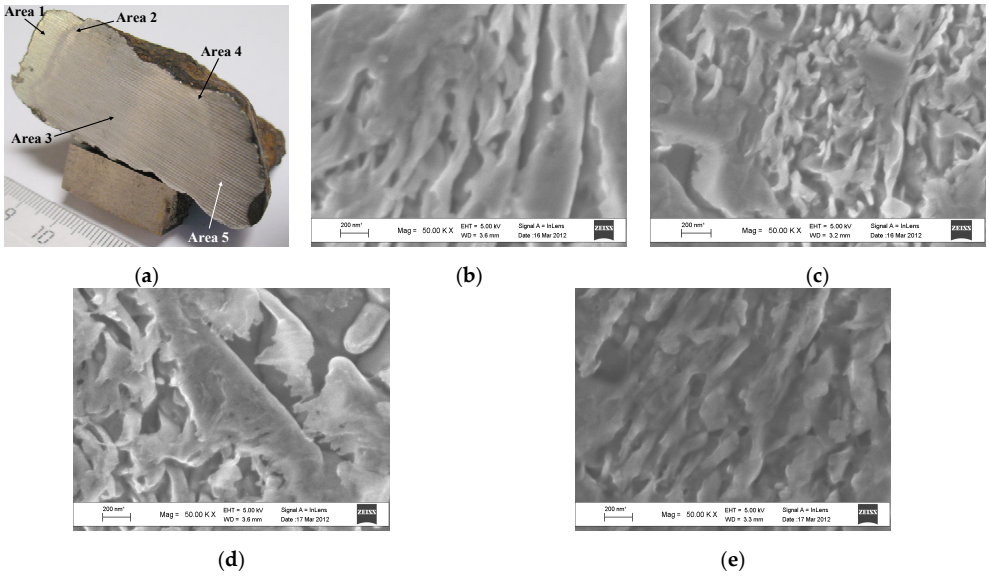

Figure 5. Visually different areas (1–5) at the saw-cut surface of Chinga iron-ung fragment (**a**) and selected SEM images of these areas: area 1 (**b**), area 2 (**c**), area 3 (**d**) and area 5 (**e**). Adapted from Ref. [25].

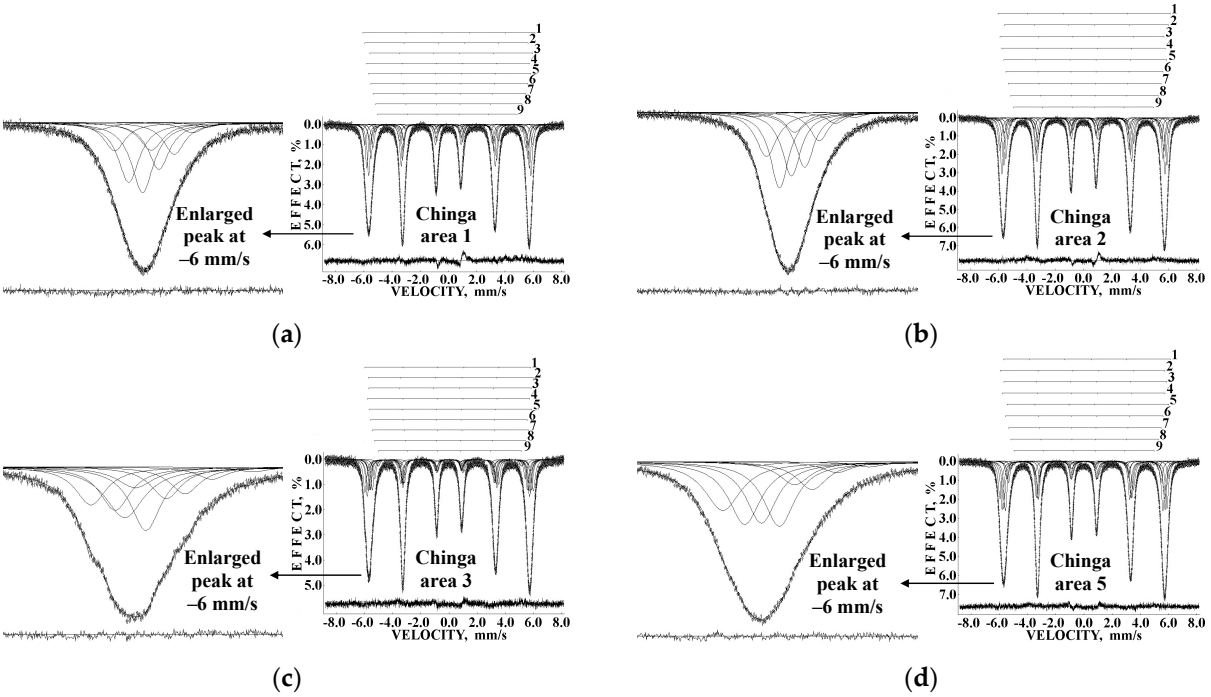

Figure 6. Mössbauer spectra of the samples from visually different areas at the saw-cut surface of Chinga iron-ung fragment measured at 295 K: area 1 (**a**), area 2 (**b**), area 3 (**c**) and area 5 (**d**). The enlarged left peak of each sextet is shown on the left. The differential spectra are shown at the bottom. Adapted from Ref. [25].

Therefore, it was possible to decompose new spectra, which demonstrate asymmetric six-line patterns, with a larger number of magnetic sextets to reach better fits. These decompositions were carried out with nine magnetic sextets for all spectra. Despite the fact that these spectra cannot be distinguished visually, a comparison of the enlarged left peaks of sextets (the most negative velocity peaks) clearly demonstrates some differences in the absorption line shapes. The most visible features of the absorption line shape were found for the spectrum of the sample from area 3. It is possible that local character of the Mössbauer spectroscopy allows one to excavate larger number of slightly different local microenvironments of the ^{57}Fe in the case of larger number of spectral points, i.e., in the Mössbauer spectra measured with a high velocity resolution. It should be noted that the ^{57}Fe hyperfine parameters for the main revealed magnetic sextets demonstrated higher values for H_{eff} (355–379 kOe) which looked strange and had never been obtained previously in the Mössbauer spectra of Fe-Ni-Co alloys measured with a low velocity resolution. Therefore, these values should be checked, verified and compared with those values obtained for analogous alloys (for the α_2-Fe(Ni, Co) phase) by means of Mössbauer spectroscopy with a high velocity resolution.

If we can accept decomposition of the Mössbauer spectra of visually different areas at the saw-cut surface of the Chinga iron-ung fragment shown in Figure 6a–d and associate large values of H_{eff} in the range of 355–379 kOe with (i) the α_2-Fe(Ni, Co) phase (Chinga contains ~18 at.% of Ni) and (ii) variations in the ^{57}Fe local microenvironments resulting from Ni distribution in the neighboring coordination spheres, it will be possible to compare the differences in the histograms of the relative areas versus magnetic hyperfine fields for components obtained from the Mössbauer spectra decomposition as demonstrated in Figure 7a–d. This comparison indicates that there are some variations in the phase compositions in these areas which may be additionally affected by the cutting process. The latter agrees with the above results for three Chinga samples prepared in different ways (see [24]).

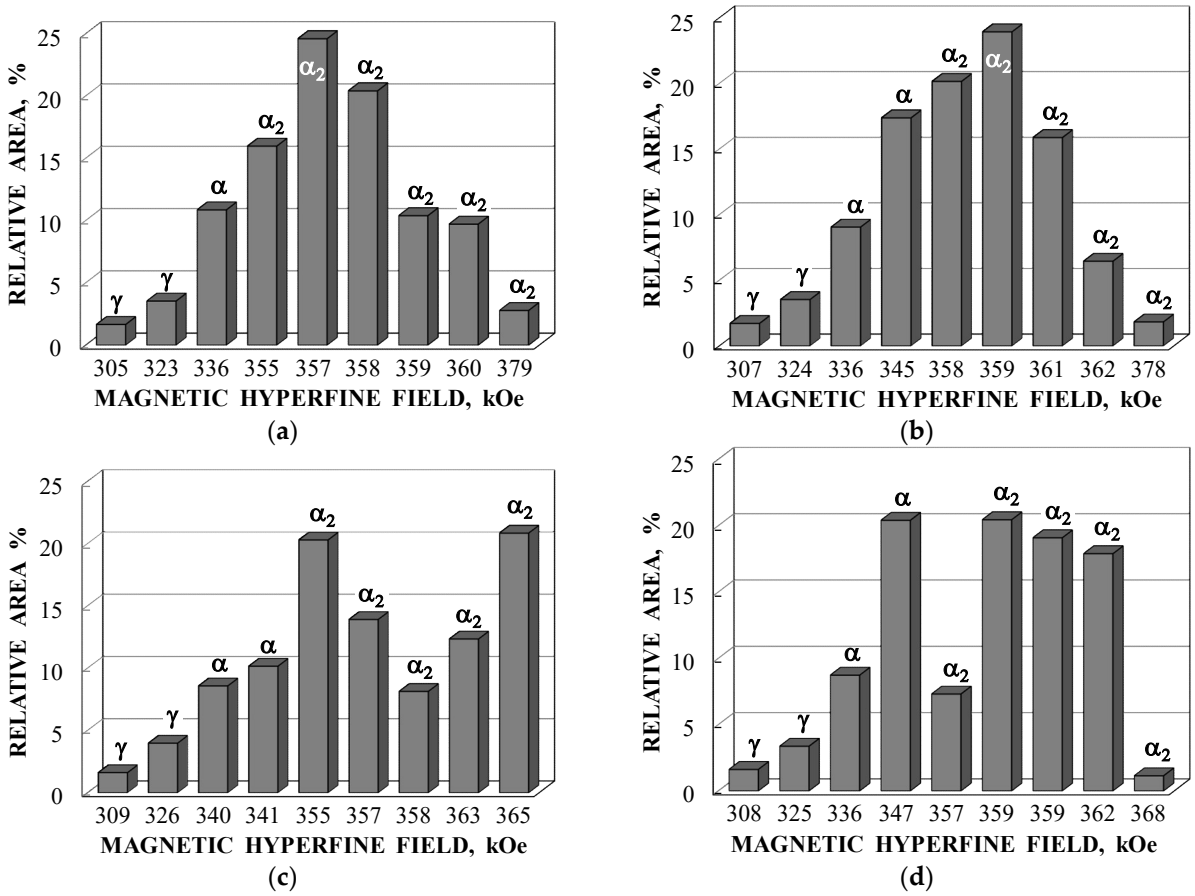

Figure 7. Comparison of the histograms of the relative areas vs. magnetic hyperfine fields for components of the Mössbauer spectra of the samples from visually different areas at the saw-cut surface of Chinga iron-ung fragment: area 1 (**a**), area 2 (**b**), area 3 (**c**) and area 5 (**d**). Indicated symbols γ, α and α_2 correspond to the γ-Fe(Ni, Co), α-Fe(Ni, Co) and α_2-Fe(Ni, Co) phases. Adapted from Ref. [25].

Another ataxite, Dronino iron-ung meteorite was re-examined in [26,27] by Mössbauer spectroscopy with a high velocity resolution, optical microscopy and XRD. Optical microphotograph of a polished section of Dronino and the XRD pattern of the powdered sample are shown in Figure 8a,b. The optical microphotograph demonstrates the duplex structure of Dronino metal: α-Fe(Ni, Co) + α_2-Fe(Ni, Co) phases, i.e., kamacite + martensite, (see [28]). XRD indicates the presence of the b.c.c. Fe-Ni-Co alloy (in fact, mainly the α-phase). A comparison of the 2048-channel Mössbauer spectrum of the Dronino iron-ung powdered sample with the 4096-channel spectrum of reference α-Fe foil with a thickness of 7 μm measured at 295 K is shown in Figure 8c,d. The latter spectrum demonstrates a symmetrical six-line pattern with higher intensity of the 2nd and the 5th lines due to the texture effect resulting from the 7 μm thickness foil preparation. This spectrum was fitted well using one magnetic sextet with Lorentzian line shapes and narrow line widths Γ. In contrast, the Mössbauer spectrum of Dronino iron-ung as well as the spectra of various samples of Chinga iron-ung shown above (see Figures 3 and 6) are asymmetrical six-line patterns with some line broadening. The best refit of the Mössbauer spectrum of Dronino iron-ung metal was achieved using six magnetic sextets with equal Γ values which were varied during the fit parameters of which are shown in Table 1.

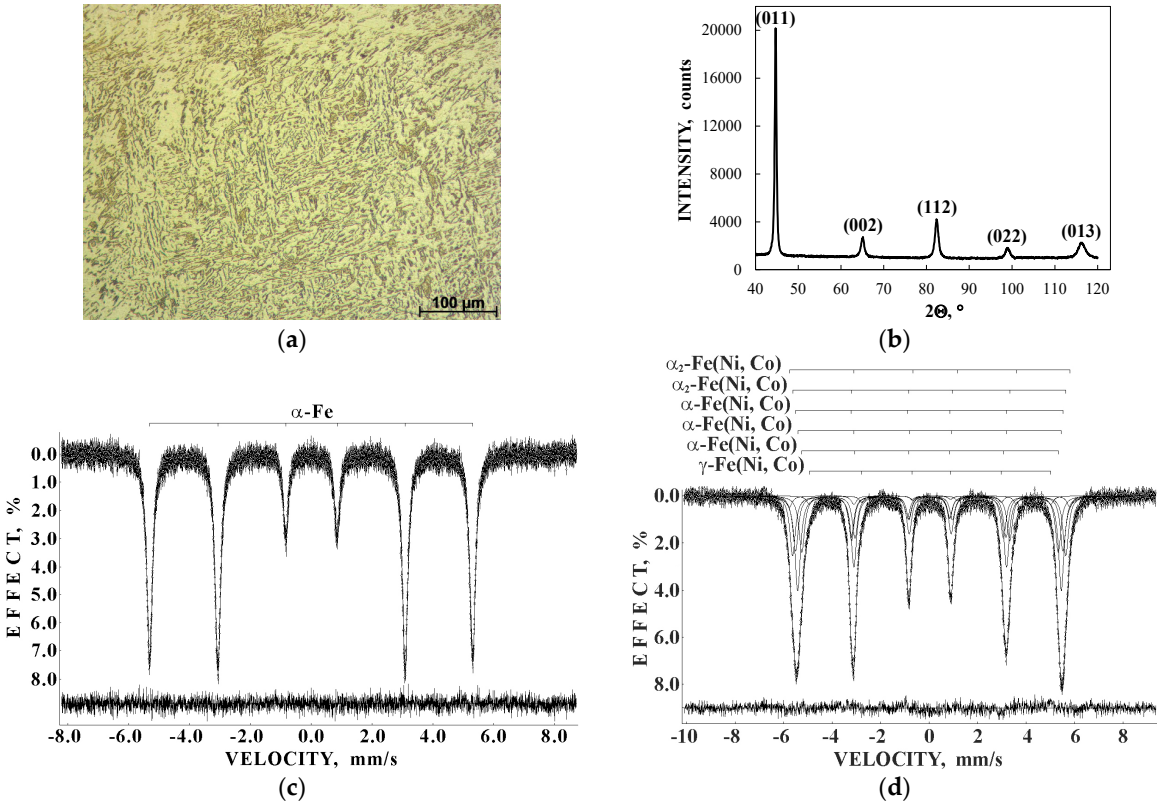

Figure 8. Dronino iron-ung meteorite: optical microphotograph of the polished section (**a**) and XRD pattern of the powdered sample with Miller indices for the α-phase (**b**) and Mössbauer spectra of reference α-Fe foil (**c**) and Dronino iron-ung meteorite powdered sample (**d**) (these spectra were measured at 295 K in 4096 channels and then the Dronino spectrum was converted into the 2048-channel αspectrum). Indicated components are the results of the best fits. The differential spectra are shown at the bottom. Adapted from Ref. [26].

Table 1. Mössbauer parameters for the Dronino iron-ung spectrum shown in Figure 8d which were obtained after refitting with equal line widths.

Γ, mm/s	δ, mm/s	2ε, mm/s	H_{eff}, kOe	*A*, %	Phase
0.276 ± 0.020	0.142 ± 0.010	−0.221 ± 0.036	359.4 ± 1.2	3.9	α_2-Fe(Ni, Co)
0.276 ± 0.020	0.042 ± 0.010	−0.057 ± 0.010	350.0 ± 0.5	20.9	α_2-Fe(Ni, Co)
0.276 ± 0.020	0.001 ± 0.010	0.030 ± 0.010	342.6 ± 0.5	19.3	α-Fe(Ni, Co)
0.276 ± 0.020	0.037 ± 0.010	−0.027 ± 0.010	337.7 ± 0.5	33.2	α-Fe(Ni, Co)
0.276 ± 0.020	0.027 ± 0.010	0.034 ± 0.010	328.4 ± 0.5	19.7	α-Fe(Ni, Co)
0.276 ± 0.020	0.071 ± 0.021	−0.058 ± 0.011	309.0 ± 0.8	2.9	γ-Fe(Ni, Co)

Using the ^{57}Fe hyperfine parameters, these components were assigned to the α_2-Fe(Ni, Co), α-Fe(Ni, Co) and γ-Fe(Ni, Co) phases. The values of H_{eff} higher than 345 kOe were associated with the α_2-Fe(Ni, Co) phase. The presence of several magnetic sextets assigned to the α_2- and α-phases was considered as a result of variations in the distribution of the number of Ni atoms in the ^{57}Fe local microenvironments even within one phase.

Two coarse octahedrites Sikhote-Alin IIAB and Anyujskij IIAB, one medium octahedrite Sterlitamak IIIAB and one octahedrite Aliskerovo IIIE-an ("an" means anomalous properties) were studied by Mössbauer spectroscopy with a high velocity resolution, optical microscopy, SEM and XRD in [26,29]. Optical microphotographs of the polished sections of Sikhote-Alin IIAB, Anyujskij IIAB, Sterlitamak IIIAB and Aliskerovo IIIE-an are shown in Figure 9a–d. These microphotographs indicate the presence of rhabdite $(Fe, Ni)_3P$ microcrystals in the α-Fe(Ni, Co) phase in Sikhote-Alin IIAB and Anyujskij IIAB metal. The Sterlitamak IIIAB metal consists of the α-Fe(Ni, Co) and γ-Fe(Ni, Co) phases and the

plessite structure α-Fe(Ni, Co)/α_2-Fe(Ni, Co) + γ-Fe(Ni, Co) while the Aliskerovo IIIE-an metal consists of the α-Fe(Ni, Co) and γ-FeNi phases as well as plessite. SEM analysis confirmed these phases.

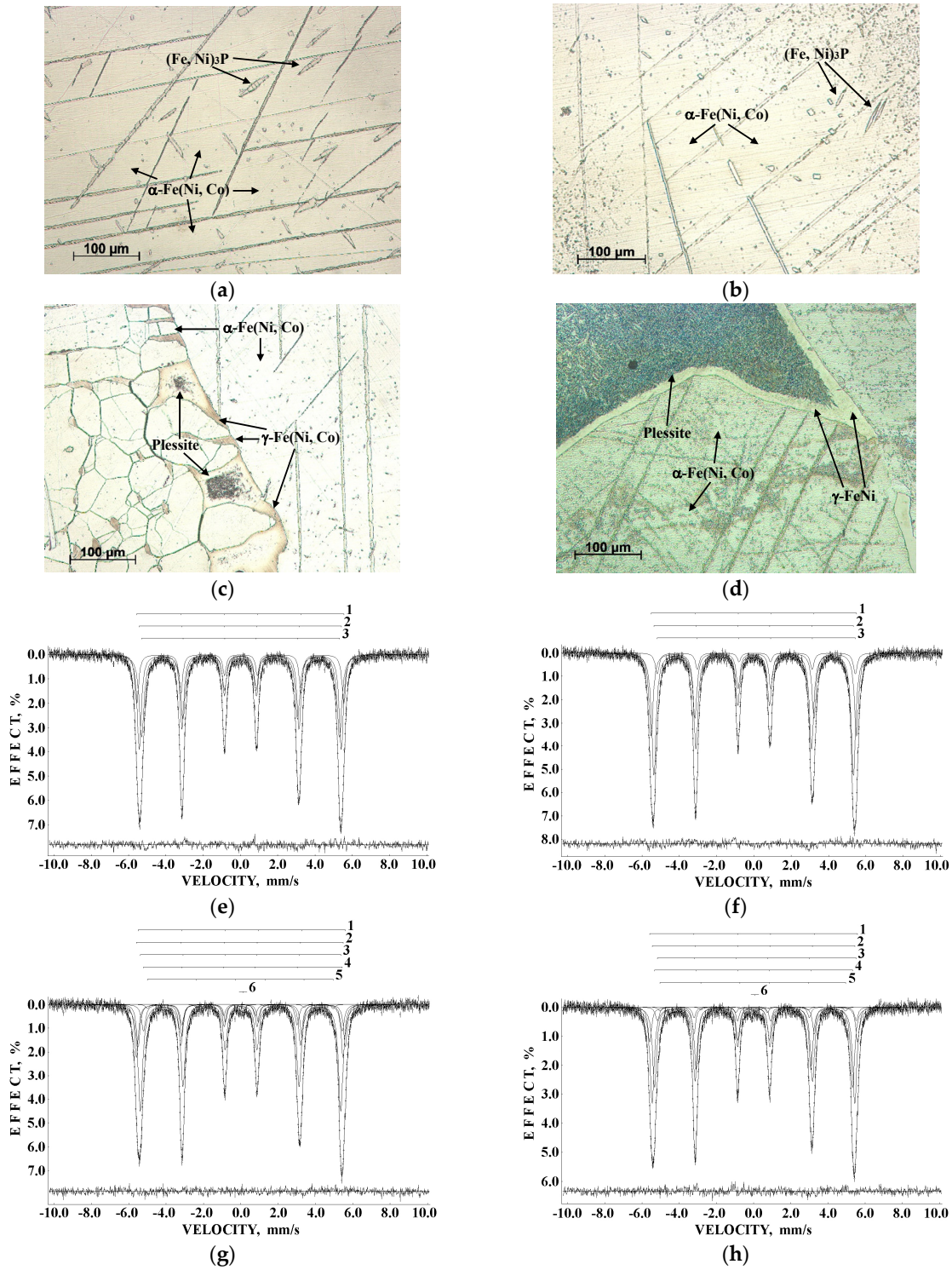

Figure 9. Optical microphotographs of the polished sections of iron meteorites Sikhote-Alin IIAB (**a**), Anyujskij IIAB (**b**), Sterlitamak IIIAB (**c**) and Aliskerovo IIIE-an (**d**) and room temperature Mössbauer spectra of Sikhote-Alin IIAB (**e**), Anyujskij IIAB (**f**), Sterlitamak IIIAB (**g**) and Aliskerovo IIIE-an (**h**). Indicated components are the results of the best fits. The differential spectra are shown at the bottom. Adapted from Ref. [26].

XRD demonstrated the presence of the α-Fe(Ni, Co) phase in Sikhote-Alin IIAB and Anyujskij IIAB meteorites while Sterlitamak IIIAB and Aliskerovo IIIE-an also contained small amount of the γ-phase in addition to the α-phase. The room temperature 1024-channel Mössbauer spectra of powdered samples of Sikhote-Alin IIAB, Anyujskij IIAB, Sterlitamak IIIAB and Aliskerovo IIIE-an are shown in Figure 9e–h. These spectra also demonstrated similar asymmetric six-line patterns. However, these spectra were well decomposed with different numbers of spectral components: three magnetic sextets for the spectra of Sikhote-Alin and Anyujskij and five magnetic sextets and one paramagnetic singlet for the spectra of Sterlitamak and Aliskerovo. The Mössbauer parameters of the revealed components associated with the corresponding metal phases are listed in Table 2. These fits were done with free variations of the Γ values and the results show close Γ values.

Table 2. Mössbauer parameters for the Sikhote-Alin IIAB, Anyujskij IIAB, Sterlitamak IIIAB and Aliskerovo IIIE-an spectra shown in Figure 9e–h (data were taken from Ref. [29]).

Meteorite	No [1]	Γ, mm/s	δ, mm/s	2ε, mm/s	H_{eff}, kOe	*A*, %	Phase
Sikhote-Alin IIAB	1	0.240 ± 0.040	0.011 ± 0.020	−0.034 ± 0.020	345.1 ± 0.6	19	α-Fe(Ni, Co)
	2	0.265 ± 0.040	−0.004 ± 0.020	−0.010 ± 0.020	336.5 ± 0.6	40	α-Fe(Ni, Co)
	3	0.313 ± 0.040	−0.001 ± 0.020	0.014 ± 0.020	329.7 ± 0.6	41	α-Fe(Ni, Co)
Anyujskij IIAB	1	0.270 ± 0.040	0.010 ± 0.020	−0.037 ± 0.031	342.3 ± 0.6	36	α-Fe(Ni, Co)
	2	0.287 ± 0.040	−0.015 ± 0.020	−0.002 ± 0.032	332.5 ± 0.6	56	α-Fe(Ni, Co)
	3	0.255 ± 0.040	0.083 ± 0.020	0.082 ± 0.020	330.0 ± 0.8	8	α-Fe(Ni, Co)
Sterlitamak IIIAB	1	0.233 ± 0.040	0.057 ± 0.020	−0.007 ± 0.020	344.7 ± 0.6	16	α-Fe(Ni, Co)
	2	0.239 ± 0.040	−0.031 ± 0.020	−0.046 ± 0.020	343.7 ± 0.6	20	α-Fe(Ni, Co)
	3	0.295 ± 0.040	0.001 ± 0.020	−0.024 ± 0.020	333.4 ± 0.6	50	α-Fe(Ni, Co)
	4	0.263 ± 0.040	0.024 ± 0.020	0.182 ± 0.020	330.7 ± 0.7	11	α-Fe(Ni, Co)
	5	0.238 ± 0.071	0.243 ± 0.020	−0.534 ± 0.041	309.1 ± 1.6	2	γ-Fe(Ni, Co)
	6	0.352 ± 0.152	0.128 ± 0.050	–	–	1	par. γ-Fe(Ni, Co) [2]
Aliskerovo IIIE-an	1	0.234 ± 0.040	0.015 ± 0.020	−0.024 ± 0.020	347.1 ± 0.6	14	α_2-Fe(Ni, Co)
	2	0.269 ± 0.040	0.003 ± 0.020	−0.020 ± 0.020	338.6 ± 0.6	43	α-Fe(Ni, Co)
	3	0.233 ± 0.040	0.036 ± 0.020	0.274 ± 0.028	332.3 ± 1.1	5	α-Fe(Ni, Co)
	4	0.259 ± 0.040	0.001 ± 0.020	0.003 ± 0.020	330.9 ± 0.6	35	α-Fe(Ni, Co)
	5	0.233 ± 0.096	0.006 ± 0.020	−0.096 ± 0.048	310.1 ± 2.1	2	γ-Fe(Ni, Co)
	6	0.664 ± 0.246	0.071 ± 0.069	–	–	1	par. γ-Fe(Ni, Co) [2]

[1] The number of spectral components. [2] The paramagnetic γ-Fe(Ni, Co) phase.

Two iron meteorites Gibeon IVA (fine octahedrite) and Mundrabilla IAB-ung (medium octahedrite) were recently studied using Mössbauer spectroscopy with a high velocity resolution, optical microscopy, SEM with EDS, XRD and magnetization measurements [30,31]. Optical microscopy and SEM images of polished sections of Gibeon IVA and Mundrabilla IAB-ung iron meteorites are shown in Figure 10. These and other images demonstrate the presence of the α-Fe(Ni, Co) phase (kamacite) and the γ-Fe(Ni, Co) phase (taenite) with plessite structures in both meteorites, although some morphological differences were observed. EDS analysis showed variations in the Fe, Ni and Co concentrations along the **A–A'** lines (Figure 10c–f). The ranges of Ni contents in the α-Fe(Ni, Co) phase matrix were ~5.0–7.5 at.% for Gibeon and ~6.3–6.5 at.% for Mundrabilla while those in the γ-Fe(Ni, Co) phase were ~26.0–36.1 at.% for Gibeon and ~22–45 at.% for Mundrabilla. The XRD patterns of Gibeon IVA and Mundrabilla IAB-ung powdered samples are shown in Figure 11a,b. These patterns demonstrate the presence of the main α-Fe(Ni, Co) phase with minor content of the γ-Fe(Ni, Co) phase in both iron meteorites (see insets in Figure 11a,b). The average content of taenite was evaluated as ~1.3 wt.% and ~1.4 wt.% in Gibeon and Mundrabilla, respectively. The Mössbauer spectra of Gibeon IVA and Mundrabilla IAB-ung powdered samples measured at 295 K with a high velocity resolution in 4096 channels and converted into the 1024-channel spectra are shown in Figure 11c,d. These spectra are also asymmetric six-line patterns which are similar to all of the spectra of iron meteorites shown above.

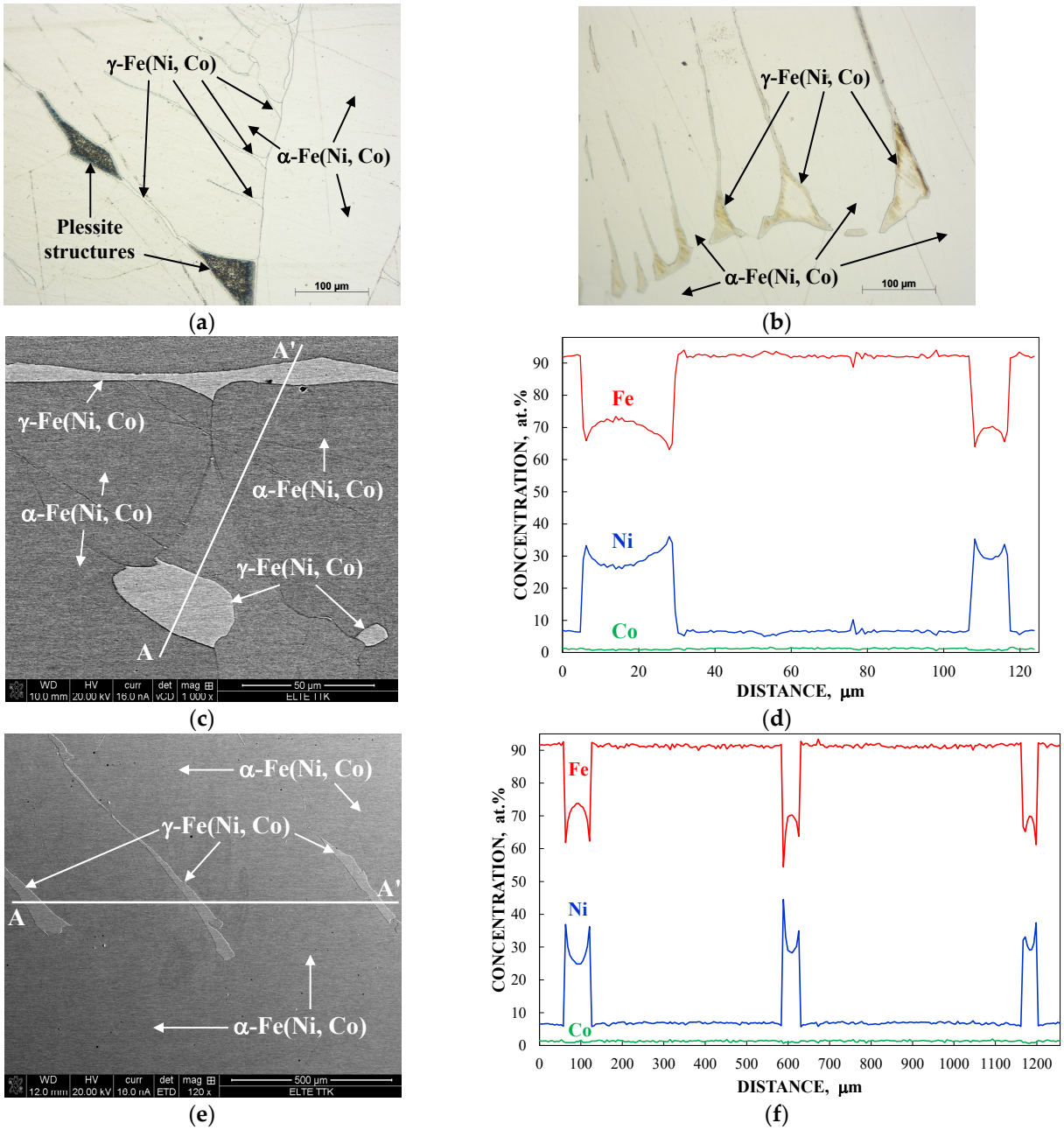

Figure 10. Selected optical microphotographs of the polished sections of Gibeon IVA (**a**) and Mundrabilla IAB-ung (**b**) and SEM images of the polished sections (**c**,**e**) with corresponding variations of the Fe, Ni and Co concentrations along the **A–A′** lines (**d**,**f**) for Gibeon IVA (**c**,**d**) and Mundrabilla IAB-ung (**e**,**f**). Adapted from Refs. [30,31].

The Mössbauer spectra of the Gibeon IVA and Mundrabilla IAB-ung powdered samples were better fitted using five magnetic sextets and one paramagnetic singlet. However, the Mössbauer parameters for these components were slightly different (see Table 3). Based on the values of H_{eff}, the magnetic sextets revealed in the Mössbauer spectrum of Gibeon IVA were assigned to the α_2-Fe(Ni, Co) phase, the α-Fe(Ni, Co) phase with three different local microenvironments with Ni content variations, and the γ-Fe(Ni, Co) phase, while those revealed in the Mössbauer spectrum of Mundrabilla IAB-ung were associated with the α_2-Fe(Ni, Co) phase, the α-Fe(Ni, Co) phase with two different local microenvironments with Ni content variations, and the γ-Fe(Ni, Co) phase with two different local microenvironments with Ni content variations. In the latter case, two components related to the

γ-Fe(Ni, Co) phase could be considered as disordered (H_{eff} = 325.8 kOe) and more ordered (H_{eff} = 312.8 kOe) taenite. The parameters of the paramagnetic singlets were similar except for small differences in the δ values which were related to the paramagnetic γ-Fe(Ni, Co) phase the presence of which was confirmed by EDS. However, some δ variations may be a result of small differences in the Ni content in the paramagnetic taenite in the Gibeon IVA and Mundrabilla IAB-ung iron meteorites.

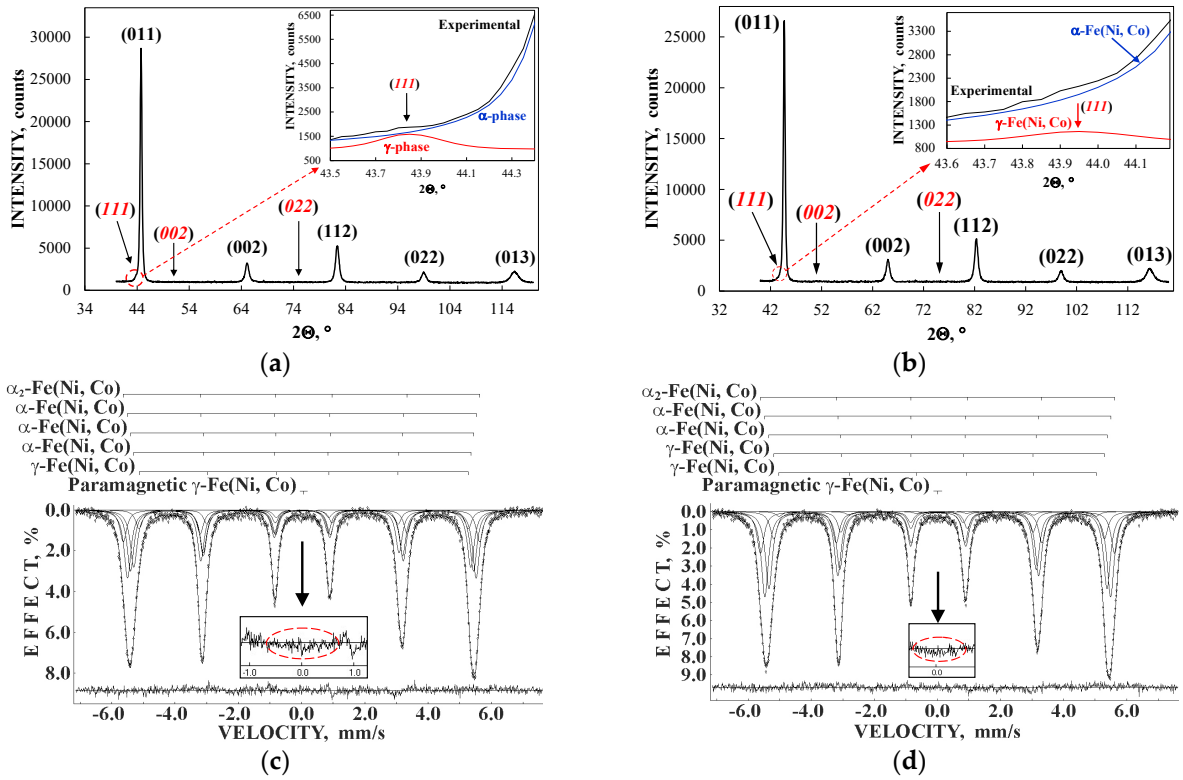

Figure 11. XRD patterns of Gibeon IVA (**a**) and Mundrabilla IAB-ung (**b**) and Mössbauer spectra of Gibeon IVA (**c**) and Mundrabilla IAB-ung (**d**). Indicated components are the results of the best fits. The differential spectra are shown at the bottom. Insets show misfits at the differential spectra in the case of the fits without paramagnetic singlet. Adapted from Refs. [30,31].

Table 3. Mössbauer parameters for the Gibeon IVA and Mundrabilla IAB-ung spectra shown in Figure 11c,d (data were taken from Refs. [30,31]).

Meteorite	Γ, mm/s	δ, mm/s	2ε, mm/s	H_{eff}, kOe	*A*, %	Phase
Gibeon IVA	0.261 ± 0.030	0.034 ± 0.015	−0.070 ± 0.015	349.9 ± 0.6	13.4	α_2-Fe(Ni, Co)
	0.261 ± 0.030	0.014 ± 0.020	−0.008 ± 0.020	342.3 ± 0.6	28.6	α-Fe(Ni, Co)
	0.261 ± 0.030	0.031 ± 0.015	−0.029 ± 0.015	336.8 ± 0.6	25.7	α-Fe(Ni, Co)
	0.261 ± 0.030	0.007 ± 0.015	0.034 ± 0.015	330.1 ± 0.6	24.0	α-Fe(Ni, Co)
	0.261 ± 0.030	0.051 ± 0.015	0.037 ± 0.015	323.3 ± 0.6	7.9	γ-Fe(Ni, Co)
	0.269 [1]	0.067 ± 0.022	–	–	0.4	par. γ-Fe(Ni, Co) [2]
Mundrabilla IAB-ung	0.268 ± 0.028	0.030 ± 0.014	−0.050 ± 0.014	348.8 ± 0.6	17.6	α_2-Fe(Ni, Co)
	0.268 ± 0.028	0.019 ± 0.014	−0.017 ± 0.014	340.6 ± 0.6	36.0	α-Fe(Ni, Co)
	0.268 ± 0.028	0.020 ± 0.014	−0.002 ± 0.014	333.1 ± 0.6	32.5	α-Fe(Ni, Co)
	0.268 ± 0.028	0.021 ± 0.014	0.066 ± 0.014	325.8 ± 0.6	11.5	γ-Fe(Ni, Co)
	0.268 ± 0.028	0.068 ± 0.014	−0.120 ± 0.022	312.8 ± 1.2	2.0	γ-Fe(Ni, Co)
	0.268 ± 0.028	0.006 ± 0.020	–	–	0.4	par. γ-Fe(Ni, Co) [2]

[1] Fixed parameter. [2] The paramagnetic γ-Fe(Ni, Co) phase.

A comparison of the relative areas of magnetic sextets resulting from decompositions of the Mössbauer spectra of Gibeon IVA and Mundrabilla IAB-ung which are roughly proportional to the relative iron fractions in these phases are shown in Figure 12. This comparison demonstrates that two different iron meteorites belonging to different groups with different history of formation and further evolution in space have some variations in their phase compositions.

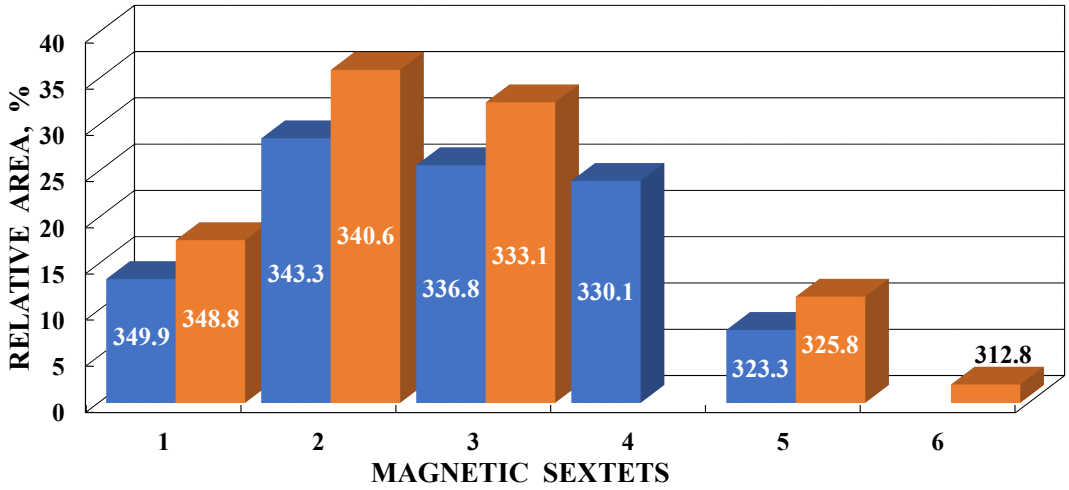

Figure 12. Comparison of the relative areas of magnetic sextets (roughly relative iron fractions) for Gibeon IVA (■) and Mundrabilla IAB-ung (■). The numbers 1–6 are magnetic sextets: 1 is the α_2-Fe(Ni, Co) phase, 2–4 are the α-Fe(Ni, Co) phase and 5, 6 are the γ-Fe(Ni, Co) phase. Indicated values are the values of the magnetic hyperfine field in kOe.

4.2. Stony-Iron Meteorites

Meteorite Seymchan is a stony-iron meteorite from the main group pallasite (PMG). Pallasites consist of stony fragments mixed with molten Fe-Ni-Co alloy and then slowly cooled. Therefore, pallasites demonstrate stony pieces "frozen" in the metal matrix as shown in Figure 13a for Seymchan PMG. Thus, it is possible to study the metal matrix and stony fragments separately which was done for Seymchan in [32]. An optical microphotograph and SEM image of the metal matrix in Seymchan are shown in Figure 13b,c. EDS analysis showed the presence of metal grains with the α-Fe(Ni, Co) and γ-Fe(Ni, Co) phases as well as plessite structures and some rhabdite $(Fe, Ni)_3P$ microcrystals in the metal matrix. Variations in Fe, Ni and Co concentrations along the **A–A′** line crossing the grain boundary (Figure 13c) are shown in Figure 13d. The powdered sample of the Seymchan PMG metal matrix was studied by XRD and Mössbauer spectroscopy (see Figure 13e,f). XRD demonstrates the presence of the main α-Fe(Ni, Co) phase with additional minor contents of the γ-Fe(Ni, Co) phase and $(Fe, Ni)_3P$. The 295 K Mössbauer spectrum of the Seymchan metal matrix demonstrates an asymmetrical six-line pattern which was fitted well using eight magnetic sextets with equal Γ values varied during the fit and one paramagnetic doublet (parameters can be seen in Table 4). Based on the H_{eff} values, components 1 and 2 were assigned to the α_2-Fe(Ni, Co) phase, components 3–6 were associated with the α-Fe(Ni, Co) phase while components 7 and 8 were related to the γ-Fe(Ni, Co) phase. The presence of several magnetic sextets for one phase was explained as a result of Ni variations within this phase. Magnetic sextet 7 with a relatively larger value of H_{eff} can be related to disordered taenite while magnetic sextet 8 with a relatively smaller value of H_{eff} can be associated with more ordered taenite.

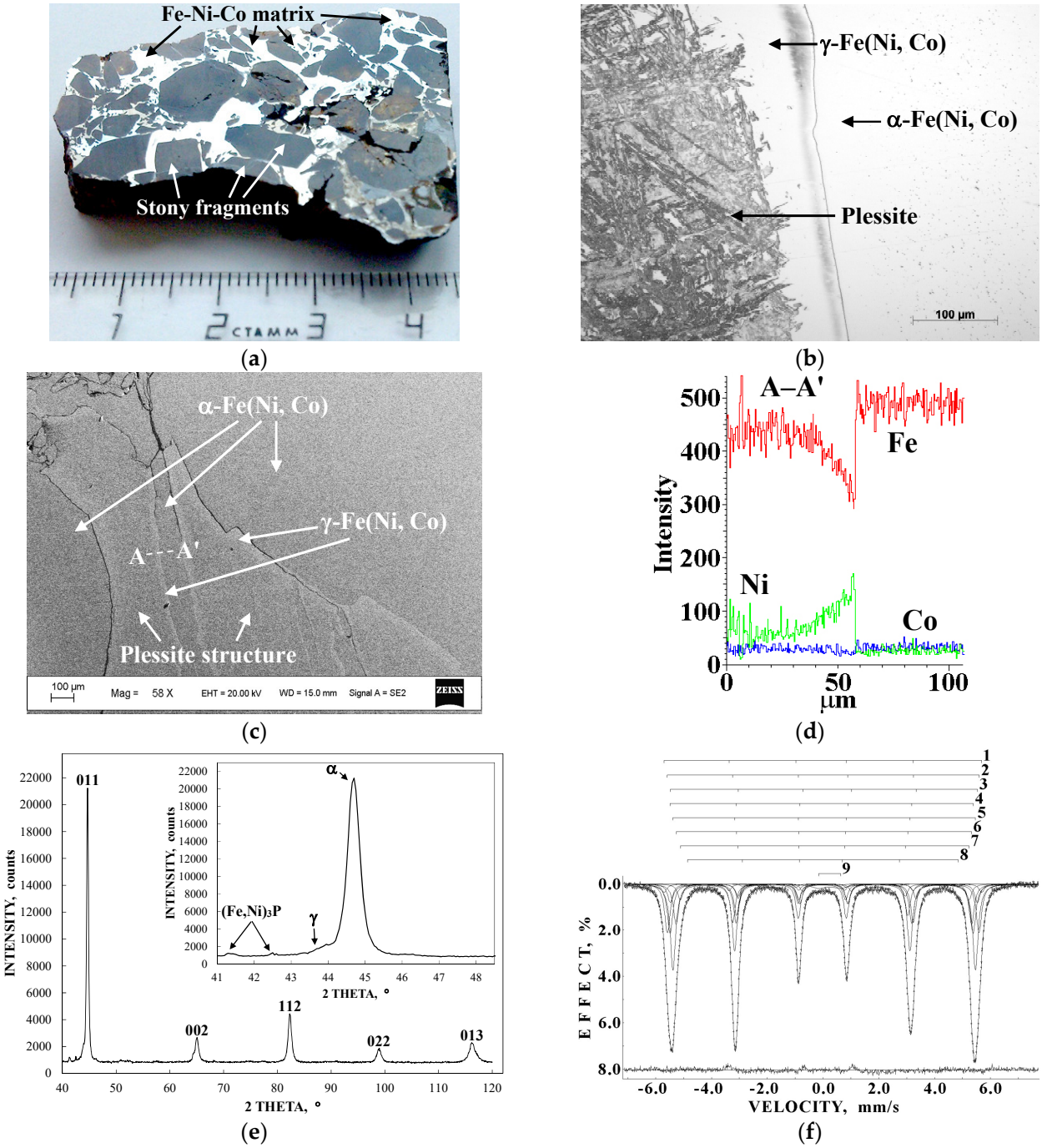

Figure 13. Seymchan PMG: photograph of the polished section (**a**), optical microphotograph of the polished section the metal matrix (**b**), SEM image of the polished section the metal matrix with indicated phases (**c**) and profiles of the Fe, Ni and Co concentration variations in the boundary between the metal grains along the **A–A'** line obtained by EDS (**d**), XRD pattern (indicated reflexes in the XRD pattern correspond to the α-Fe(Ni, Co) phase, inset shows additional minor peaks for the γ-Fe(Ni, Co) phase (**γ**) and (Fe, Ni)$_3$P in addition to the α phase (**α**)) (**e**) and the Mössbauer spectrum of the metal matrix from Seymchan PMG (indicated components in the Mössbauer spectrum are the results of the best fits; the differential spectrum is shown at the bottom) (**f**). Adapted from Ref. [32].

Table 4. Mössbauer parameters for the metal matrix from the Seymchan PMG spectrum shown in Figure 13f (data were taken from Ref. [32]).

Component	Γ, mm/s	δ, mm/s	2ε/Δ, mm/s	H_{eff}, kOe	*A*, %	Phase/Component
1	0.233 ± 0.030	−0.036 ± 0.015	0.061 ± 0.015	353.3 ± 0.6	3.8	α_2-Fe(Ni, Co)
2	0.233 ± 0.030	0.003 ± 0.015	−0.002 ± 0.015	346.9 ± 0.6	17.4	α_2-Fe(Ni, Co)
3	0.233 ± 0.030	0.086 ± 0.015	−0.128 ± 0.015	341.9 ± 0.6	6.9	α-Fe(Ni, Co)
4	0.233 ± 0.030	−0.010 ± 0.015	−0.082 ± 0.015	337.2 ± 0.6	18.0	α-Fe(Ni, Co)
5	0.233 ± 0.030	0.006 ± 0.015	0.070 ± 0.015	336.8 ± 0.6	30.6	α-Fe(Ni, Co)
6	0.233 ± 0.030	−0.003 ± 0.015	0.065 ± 0.015	328.8 ± 0.6	15.1	α-Fe(Ni, Co)
7	0.233 ± 0.030	0.004 ± 0.015	0.114 ± 0.015	321.0 ± 0.6	5.1	γ-Fe(Ni, Co)
8	0.233 ± 0.030	−0.037 ± 0.015	0.068 ± 0.020	301.3 ± 0.8	1.1	γ-Fe(Ni, Co)
9	0.613 ± 0.051	0.270 ± 0.018	0.825 ± 0.035	–	1.9	Fe^{3+}

4.3. Carbonaceous Chondrites

Meteorite Isheyevo CH/CBb is a carbonaceous chondrite which is transitional between the CH group (H means high metal content) and the b-subgroup of the CB group (B means the Bencubbin-like meteorite group). Isheyevo contains from 50 to 70 vol.% of Fe-Ni-Co alloy, its weathering grade is W1. The external and internal parts of one Isheyevo fragment were studied by Mössbauer spectroscopy with a high velocity resolution at room temperature in [33]. The measured spectra are shown in Figure 14a,b.

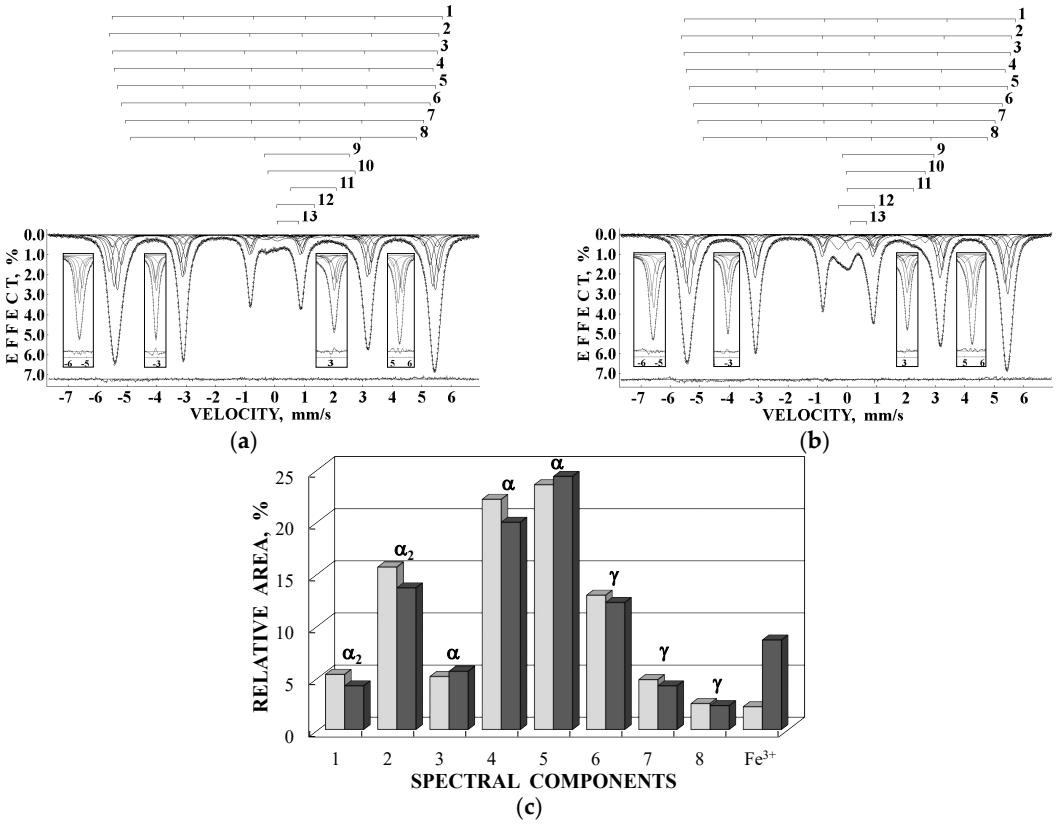

Figure 14. Room temperature Mössbauer spectra of Isheyevo CH/CBb carbonaceous chondrite: internal part (**a**) and external part (**b**); indicated components are the results of the new fits, the differential spectra are shown at the bottom, insets show misfits at the differential spectra resulting from earlier fits in [33] and a comparison of the relative areas of the magnetic sextets 1–8 and quadrupole doublets associated with Fe^{3+} compounds as revealed from the Mössbauer spectra of Isheyevo CH/CBb carbonaceous chondrite: internal part (■) and external part (■). α_2, α and γ indicate Fe-Ni-Co phases (**c**).

These spectra were refitted with a larger number of components, than that used earlier in [33]. Equal Γ values for magnetic sextets which were varied during the new fit were also used. An improvment of the differential spectra can be clearly seen by comparison of the new spectra fits with the previous fits shown in insets. New parameters are listed in Table 5 while a comparison of the relative areas of the magnetic sextets and ferric compounds for the internal and external parts of the Isheyevo fragment is shown in Figure 14c).

Table 5. Mössbauer parameters for the internal and external parts of Isheyevo CH/CBb obtained in the new fits. Component numbers correspond to those shown in Figure 14a,b.

Part	No [1]	Γ, mm/s	δ, mm/s	2ε/Δ, mm/s	H_{eff}, kOe	*A*, %	Phase/Component
Internal	1	0.261 ± 0.029	0.126 ± 0.014	−0.069 ± 0.014	348.0 ± 0.5	5.3	α_2-Fe(Ni, Co)
	2	0.261 ± 0.029	0.017 ± 0.014	−0.067 ± 0.014	347.9 ± 0.5	15.6	α_2-Fe(Ni, Co)
	3	0.261 ± 0.029	−0.060 ± 0.014	0.141 ± 0.014	342.6 ± 0.5	5.1	α-Fe(Ni, Co)
	4	0.261 ± 0.029	0.022 ± 0.014	−0.111 ± 0.014	336.6 ± 0.5	22.1	α-Fe(Ni, Co)
	5	0.261 ± 0.029	0.038 ± 0.014	0.051 ± 0.014	335.8 ± 0.5	23.5	α-Fe(Ni, Co)
	6	0.261 ± 0.029	0.030 ± 0.014	0.013 ± 0.014	325.8 ± 0.5	12.9	γ-Fe(Ni, Co)
	7	0.261 ± 0.029	0.016 ± 0.014	−0.018 ± 0.014	314.9 ± 0.5	4.8	γ-Fe(Ni, Co)
	8	0.261 ± 0.029	0.030 ± 0.014	−0.131 ± 0.014	301.1 ± 0.5	2.5	γ-Fe(Ni, Co)
	9	0.307 ± 0.029	1.260 ± 0.014	2.960 ± 0.015	–	1.2	Fe^{2+}
	10	0.449 ± 0.055	1.103 ± 0.016	2.878 ± 0.027	–	1.9	Fe^{2+}
	11	0.557 ± 0.112	1.317 ± 0.021	1.549 ± 0.068	–	1.2	Fe^{2+}
	12	0.716 ± 0.029	0.717 ± 0.078	1.289 ± 0.134	–	1.7	Fe^{2+}
	13	0.497 ± 0.040	0.452 ± 0.023	0.726 ± 0.050	–	2.2	Fe^{3+}
External	1	0.265 ± 0.029	−0.117 ± 0.014	−0.041 ± 0.014	348.7 ± 0.5	4.2	α_2-Fe(Ni, Co)
	2	0.265 ± 0.029	−0.015 ± 0.014	−0.067 ± 0.014	347.9 ± 0.5	13.6	α_2-Fe(Ni, Co)
	3	0.265 ± 0.029	−0.059 ± 0.014	0.130 ± 0.014	343.7 ± 0.5	5.6	α-Fe(Ni, Co)
	4	0.265 ± 0.029	−0.017 ± 0.014	−0.121 ± 0.014	336.6 ± 0.5	19.9	α-Fe(Ni, Co)
	5	0.265 ± 0.029	0.037 ± 0.014	0.034 ± 0.014	335.8 ± 0.5	24.3	α-Fe(Ni, Co)
	6	0.265 ± 0.029	0.027 ± 0.014	0.011 ± 0.014	325.5 ± 0.5	12.2	γ-Fe(Ni, Co)
	7	0.265 ± 0.029	0.006 ± 0.014	−0.040 ± 0.014	313.0 ± 0.5	4.2	γ-Fe(Ni, Co)
	8	0.265 ± 0.029	0.008 ± 0.014	−0.115 ± 0.014	299.5 ± 0.5	2.3	γ-Fe(Ni, Co)
	9	0.233 ± 0.029	1.401 ± 0.017	3.105 ± 0.027	–	0.5	Fe^{2+}
	10	0.323 ± 0.029	1.311 ± 0.014	2.671 ± 0.018	–	2.0	Fe^{2+}
	11	0.534 ± 0.034	1.129 ± 0.014	2.234 ± 0.027	–	2.6	Fe^{2+}
	12	0.454 ± 0.029	0.317 ± 0.014	1.232 ± 0.017	–	5.0	Fe^{3+}
	13	0.338 ± 0.029	0.392 ± 0.014	0.536 ± 0.014	–	3.6	Fe^{3+}

[1] The number of spectral components.

After [33], the chemical composition and mineralogy of Isheyevo CH/CBb were studied in [34]. These results showed that the metal-rich lithologies with 50–60 vol.% of Fe-Ni-Co alloy were dominant. There are different metal grains in Isheyevo with variations in Ni content (4.2–14.3 wt.%, >25 wt.%) [34]. Based on these data and using the H_{eff} values, the revealed magnetic spectral components for both internal and external parts can be related to the following metal phases: the α_2-Fe(Ni, Co) phase (1 and 2), the α-Fe(Ni, Co) phase (3–5), and the γ-Fe(Ni, Co) phase (6–8). The presence of several magnetic sextets for one phase was also explained as a result of variations in Ni content within one phase. Paramagnetic quadrupole doublets demonstrate ^{57}Fe hyperfine parameters corresponding to ferrous compounds (9–12 for the internal part and 9–11 for the external part) and to ferric compounds (13 for the internal part and 12 and 13 for the external part). It is possible that ferrous compounds can be attributed to some silicate crystals and other undetermined compounds. The ferric compounds have ^{57}Fe hyperfine parameters similar to some ferric oxides and oxyhydroxides as well as, probably, phyllosilicates. It is possible that the presence of ferric compounds in the internal part of the Isheyevo fragment can be related to hydration processes at the early stage of carbonaceous chondrites formation while those in the external part can also be a result of terrestrial weathering. The total relative areas of the magnetic sextets are the following: $A_{tot}{}^{mag}$ = 91.8% for the internal part and $A_{tot}{}^{mag}$ = 86.3% for the external part while those for ferric compounds are: $A_{tot}{}^{Fe3+}$ = 2.2% for the internal part and $A_{tot}{}^{Fe3+}$ = 8.6% for the external part. These results may indicate the presence of terrestrial weathering of Fe-Ni-Co alloy.

4.4. Ordinary Chondrites

Ordinary chondrites usually contain up to 19 wt.% of Fe-Ni-Co alloy (for the H group). However, some ordinary chondrites demonstrate higher metal contents than those known for the corresponding ordinary chondrite groups. Annama H5 [35] and Bursa L6 [36] are examples of metal alloy excess. SEM images of Annama H5 and Bursa L6 are shown in Figure 15a,c, respectively, with variations in the concentrations of Fe, Ni and Co along the chosen **A–A′** lines. An analysis of chemical compositions of the selected metal grains in both ordinary chondrites showed the ranges of Ni contents which could be assigned to the following phases: α_2-Fe(Ni, Co), α-Fe(Ni, Co), γ-Fe(Ni, Co), γ-FeNi(Co) and paramagnetic γ-Fe(Ni, Co) as shown in Table 6. The content of Co varied in the range of ~1.0–0.2 at.% for all phases in both meteorites. Variations in the Fe and Ni contents within one phase were observed (see also Figure 15b,d).

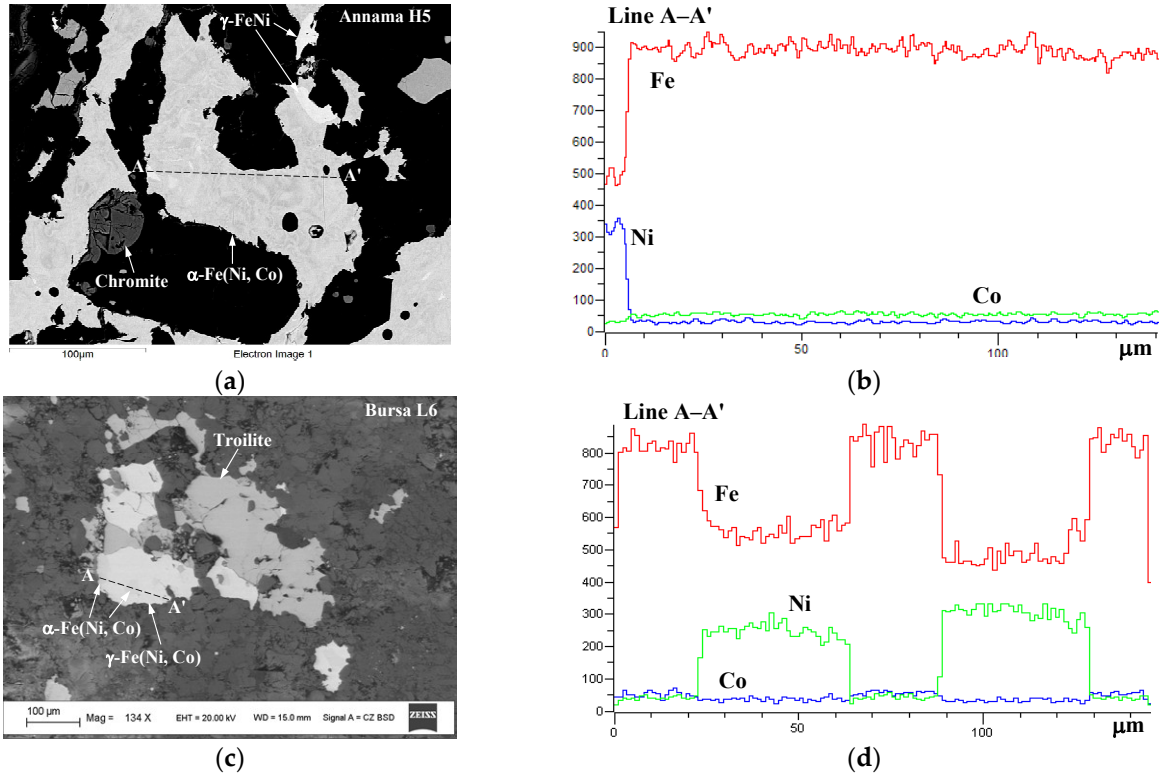

Figure 15. Scanning electron microscopy images of polished sections of Annama H5 (**a**) and Bursa L6 (**c**) polished sections with indicated selected phases and variations of Fe, Ni and Co concentrations along the **A–A′** lines obtained using energy dispersive spectroscopy for Annama H5 (**b**) and Bursa L6 (**d**); (**c**,**d**) were adapted from Ref. [36].

Table 6. Ni concentrations in the metal grains and related phases in Annama H5 and Bursa L6 ordinary chondrites (data were taken from Refs. [35,36]).

Meteorite	Ni Concentration (at.%) in the Phases				
	α_2-Fe(Ni, Co)	α-Fe(Ni, Co)	γ-Fe(Ni, Co)	γ-FeNi(Co)	par. γ-Fe(Ni, Co) [1]
Annama H5	8.9	3.4–6.6	39.1–44.7	47.2–50.7	31.3–33.4
Bursa L6	17.0–18.9	3.3–6.8	34.6–46.3	47.0–55.3	28.9

[1] The paramagnetic γ-Fe(Ni, Co) phase.

The XRD patterns and Mössbauer spectra of Annama H5 and Bursa L6 are shown in Figure 16. XRD showed the presence of ~9.0 wt.% and ~7.7 wt.% of the α-Fe(Ni, Co) phase, and ~1.3 wt.% and ~0.6 wt.% of the γ-Fe(Ni, Co) phase in Annama and Bursa, respectively. The Mössbauer spectrum of Annama H5 demonstrates the presence of a very

high contribution of the magnetic six-line pattern related to various phases in Fe-Ni-Co alloy in comparison with other ordinary chondrites from the H group. The spectrum of Bursa L6 shows a smaller part of the magnetic six-line pattern associated with Fe-Ni-Co alloy compared to that for Annama H5; however, this contribution is larger than similar contributions in the spectra of other ordinary chondrites from the L group. Components related to the metallic phases in both spectra were fitted well using seven magnetic sextets and one paramagnetic singlet for Annama H5 and five magnetic sextets and one paramagnetic singlet for Bursa L6. All Mössbauer parameters are listed in Table 7. The total relative areas for Fe-Ni-Co alloy were ~53% for Annama H5 and ~31.6% for Bursa L6 (taking into account a part of the metal which was oxidized due to terrestrial weathering of the latter meteorite: XRD showed ~0.5 wt.% of ferrihydrite $5Fe_2O_3 \times 9H_2O$ in Bursa L6, the relative area of the corresponding component in the Mössbauer spectrum was ~1.3%).

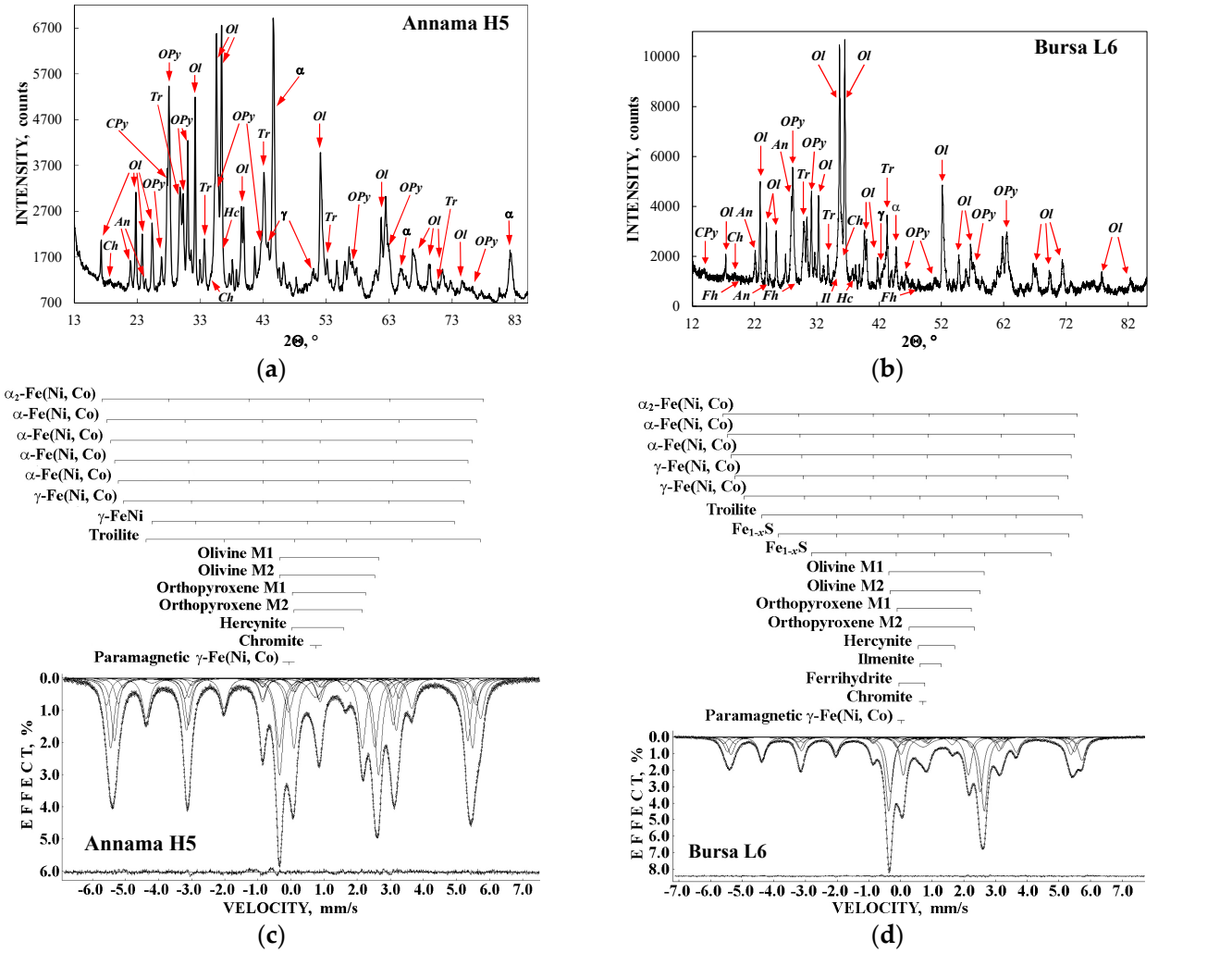

Figure 16. XRD patterns (**a**,**b**) and the room temperature Mössbauer spectra (**c**,**d**) of Annama H5 (**a**,**c**) and Bursa L6 (**b**,**d**). Indicated reflexes in the XRD patterns are: olivine (***Ol***), orthopyroxene (***OPy***), anorthite (***An***), Ca-rich clinopyroxene (***CPy***), α-Fe(Ni, Co) phase (**α**), troilite (***Tr***), γ-Fe(Ni, Co) phase (**γ**), chromite (***Ch***), hercynite (***Hc***), ilmenite (***Il***) and ferrihydrite (***Fh***). Indicated components in the Mössbauer spectra are the results of the best fits, the differential spectra are shown at the bottom. Adapted from Refs. [35,36].

Table 7. Mössbauer parameters for Annama H5 and Bursa L6 ordinary chondrites; components (phases) correspond to those shown in Figure 16c,d (data were taken from [35,36]).

Meteorite	Γ, mm/s	δ, mm/s	2ε/Δ, mm/s	H_{eff}, kOe	*A*, %	Phase/Compound
Annama H5	0.233 ± 0.014	−0.164 ± 0.009	0.420 ± 0.018	356.2 ± 0.7	0.7	α_2-Fe(Ni, Co)
	0.257 ± 0.014	0.022 ± 0.007	−0.012 ± 0.007	345.5 ± 0.5	10.2	α-Fe(Ni, Co)
	0.236 ± 0.014	0.015 ± 0.007	0.012 ± 0.007	338.2 ± 0.5	17.1	α-Fe(Ni, Co)
	0.233 ± 0.014	0.004 ± 0.007	0.015 ± 0.007	330.4 ± 0.5	15.1	α-Fe(Ni, Co)
	0.233 ± 0.014	0.055 ± 0.007	0.140 ± 0.009	328.0 ± 0.5	4.5	α-Fe(Ni, Co)
	0.233 ± 0.014	0.044 ± 0.007	0.131 ± 0.013	315.6 ± 0.6	1.1	γ-Fe(Ni, Co)
	0.401 ± 0.021	0.061 ± 0.008	0.606 ± 0.015	283.9 ± 0.7	2.1	γ-FeNi
	0.275 ± 0.014	0.762 ± 0.007	*Not determined* [1]	313.8 ± 0.5	11.4	Troilite
	0.260 ± 0.014	1.150 ± 0.007	2.992 ± 0.007	–	12.5	Olivine M1
	0.260 ± 0.014	1.093 ± 0.007	2.878 ± 0.007	–	8.8	Olivine M2
	0.260 ± 0.014	1.139 ± 0.007	2.200 ± 0.014	–	2.0	Orthopyroxene M1
	0.260 ± 0.014	1.121 ± 0.007	2.069 ± 0.007	–	8.7	Orthopyroxene M2
	0.260 ± 0.014	0.852 ± 0.007	1.465 ± 0.007	–	0.9	Hercynite
	0.498 ± 0.014	0.748 ± 0.007	–	–	2.4	Chromite
	0.307 ± 0.014	−0.068 ± 0.007	–	–	2.6	par. γ-Fe(Ni,Co) [2]
Bursa L6	0.258 ± 0.030	0.007 ± 0.015	−0.029 ± 0.015	347.4 ± 0.5	3.9	α_2-Fe(Ni, Co)
	0.258 ± 0.030	0.008 ± 0.015	0.007 ± 0.015	340.3 ± 0.5	8.7	α-Fe(Ni, Co)
	0.258 ± 0.030	0.006 ± 0.015	0.024 ± 0.015	333.8 ± 0.5	10.3	α-Fe(Ni, Co)
	0.258 ± 0.030	0.001 ± 0.015	0.066 ± 0.015	326.4 ± 0.5	4.0	γ-Fe(Ni, Co)
	0.258 ± 0.030	−0.072 ± 0.015	0.186 ± 0.015	308.0 ± 0.5	1.1	γ-Fe(Ni, Co)
	0.268 ± 0.030	0.752 ± 0.015	*Not determined* [1]	314.2 ± 0.5	13.7	Troilite
	0.442 ± 0.035	0.687 ± 0.015	0.086 ± 0.034	285.0 ± 1.5	1.7	$Fe_{1-x}S$
	0.261 [3]	0.716 ± 0.015	0.496 ± 0.016	234.9 ± 0.5	1.0	$Fe_{1-x}S$
	0.246 ± 0.030	1.134 ± 0.015	3.012 ± 0.015	–	19.8	Olivine M1
	0.246 ± 0.030	1.096 ± 0.015	2.834 ± 0.015	–	14.6	Olivine M2
	0.246 ± 0.030	1.065 ± 0.015	2.343 ± 0.015	–	2.9	Orthopyroxene M1
	0.246 ± 0.030	1.114 ± 0.015	2.053 ± 0.015	–	10.1	Orthopyroxene M2
	0.246 ± 0.030	1.137 ± 0.015	1.149 ± 0.015	–	0.8	Hercynite
	0.246 ± 0.030	0.949 ± 0.015	0.654 ± 0.026	–	0.5	Ilmenite
	0.234 [3]	0.358 ± 0.015	0.811 ± 0.015	–	1.3	Ferrihydrite

[1] See explanation in Section 5.2. [2] The paramagnetic γ-Fe(Ni, Co) phase. [3] Fixed parameter.

Another example is the Kemer L4 ordinary chondrite [37] which contains a lower amount of Fe-Ni-Co alloy than Bursa L6 but a larger one than that in other ordinary chondrites from the L group. The results of Kemer L4 studies by SEM with EDS, XRD and Mössbauer spectroscopy are shown in Figure 17. Chemical compositions of the selected metal grains in Kemer L4 showed the following phases (minerals) with the corresponding ranges of Ni contents: (i) 14.2 at.%, α_2-Fe(Ni, Co) (martensite), (ii) 3.9–7.4 at.%, α-Fe(Ni, Co) (kamacite), (iii) 41.1–41.8 at.%, γ-Fe(Ni, Co) (taenite), (iv) 53.7–54.0 at.%, γ-FeNi(Co) (tetrataenite), and (v) 29.4–30.5 at.%, paramagnetic γ-Fe(Ni, Co) (paramagnetic taenite). The content of Co varied in the range of ~1.1–0.2 at.% for all phases. There was a variation of Ni content within the one metal grain and within one phase as shown in Figure 17b. XRD indicated the presence of ~4.4 wt.% of the α-Fe(Ni, Co) phase and ~0.7 wt.% of the γ-Fe(Ni, Co) phase in Kemer L4, as well as ~0.5 wt.% of ferrihydrite resulting from terrestrial weathering. The result of the best fit of the Mössbauer spectrum of Kemer L4 is shown in Figure 17d and the parameters are listed in Table 8. Two magnetic sextets were assigned to the α-Fe(Ni, Co) phase and one magnetic sextet was related to the γ-Fe(Ni, Co) phase.

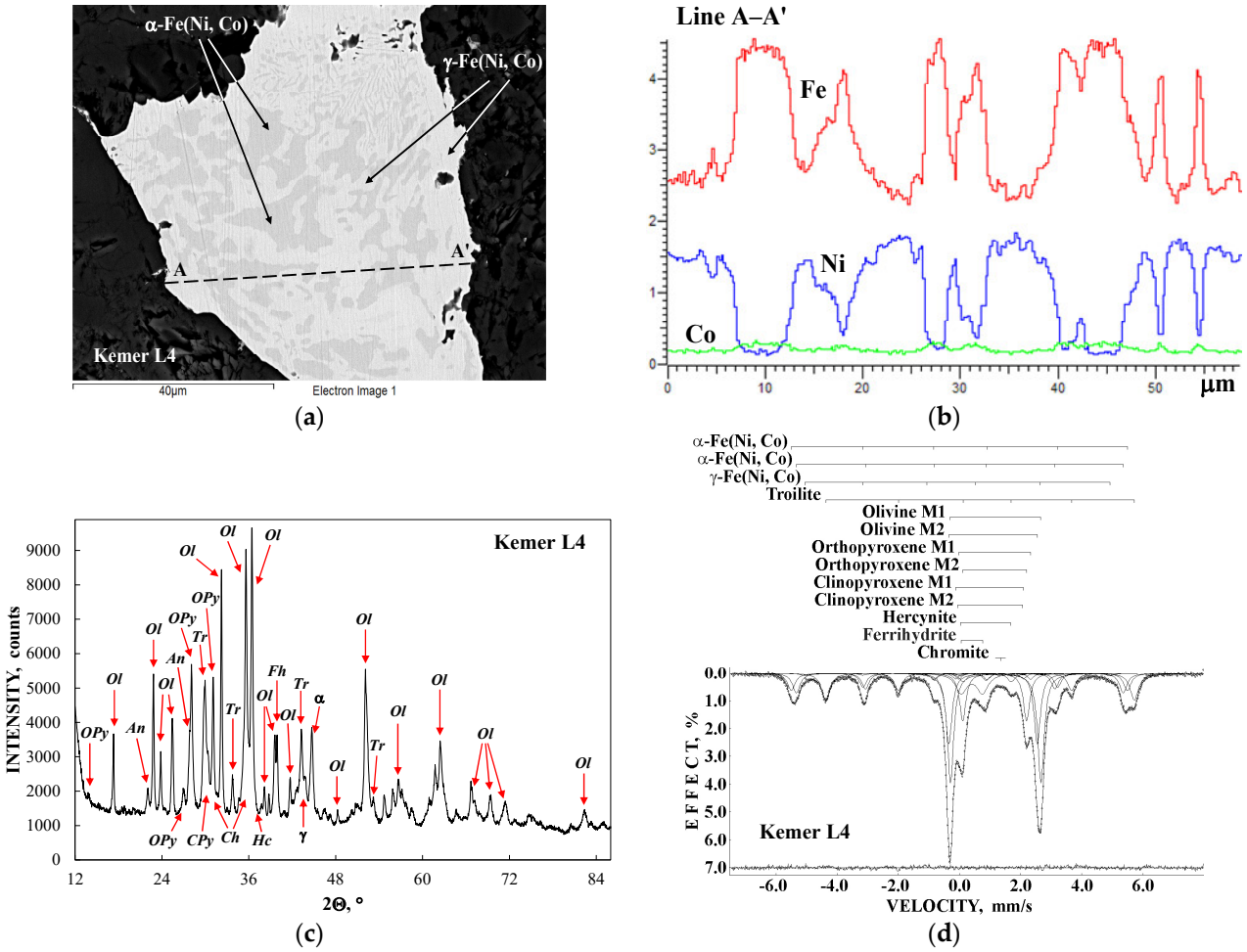

Figure 17. SEM image of Kemer L4 polished section with indicated selected α- and γ-phases (**a**) and variations of Fe, Ni and Co concentrations along the line **A–A′** obtained using EDS (**b**), XRD pattern of Kemer L4 with indicated reflexes of olivine (***Ol***), orthopyroxene (***OPy***), anorthite (***An***), Ca-rich clinopyroxene (***CPy***), α-Fe(Ni, Co) phase (**α**), troilite (***Tr***), γ-Fe(Ni, Co) phase (**γ**), chromite (***Ch***), hercynite (***Hc***) and ferrihydrite (***Fh***) (**c**) and room temperature Mössbauer spectrum of Kemer L4, indicated components are the result of the best fit, the differential spectrum is shown at the bottom (**d**). Adapted from Ref. [37].

Table 8. Mössbauer parameters for Kemer L4 ordinary chondrite; components (phases) correspond to those shown in Figure 17d (data were taken from [37]).

Γ, mm/s	δ, mm/s	2ε/Δ, mm/s	H_{eff}, kOe	*A*, %	Phase/Compound
0.296 ± 0.030	0.013 ± 0.015	−0.037 ± 0.015	341.4 ± 0.5	9.7	α-Fe(Ni, Co)
0.296 ± 0.030	0.017 ± 0.015	−0.013 ± 0.015	332.1 ± 0.5	10.9	α-Fe(Ni, Co)
0.354 ± 0.042	−0.169 ± 0.015	0.203 ± 0.031	310.0 ± 0.9	1.7	γ-Fe(Ni, Co)
0.327 ± 0.030	0.763 ± 0.015	*Not determined* [1]	313.4 ± 0.5	15.0	Troilite
0.251 ± 0.030	1.186 ± 0.015	2.961 ± 0.015	–	24.4	Olivine M1
0.251 ± 0.030	1.098 ± 0.015	2.892 ± 0.015	–	15.8	Olivine M2
0.251 ± 0.030	1.152 ± 0.018	2.346 ± 0.015	–	1.4	Orthopyroxene M1
0.251 ± 0.030	1.151 ± 0.015	2.089 ± 0.015	–	10.6	Orthopyroxene M2
0.251 ± 0.030	0.982 ± 0.016	2.215 ± 0.034	–	1.3	Clinopyroxene M1
0.251 ± 0.030	1.004 ± 0.052	2.121 ± 0.118	–	0.4	Clinopyroxene M2
0.251 ± 0.030	0.855 ± 0.039	1.645 ± 0.106	–	0.7	Hercynite
0.442 ± 0.030	0.406 ± 0.015	0.696 ± 0.019	–	7.6	Ferrihydrite
0.444 ± 0.079	1.361 ± 0.027	–	–	0.5	Chromite

[1] See explanation in Section 5.2.

The total relative area of spectral components assigned to the metallic phases is ~22.3% and the relative area of the ferrihydrite subspectrum is ~7.6%. Considering the ferrihydrite formation as a result of Fe-Ni-Co alloy oxidation due to terrestrial weathering, the initial Fe-Ni-Co alloy total relative area for Kemer L4 can be roughly estimated as ~29.9% which is slightly smaller than that for Bursa L6. In contrast, the two or three magnetic sextets and sometimes paramagnetic singlet assigned to Fe-Ni-Co alloy with substantially smaller total relative area were observed in the Mössbauer spectra of other ordinary chondrites measured with a high velocity resolution. Figure 18 shows the Mössbauer spectra of the Ozerki L6 [38] and Bjurböle L/LL4 [39] ordinary chondrites.

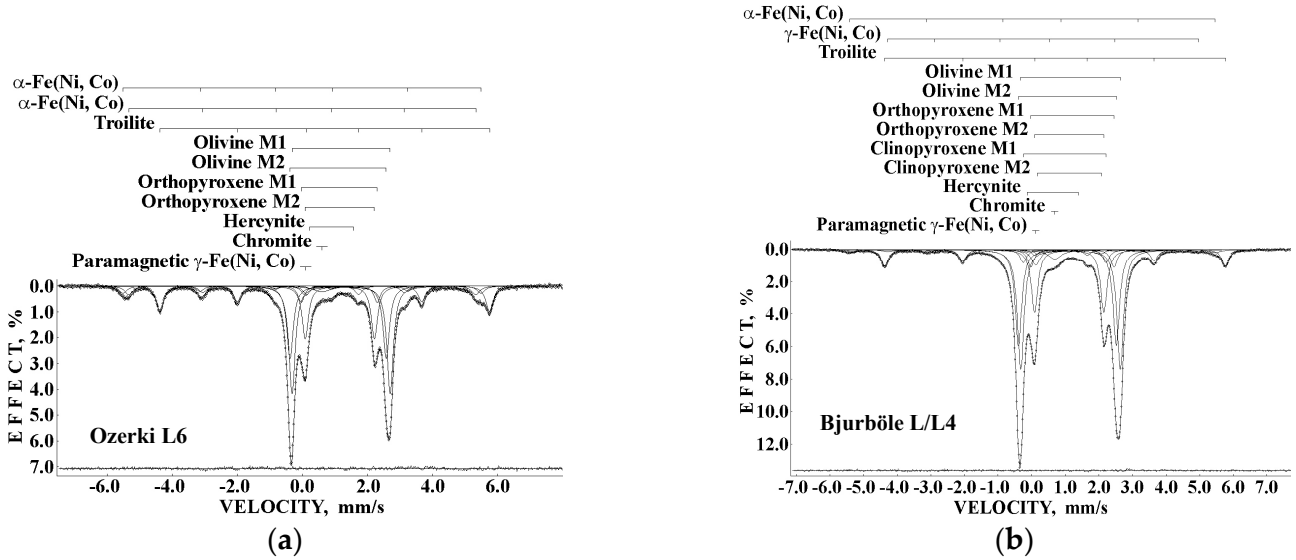

Figure 18. Room temperature Mössbauer spectra of Ozerki L6 (**a**) and Bjurböle L/LL4 (**b**). Indicated components are the results of the best fits. The differential spectra are shown at the bottom. Adapted from Refs. [38,40].

Selected Mössbauer parameters of spectral components assigned to Fe-Ni-Co alloy and ferric compounds resulting from terrestrial weathering of metallic phases obtained for the ordinary chondrites Vengerovo H5, Zvonkov H6, Richardton H5, Mount Tazerzait L5, Kunashak L6 [40], Tsarev L5 (fragment No 2) [41], Ozerki L6 [38], Bjurböle L/L4 [39], Northwest Africa (NWA) 6286 LL6 [42], and Chelyabinsk LL5 (fragment No 2) [43] are listed in Table 9.

For the H ordinary chondrites mentioned in Table 9, the initial total relative areas for Fe-Ni-Co alloy spectral components are the following: ~19% (Vengerovo H5), ~20.3% (Zvonkov H6) and ~13.2% (Richardton H5) that is substantially smaller than that for Annama H5 (~53%). The initial total relative areas of the spectral components for Fe-Ni-Co alloy for the L ordinary chondrites presented in Table 9 were the following: ~10.7% (Mount Tazerzait L5), ~11.2% (Kunashak L6), ~14.2% (Tsarev L5 No 2), ~13.0% (Ozerki L6) and ~7.2% (Bjurböle L/LL4) that is smaller than those for Bursa L6 (~31.6%) and Kemer L4 (~29.9%). As for the LL ordinary chondrites studied herein, the Mössbauer spectrum of Chelyabinsk LL5 fragment No 2 demonstrated the total relative area for Fe-Ni-Co alloy of ~10.2% which is larger than that obtained for the other studied samples (e.g., 6.4% for NWA 6286 LL6).

Table 9. Mössbauer parameters for spectral components assigned to Fe-Ni-Co alloy and ferric compounds in selected ordinary chondrites (data were taken from Refs. [38–43]).

Meteorite	Γ, mm/s	δ, mm/s	2ε/Δ, mm/s	H_{eff}, kOe	*A*, %	Phase/Compound
Vengerovo	0.300 ± 0.028	0.031 ± 0.014	−0.097 ± 0.014	342.3 ± 0.8	4.5	α-Fe(Ni,Co)
H5	0.300 ± 0.028	0.021 ± 0.014	−0.038 ± 0.014	334.4 ± 0.5	7.2	α-Fe(Ni,Co)
	0.300 ± 0.028	−0.134 ± 0.014	0.226 ± 0.023	319.9 ± 0.8	2.1	γ-Fe(Ni,Co)
	0.444 [1]	0.402 ± 0.014	0.764 ± 0.024	–	5.1	Fe^{3+}
Zvonkov H6	0.300 ± 0.028	0.036 ± 0.014	−0.066 ± 0.014	342.4 ± 0.5	7.1	α-Fe(Ni,Co)
	0.300 ± 0.028	0.031 ± 0.014	−0.022 ± 0.014	333.1 ± 0.5	8.0	α-Fe(Ni,Co)
	0.300 ± 0.028	−0.099 ± 0.014	0.251 ± 0.022	320.4 ± 0.8	1.7	γ-Fe(Ni,Co)
	0.575 [1]	0.396 ± 0.024	0.788 ± 0.044	–	3.5	Fe^{3+}
Richardton	0.300 ± 0.028	0.029 ± 0.014	−0.122 ± 0.019	342.8 ± 0.6	2.9	α-Fe(Ni,Co)
H5	0.300 ± 0.028	0.019 ± 0.014	−0.010 ± 0.014	336.1 ± 1.1	4.0	α-Fe(Ni,Co)
	0.300 ± 0.028	0.033 ± 0.014	−0.095 ± 0.017	327.7 ± 0.7	2.5	α-Fe(Ni,Co)
	0.440 [1]	0.347 ± 0.028	0.733 ± 0.017	–	3.9	Fe^{3+}
Mount	0.294 ± 0.028	0.110 ± 0.014	−0.349 ± 0.028	348.7 ± 1.0	1.0	α_2-Fe(Ni,Co)
Tazerzait L5	0.294 ± 0.028	0.038 ± 0.014	−0.079 ± 0.014	340.4 ± 0.5	3.1	α-Fe(Ni,Co)
	0.294 ± 0.028	−0.151 ± 0.014	0.267 ± 0.014	324.0 ± 0.5	1.8	γ-Fe(Ni,Co)
	0.523 ± 0.028	0.316 ± 0.014	0.877 ± 0.015	–	4.9	Fe^{3+}
Kunashak L6	0.300 ± 0.028	0.055 ± 0.014	−0.111 ± 0.014	348.9 ± 0.6	3.2	α_2-Fe(Ni,Co)
	0.300 ± 0.028	0.042 ± 0.014	−0.027 ± 0.014	337.3 ± 0.5	4.4	α-Fe(Ni,Co)
	0.300 ± 0.028	−0.123 ± 0.014	0.303 ± 0.021	325.4 ± 0.7	1.9	γ-Fe(Ni,Co)
	0.360 [1]	0.480 ± 0.028	0.658 ± 0.053	–	1.7	Fe^{3+}
Tsarev L5	0.254 [1]	−0.013 ± 0.015	−0.029 ± 0.024	340.0 ± 0.8	0.9	α-Fe(Ni,Co)
(No 2)	0.387 ± 0.053	−0.237 ± 0.020	0.216 ± 0.042	307.6 ± 1.0	1.2	γ-Fe(Ni,Co)
	0.452 ± 0.030	0.335 ± 0.015	0.577 ± 0.015	–	12.2	Fe^{3+}
Ozerki L6	0.296 ± 0.030	0.018 ± 0.015	−0.060 ± 0.015	341.5 ± 0.5	5.1	α-Fe(Ni,Co)
	0.296 ± 0.030	0.014 ± 0.015	−0.039 ± 0.015	331.0 ± 0.5	6.3	α-Fe(Ni,Co)
	0.296 [1]	0.102 ± 0.015	–	–	1.7	par. γ-Fe(Ni,Co) [2]
Bjurböle	0.403 ± 0.029	0.015 ± 0.014	0.006 ± 0.014	337.4 ± 0.5	2.8	α-Fe(Ni,Co)
L/LL4	0.403 ± 0.029	0.067 ± 0.014	0.550 ± 0.026	287.0 ± 0.9	1.7	γ-Fe(Ni,Co)
	0.313 ± 0.029	0.124 ± 0.014	–	–	2.7	par. γ-Fe(Ni,Co) [2]
NWA 6286	0.240 ± 0.028	0.288 ± 0.014	−0.241 ± 0.018	347.9 ± 0.6	1.0	α_2-Fe(Ni,Co)
LL6	0.401 ± 0.032	−0.154 ± 0.014	0.086 ± 0.021	304.6 ± 0.6	1.8	γ-Fe(Ni,Co)
	0.346 ± 0.029	−0.086 ± 0.014	0.376 ± 0.020	293.8 ± 0.5	1.9	γ-Fe(Ni,Co)
	0.248 ± 0.028	0.035 ± 0.014	–	–	1.7	par. γ-Fe(Ni,Co) [2]
Chelyabinsk	0.240 ± 0.087	−0.096 ± 0.025	−0.220 ± 0.050	341.2 ± 1.3	0.9	α-Fe(Ni,Co)
LL5 (No 2)	0.467 ± 0.033	0.024 ± 0.017	−0.003 ± 0.021	336.5 ± 0.5	6.4	α-Fe(Ni,Co)
	0.372 ± 0.033	−0.029 ± 0.017	0.155 ± 0.029	304.6 ± 1.0	2.3	γ-Fe(Ni,Co)
	0.233 ± 0.017	−0.191 ± 0.043	–	–	0.6	par. γ-Fe(Ni,Co) [2]

[1] Fixed parameter. [2] The paramagnetic γ-Fe(Ni, Co) phase.

These results show that in the case of ordinary chondrites when the Fe-Ni-Co alloy content is relatively small in comparison with other iron-bearing phases/minerals, it is not easy to extract the real number of magnetic sextets from the Mössbauer spectra like it was done for iron and stony-iron meteorites. However, to study Fe-Ni-Co alloy in ordinary chondrites deeply, an extracting of the metal grains, e.g., by magnetic separation, should be used. The study of magnetically separated Fe-Ni-Co grains from Tsarev L5 (fragment No 1) was carried out by Mössbauer spectroscopy in [44,45]. The measured room temperature Mössbauer spectrum of metal grains separate measured in 4096 channels and converted into the 1024-channel spectrum was refitted in the present work, based on our experience with the study of Fe-Ni-Co alloys in meteorites mentioned above. We included control of the fitting quality with the differential spectra and used equal Γ values for the sextets which were varied during the fits. The new result is shown in Figure 19 in comparison with the spectrum of bulk Tsarev L5 (No 1) parameters of which were obtained in [40]. New parameters are shown in Table 10.

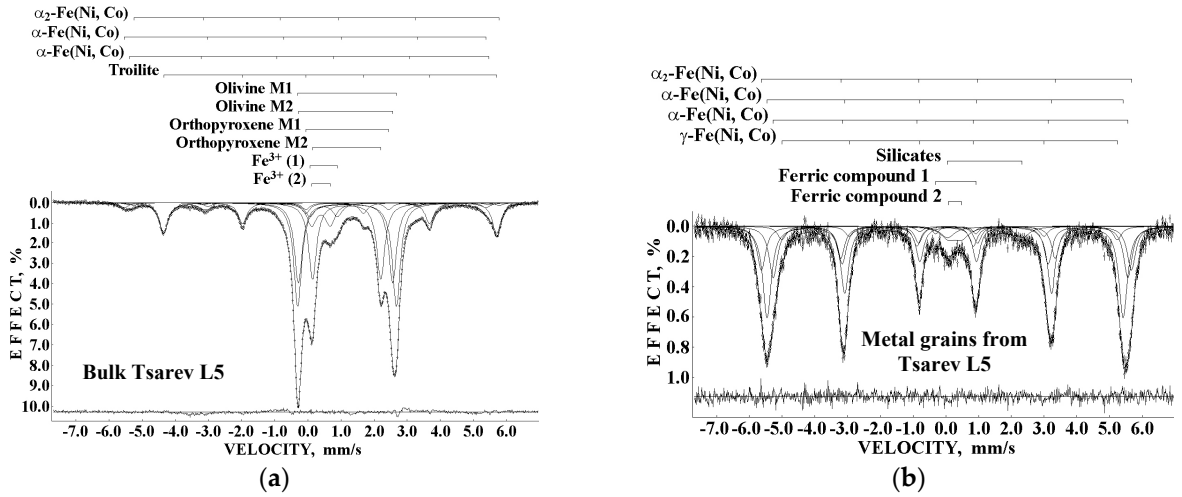

Figure 19. Room temperature Mössbauer spectra of the bulk Tsarev L5 No 1 ordinary chondrite (**a**) and separated metal grains from Tsarev L5 No 1 (**b**). Indicated components are the results of the best fits. The differential spectra are shown at the bottom.

Table 10. Mössbauer parameters for the metal grains extracted from the fragment No 1 of Tsarev L5 ordinary chondrite.

Γ, mm/s	δ, mm/s	2ε/Δ, mm/s	H_{eff}, kOe	*A*, %	Phase/Compound
0.313 ± 0.028	0.044 ± 0.014	−0.052 ± 0.014	351.6 ± 0.6	19.8	α_2-Fe(Ni,Co)
0.313 ± 0.028	0.025 ± 0.014	−0.095 ± 0.014	337.9 ± 0.5	41.2	α-Fe(Ni,Co)
0.313 ± 0.028	0.063 ± 0.014	0.164 ± 0.014	336.6 ± 0.6	23.2	α-Fe(Ni,Co)
0.313 ± 0.028	0.069 ± 0.014	0.097 ± 0.021	318.4 ± 1.1	6.1	γ-Fe(Ni,Co)
0.529 ± 0.078	1.191 ± 0.139	2.277 ± 0.275	–	4.3	Silicates
0.233 ± 0.096	0.302 ± 0.020	1.228 ± 0.042	–	4.2	Fe^{3+} (1)
0.545 ± 0.145	0.275 ± 0.143	0.404 ± 0.293	–	1.7	Fe^{3+} (2)

The spectrum of the separated metal grains has a small absorption effect and high noise because the grains were of different sizes. This is why, when the thin absorber thickness was retained, the sample was not homogeneous after the gluing of grains on the Al foil. The high noise and insufficient signal-to-noise ratio for the minor components were the reasons for the large errors calculated for the minor components. The hyperfine parameters for residual silicate phases corresponded to orthopyroxene. However, the broad line width for this component with a smaller relative area may be a result of the averaging minor contributions from the residual olivine and orthopyroxene contents.

The Mössbauer spectra of the extraterrestrial Fe-Ni-Co alloy from various meteorites (iron, stony-iron and stony) demonstrate an asymmetric six-line pattern with broadened lines while the spectrum of the reference thin α-Fe foil is a symmetrical sextet with narrow lines. Therefore, the meteoritical Fe-Ni-Co alloy Mössbauer spectra measured with a high velocity resolution were fitted well using a superposition of several magnetic sextets and sometimes with a small paramagnetic singlet. These spectral components were assigned to different metal phases (minerals) as well as to variations in Ni content within one phase. Taking into consideration the results of [46] and our data we can suppose that magnetic sextets with: (i) H_{eff} > ~345 kOe are related to the α_2-Fe(Ni, Co) phase (martensite), (ii) ~327 kOe < H_{eff} < ~345 kOe are attributed to the α-Fe(Ni, Co) phase (kamacite), (iii) ~283 kOe < H_{eff} < ~327 kOe are associated with the γ-Fe(Ni, Co) phase (taenite) with the values of H_{eff} < ~290 kOe which may also be assigned to the γ-FeNi(Co) phase (tetrataenite). The values of δ for the paramagnetic γ-Fe(Ni, Co) phase (paramagnetic taenite) are in the range from ~−0.20 mm/s to ~0.15 mm/s.

5. Iron-Bearing Minerals in Meteorites

Different meteorites contain various contents of iron-bearing minerals such as olivine, orthopyroxene and clinopyroxene (silicate crystals), stoichiometric troilite and pyrrhotite (probably nonstoichiometric troilite with $x \leq 0.05$), chromite, hercynite, ilmenite, schreibersite and its prismatic idiomorphic microcrystals called rhabdites, daubréelite, etc. besides Fe-Ni-Co alloy.

5.1. Silicate Crystals

Olivine, orthopyroxene and clinopyroxene are silicate crystals which can be found mainly in stony and stony-iron meteorites. These minerals contain two crystallographically nonequivalent M1 and M2 sites for Fe^{2+} and Mg^{2+} cations as shown in Figure 20. These sites are occupied by Fe^{2+} and Mg^{2+} cations in different ways: in olivine Fe^{2+} occupancies are slightly higher for the M1 sites while in orthopyroxene the M2 sites are the most preferable for Fe^{2+}. In the case of Ca-poor clinopyroxene, Fe^{2+} cations mainly occupy the M2 sites similarly to that in orthopyroxene. In contrast, in Ca-rich clinopyroxene Ca^{2+} cations occupy the larger M2 sites, therefore, the M1 sites occupations by Fe^{2+} are relatively higher. The variations in the M1 and M2 sites cation partitioning are related to the thermal history of silicate crystals, therefore, the distribution of Fe^{2+} among the M1 and M2 sites in silicates as well as its variations after thermal effects is of interest. Mössbauer spectroscopy is widely used to study various terrestrial (natural and synthetic) silicate crystals and demonstrates a superposition of two well-distinguished quadrupole doublets associated with ^{57}Fe in the M1 and M2 sites (see, e.g., [47–49]). However, in the case of ordinary chondrites, the spectra which consist of several magnetic sextets and paramagnetic quadrupole doublets and singlets, it is too difficult to distinguish spectral components which can be assigned to the M1 and M2 sites in corresponding silicate crystals due to the overlapping of these components. Nevertheless, the application of Mössbauer spectroscopy with a high velocity resolution allowed us to overcome this problem.

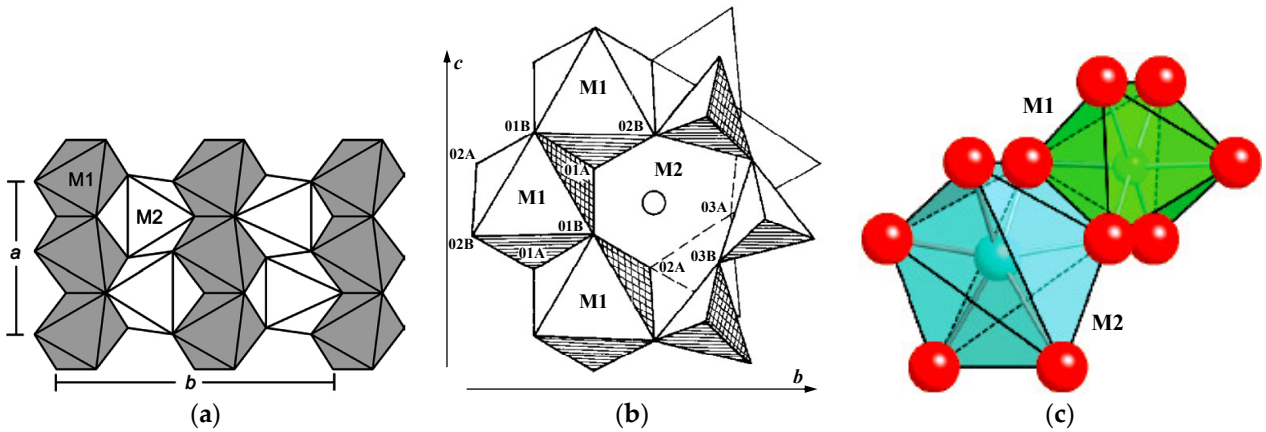

Figure 20. Two crystallographically non-equivalent M1 and M2 sites for Fe^{2+} and Mg^{2+} cations in olivine (**a**), orthopyroxene (**b**) and clinopyroxene (**c**). Adapted from Refs. [47–49].

Some Mössbauer spectra of ordinary chondrites shown in Figure 16c,d, Figure 17d, Figure 18a,b and Figure 19a demonstrate revealing of the spectral components associated with the M1 and M2 sites in olivine, orthopyroxene and clinopyroxene (if the content of the latter silicate is more than ~4 wt.%). Similar results were obtained in the studies of (i) Sariçiçek howardite (there is not olivine) [50] and (ii) the stony part of Seymchan PMG (there is not orthopyroxene) [32]. The XRD patterns and the room temperature Mössbauer spectra of Sariçiçek howardite and the stony part of Seymchan PMG are shown in Figure 21. XRD analysis demonstrated the presence of (i) ~37.6 wt.% of orthopyroxene, ~23.9 wt.% of Ca-poor clinopyroxene and ~12.3 wt.% of Ca-rich clinopyroxene in Sariçiçek

and (ii) ~95.5 wt.% of olivine and ~2.3 wt.% of Ca-rich clinopyroxene in the stony part of Seymchan.

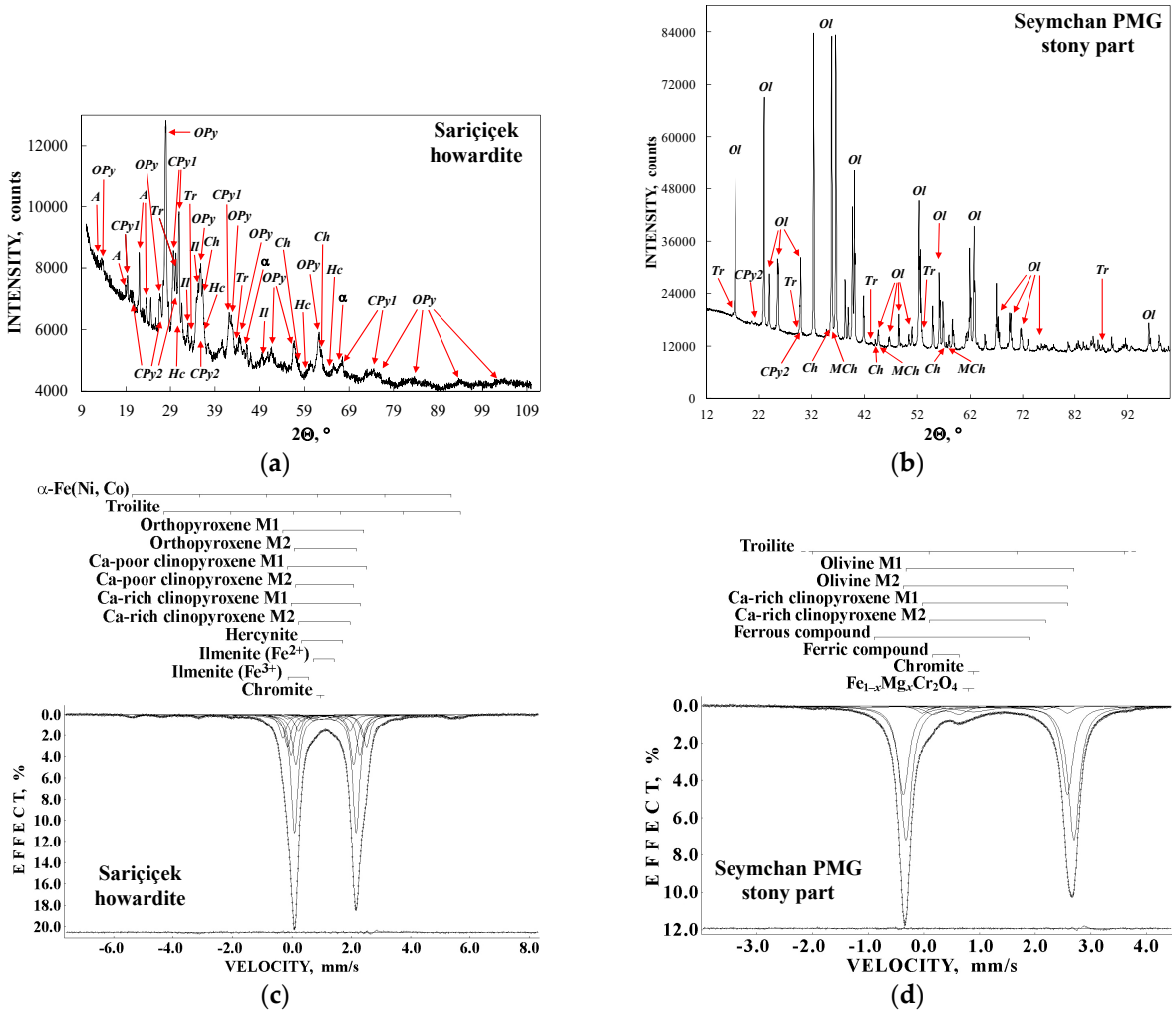

Figure 21. XRD patterns (**a**,**b**) and the room temperature Mössbauer spectra (**c**,**d**) of Sariçiçek howardite (**a**,**c**) and the stony part of Seymchan PMG (**b**,**d**). Indicated reflexes in the XRD patterns are: olivine (***Ol***), orthopyroxene (***OPy***), anorthite (***A***), Ca-poor clinopyroxene (***CPy1***), Ca-rich clinopyroxene (***CPy2***), α-Fe(Ni, Co) phase (***α***), troilite (***Tr***), chromite (***Ch***), hercynite (***Hc***), ilmenite (***Il***) and magnesiochromite (***MCh***). Indicated components in the Mössbauer spectra are the results of the best fits, the differential spectra are shown at the bottom. Adapted from Refs. [32,50].

The best fits of the Mössbauer spectra of Sariçiçek howardite and the stony part of Seymchan PMG are shown in Figure 21c,d. It was possible to reveal spectral components associated with the M1 and M2 sites in orthopyroxene, Ca-poor and Ca-rich clinopyroxenes in the spectrum of Sariçiçek and in olivine and Ca-rich clinopyroxene in the spectrum of Seymchan PMG. Using the relative areas of spectral components assigned to the M1 and M2 sites in olivine, orthopyroxene and clinopyroxene for the studied ordinary chondrites, howardite and the stony part of the main group pallasite, the Fe^{2+} partitioning among these sites in different silicate crystals for various meteorites can be compared as shown in Figure 22. These results agree with well-known data for silicates structure and chemical composition indicating the slightly higher Fe^{2+} occupancies of the M1 sites in olivine, a significant preference in the Fe^{2+} occupancies of the M2 sites in orthopyroxene and M1 sites in Ca-rich clinopyroxene, while the larger Fe^{2+} occupancy of the M2 sites in Ca-poor clinopyroxene. Moreover, Figure 22 indicates some differences in the Fe^{2+} partitioning between two sites in each silicate crystal in various meteorites. The latter can be related to

the thermal history of silicate crystals and meteorites. Using these results, it is possible to estimate the distribution coefficient K_D ($K_D = ({X_{Fe}}^{M1} \times {X_{Mg}}^{M2})/({X_{Fe}}^{M2} \times {X_{Mg}}^{M1})$ where ${X_{Fe}}^{M1}$, ${X_{Mg}}^{M1}$, ${X_{Fe}}^{M2}$ and ${X_{Mg}}^{M2}$ are the Fe^{2+} and Mg^{2+} cations occupancies of the M1 and M2 sites in olivine and orthopyroxene) and then calculate the temperature of equilibrium cation distribution T_{eq} using the following equations: $\ln K_D = -\Delta G^{\circ}/(R \times T_{eq})$ for olivine and $\ln K_D = 0.391 - 2205/T_{eq}$ for orthopyroxene. This is described in detail in [51] and the references therein. The plots of $\ln K_D$ vs. $1/T_{eq}$ for these silicate crystals in stony and stony-iron meteorites as studied by Mössbauer spectroscopy with a high velocity resolution are shown in Figure 23.

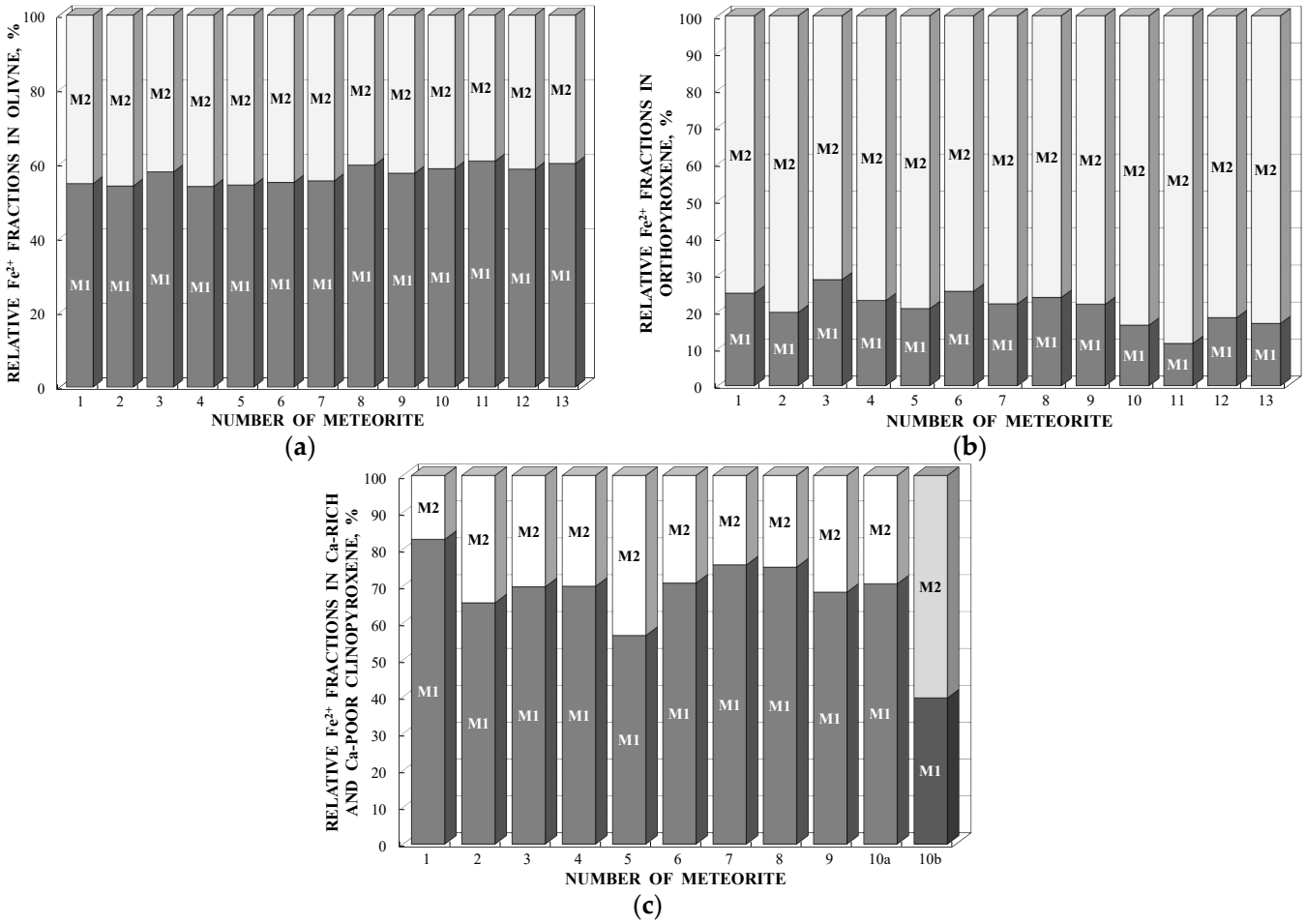

Figure 22. Relative Fe^{2+} fractions in the M1 (■) and M2 (□) sites in olivine (**a**) orthopyroxene (**b**) and clinopyroxene (**c**) obtained from the Mössbauer spectra of various meteorites. (**a**) 1—Chelyabinsk No 1a LL5, 2—Chelyabinsk No 2 LL5, 3—Chelyabinsk No 2a LL5, 4—Chelyabinsk No 3 LL5, 5—NWA 6286 LL6, 6—NWA 7857 LL6, 7—Bjurböle L/LL4, 8—Ozerki L6, 9—Bursa L6, 10—Tsarev L5 No 2, 11—Kemer L4, 12—Annama H5, 13—Seymchan PMG; (**b**) 1—Chelyabinsk No 1a LL5, 2—Chelyabinsk No 2 LL5, 3—Chelyabinsk No 2a LL5, 4—Chelyabinsk No 3 LL5, 5—NWA 6286 LL6, 6—NWA 7857 LL6, 7—Bjurböle L/LL4, 8—Ozerki L6, 9—Bursa L6, 10—Tsarev L5 No 2, 11—Kemer L4, 12—Annama H5, 13—Sariçiçek howardite; (**c**) Ca-rich clinopyroxene: 1—Chelyabinsk No 1a LL5, 2—Chelyabinsk No 2 LL5, 3—Chelyabinsk No 2a LL5, 4—Chelyabinsk No 3 LL5, 5—NWA 6286 LL6, 6—NWA 7857 LL6, 7—Bjurböle L/LL4, 8—Kemer L4, 9—Seymchan PMG, 10a—Sariçiçek howardite; Ca-poor clinopyroxene: 10b—Sariçiçek howardite. Data were taken from Refs. [32,35–39,42,43,50].

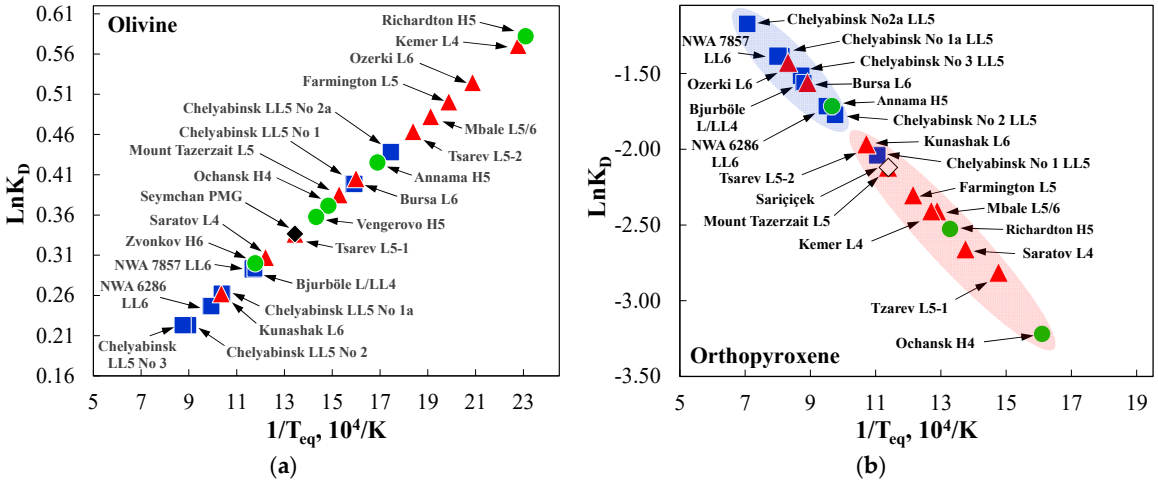

Figure 23. Plots of the natural logarithm of the distribution coefficient K_D vs. the reciprocal temperature of equilibrium cation distribution T_{eq} for olivine (**a**) and orthopyroxene (**b**) for the indicated meteorites. ●—H ordinary chondrites, ▲—L ordinary chondrites, ■—LL ordinary chondrites, ♦—main group pallasite, ◇—howardite. Blue and rose areas in (**b**) indicate a preference for the LL and L ordinary chondrites, respectively. Data were taken from Refs. [32,35–43,50], adapted from Ref. [51].

Different Fe^{2+} and Mg^{2+} partitioning among the M1 and M2 sites in silicate crystals as well as different contents of these cations in the same silicates in different meteorites may affect the local iron microenvironments and the ^{57}Fe hyperfine parameters. A comparison of Δ vs. δ for the M1 and M2 sites in olivine, orthopyroxene and clinopyroxene of the studied stony and stony-iron meteorites are shown in Figures 24 and 25. It can clearly be seen that there are several groups of the ^{57}Fe hyperfine parameters which are slightly different from the other groups beyond the indicated errors. This means that there are some variations in the local iron microenvironments in each site in olivine, orthopyroxene and clinopyroxene in the studied H, L and LL ordinary chondrites, the stony part of the main group pallasite and howardite. However, there is no relation to the type of meteorite. This may be a result of the silicate crystals formation and their further evolution and metamorphism in the parent bodies and meteorites.

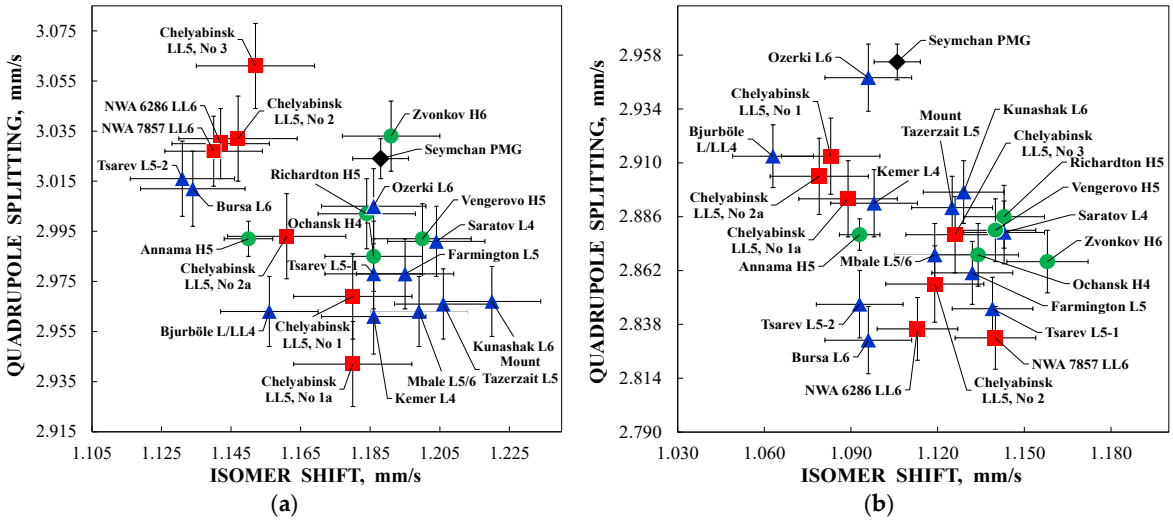

Figure 24. Comparison of the ^{57}Fe hyperfine parameters for the M1 (**a**) and M2 (**b**) sites in olivine for the indicated meteorites. ●—H ordinary chondrites, ▲—L ordinary chondrites, ■—LL ordinary chondrites, ♦—main group pallasite. Data were taken from Refs. [32,35–43].

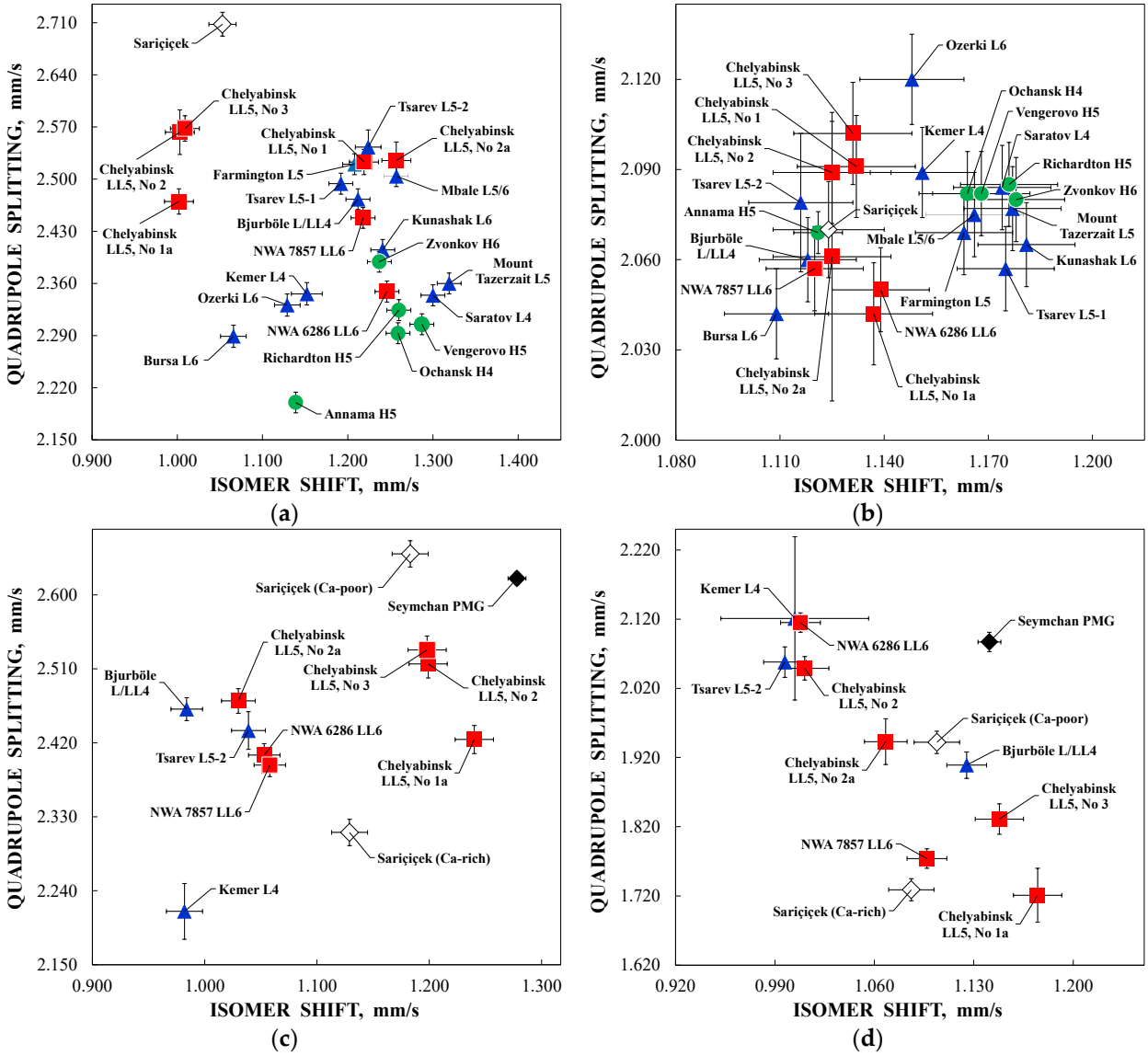

Figure 25. Comparison of the ^{57}Fe hyperfine parameters for the M1 (**a**,**c**) and M2 (**b**,**d**) sites in orthopyroxene (**a**,**b**) and clinopyroxene (**c**,**d**) for the indicated meteorites. ●—H ordinary chondrites, ▲—L ordinary chondrites, ■—LL ordinary chondrites, ♦—main group pallasite, ◇—howardite. Data were taken from Refs. [32,35–43,50].

5.2. Troilite and Daubréelite

Troilite inclusions can be found in various meteorites (iron, stony-iron and stony). The main feature of troilite with respect to Mössbauer spectroscopy is related to similar energies of the electric quadrupole interaction and the magnetic dipole interaction in contrast to, e.g., the Fe-Ni-Co alloy in which the former energy is substantially smaller than the latter. Therefore, the magnetic sextet in the Mössbauer spectrum of troilite should be fitted correctly using the full static Hamiltonian (see, e.g., [52]), while the magnetic sextet in the spectrum of the Fe-Ni-Co alloy can be fitted using the perturbation of the first order.

A detailed study of the troilite inclusion found in Sikhote-Alin IIAB iron meteorite using various techniques including Mössbauer spectroscopy with a high velocity resolution was carried out in [53]. The photograph of troilite inclusion and the SEM image of one particle of the extracted powdered troilite are shown in Figure 26a,b. EDS analysis of this troilite sample showed the presence of ~34 wt.% S, ~65 wt.% Fe and ~1 wt.% Cr. This indicates that there is a minor phase of daubréelite $FeCr_2S_4$ in addition to troilite. The XRD pattern of the troilite sample and the zero-field-cooled (ZFC) and field-cooled (FC)

magnetization curves of troilite are shown in Figure 26c,d. XRD demonstrated the presence of ~93 wt.% of FeS and ~7 wt.% of $FeCr_2S_4$. The crystal structures of troilite and daubréelite from the Sikhote-Alin IIAB iron meteorite were determined using XRD data and are shown in Figure 27. The unit cell parameters are the following: $a = b = 5.9696(8)$ Å, $c = 1.715(6)$ Å for troilite and $a = b = c = 9.98(5)$ Å for daubréelite. A degree of non-stoichiometry of troilite was determined by XRD as 0.0145–0.0148.

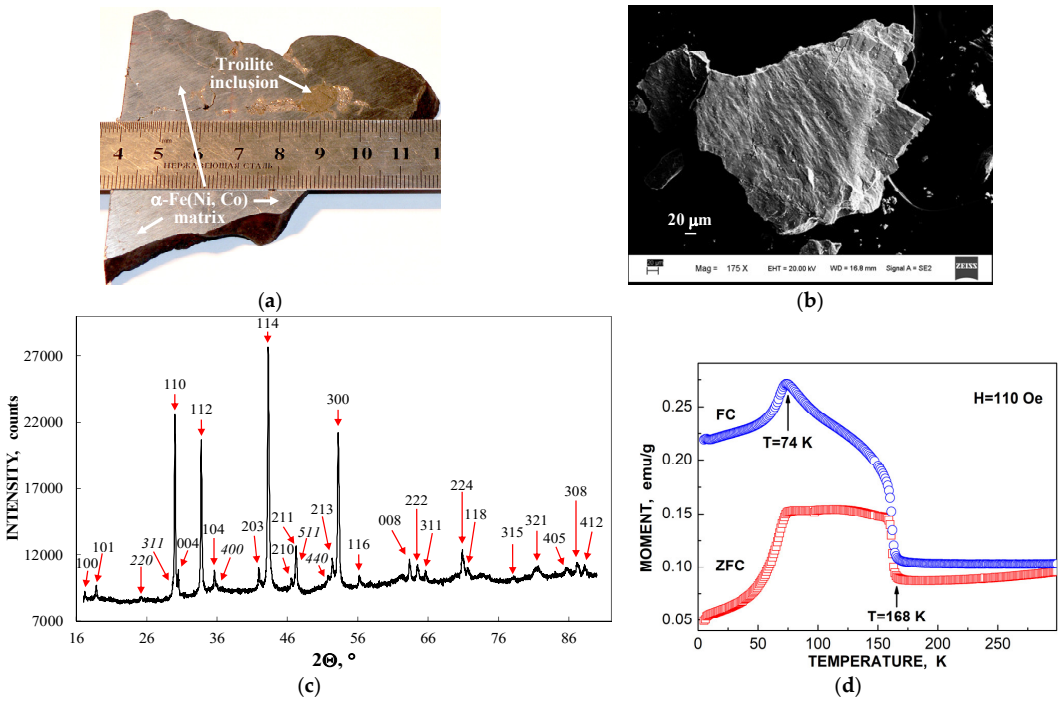

Figure 26. Massive troilite inclusion in the Sikhote-Alin IIAB iron meteorite (**a**), SEM image of the troilite particle (**b**), XRD pattern for troilite from the Sikhote-Alin IIAB iron meteorite, Miller indices in normal font indicate troilite reflections while those in Italic indicate daubréelite reflections (**c**) and zero-field-cooled (ZFC) and field-cooled (FC) magnetization curves of troilite (**d**). Adapted from Ref. [53].

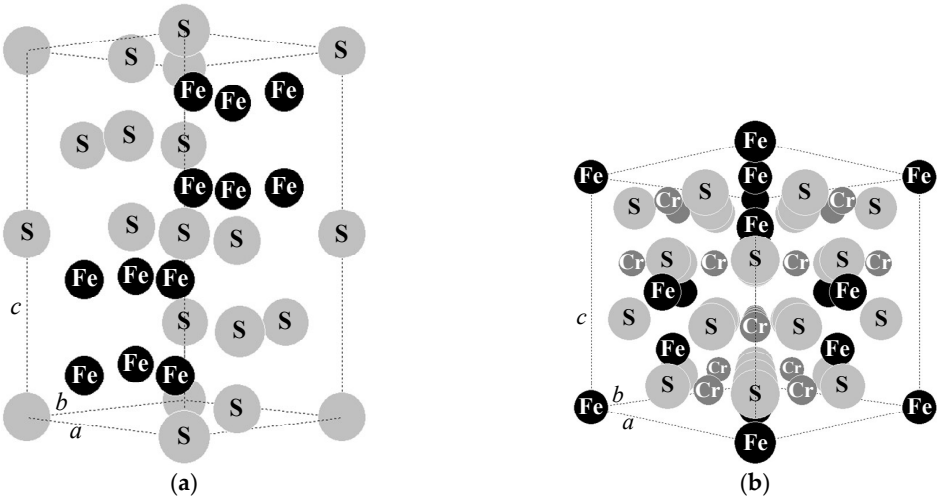

Figure 27. Crystal structures of troilite (**a**) and daubréelite (**b**) extracted from Sikhote-Alin IIAB iron meteorite and determined by XRD. The indicated atoms are: ●—Fe, ●—Cr and ●—S; *a*, *b* and *c* are the unit cell parameters. Adapted from Ref. [53].

The presence of daubréelite can be supported by the ZFC/FC curves in Figure 26d. There are two features at ~168 K and ~74 K. The antiferromagnetic ordering in FeS is well above room temperature with the Néel temperature of ~600 K [54]. Therefore, the observed features cannot be related to the phase transitions in troilite. The first feature indicates the magnetic phase transition for ferrimagnetic $FeCr_2S_4$ the Curie temperature of which is around 177 K [55]. The second feature was associated with the possible partial reorientation of the daubréelite ferrimagnetic structure at ~74 K. Therefore, the presence of minor daubréelite content in the troilite inclusion extracted from the Sikhote-Alin iron meteorite was confirmed by EDS, XRD and magnetization measurements.

The different fits of the room temperature Mössbauer spectrum of troilite extracted from the Sikhote-Alin IIAB iron meteorite are shown in Figure 28. The fit of the troilite magnetic sextet using the perturbation of the first order with the UNIVEM-MS program demonstrates significant misfits at the differential spectrum indicating an incorrect fit. Therefore, this spectrum was fitted using the full static Hamiltonian for the troilite magnetic sextet, the distribution of magnetic hyperfine field for the minor non-stoichiometric troilite and a singlet peak for daubréelite by MossWinn code (see [23]) in [53] with a good differential spectrum.

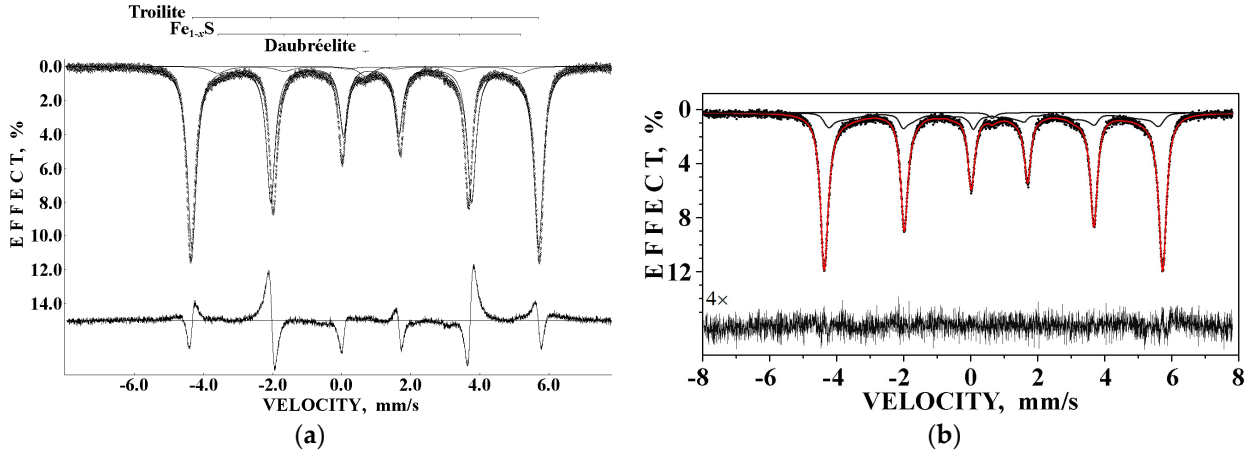

Figure 28. Room temperature Mössbauer spectrum of troilite extracted from the Sikhote-Alin IIAB iron meteorite with different fits: the fit of troilite and $Fe_{1-x}S$ sextets using the perturbation of the first order with the fit of daubréelite with a singlet (**a**) and the fit of troilite sextet using the full static Hamiltonian with the fit of non-stoichiometric troilite sextets using the distribution of hyperfine magnetic field and the fit of daubréelite with a single peak, adapted from [53] (**b**). The differential spectra are shown at the bottom.

A broad single peak in the room temperature Mössbauer spectrum of troilite extracted from the Sikhote-Alin IIAB iron meteorite with δ ~ 0.65 mm/s and A ~ 2.5% was assigned to daubréelite. However, at 90 K this peak disappeared due to the ferrimagnetic phase transition at ~177 K and smaller peak intensities in the six-line pattern which could not be revealed well from the spectrum noise. The fit of the troilite sextet in the complex Mössbauer spectra of ordinary chondrites was very difficult. The successful results of such fits of the room temperature Mössbauer spectra of Farmington L5, Tsarev L5 and Chelyabinsk LL5 using MossWinn code were presented in [56]. The Mössbauer parameters for the troilite magnetic sextet for that extracted from the Sikhote-Alin IIAB iron meteorite and these three ordinary chondrites obtained by the fits with MossWinn code and application of the full static Hamiltonian are shown in Table 11. Some variations of the Mössbauer parameters for troilite in different meteorites beyond the errors can be clearly seen indicating some variations in the FeS structure. For example, the troilite electric field gradient (EFG) varies from -4.66×10^{-21} V/m^2 for Chelyabinsk LL5 to -5.02×10^{-21} V/m^2 for Sikhote-Alin IIAB. However, all other Mössbauer spectra of ordinary chondrites were not fitted using the

full static Hamiltonian for troilite sextet due to the absence of convergence. To overcome this problem a simple method for the full static Hamiltonian simulation was supposed, and the results demonstrated good consistency with the cases in which the full static Hamiltonian was used [57,58]. This simulation is demonstrated in Figure 29 for the Mössbauer spectrum of troilite extracted from Sikhote-Alin IIAB. In this case it is not possible to estimate the ε values but it is possible to roughly estimate the δ and H_{eff} values. The results of the fits of Mössbauer spectra of various ordinary chondrites and howardite using a simulation of the full static Hamiltonian for the troilite sextet are shown in Figure 16c,d, Figure 17d, Figure 18a,b and Figure 19a. The quality of these spectra fits was substantially improved using this simulation.

Table 11. Mössbauer parameters for troilite obtained by the fits with the full static Hamiltonian for some meteorites using MossWinn code (data were taken from [53,56]).

Parameter [1]	Troilite in Meteorite			
	Sikhote-Alin IIAB	**Farmington L5**	**Tsarev L5**	**Chelyabinsk LL5**
δ, mm/s	0.766 ± 0.004	0.768 ± 0.007	0.766 ± 0.009	0.766 ± 0.016
H_{eff}, kOe	310.0 ± 0.2	308.6 ± 0.2	310.4 ± 0.3	309.8 ± 0.5
V_{zz}, 10^{21} × V/m^2	−5.02 ± 0.04	−4.85 ± 0.03	−4.68 ± 0.05	−4.66 ± 0.04
η	0.3 [2]	0.3 [2]	0.3 [2]	0.3 [2]
β, °	45.6 ± 0.3	45.3 [2]	45.3 [2]	45.3 [2]
α, °	51.1 ± 2.1	53.7 [2]	53.7 [2]	53.7 [2]
Γ, mm/s	0.259 ± 0.008	0.30 ± 0.02	0.26 ± 0.02	0.25 ± 0.03
Δ, mm/s	−0.85 ± 0.01	−0.82 ± 0.01	−0.79 ± 0.01	−0.79 ± 0.02
S_0, mm/s	2.08 ± 0.02	2.01 ± 0.01	1.94 ± 0.02	1.93 ± 0.02
S_1, mm/s	−0.36 ± 0.02	−0.355 ± 0.002	−0.342 ± 0.003	−0.340 ± 0.003
S_2, mm/s	1.34 ± 0.02	1.31 ± 0.01	1.26 ± 0.01	1.25 ± 0.01

[1] V_{zz} is electric field gradient (EFG), η is the asymmetry parameter, β and α are the polar and azimuthal angles of the hyperfine magnetic field in the eigensystem of the EFG, and S_0, S_1 and S_2 are invariants. [2] Fixed parameter.

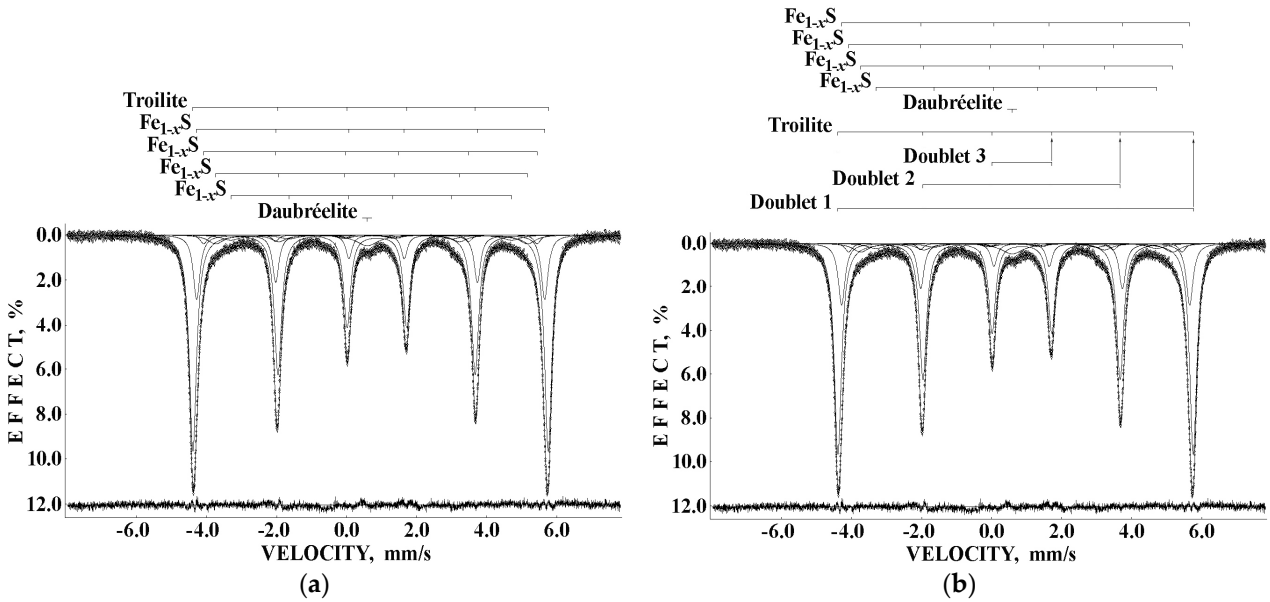

Figure 29. Room temperature Mössbauer spectrum of troilite extracted form Sikhote-Alin iron meteorite with the fit of troilite sextet using the simulation of the full static Hamiltonian (**a**) and its explanation, i.e., the substitution of troilite sextet by three doublets (**b**). The differential spectra are shown at the bottom.

The values of H_{eff} for troilite obtained using the full static Hamiltonian (see Table 11) demonstrate some small variations beyond the errors: from 308.6 kOe to 310.4 kOe. These

small differences in the magnetic hyperfine field may be related to the variations in the number of Fe vacancies in FeS as shown in [59]. A comparison of the ^{57}Fe hyperfine parameters for troilite in the Mössbauer spectra of ordinary chondrites and howardite, which were obtained using a simulation of the full static Hamiltonian, is shown in Figure 30. There are several groups of the ^{57}Fe hyperfine parameters related to the corresponding meteorite samples. The smallest value of H_{eff} is for Sariçiçek howardite which may be related to the largest number of Fe vacancies in FeS in comparison with ordinary chondrites. This fact may be a result of the differentiation of Sariçiçek howardite in the parent body (asteroid (4) Vesta) accompanied by thermal metamorphism of its matter. In contrast, considered ordinary chondrites as undifferentiated meteorites, which did not undergo thermal metamorphism similar to differentiated meteorites, demonstrate larger values of H_{eff}. Nevertheless, the values of H_{eff} for the considered ordinary chondrites show some small differences for at least two groups beyond the errors. These differences may be a result of some variations in the number of Fe vacancies in troilite in these groups of ordinary chondrites which may be a result of differences in the thermal history of these meteorites.

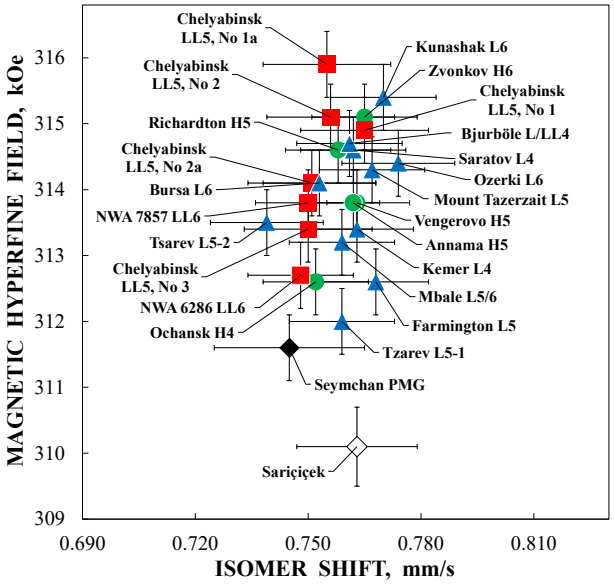

Figure 30. Comparison of the ^{57}Fe hyperfine parameters for troilite obtained by the fit of the Mössbauer spectra of ordinary chondrites and howardite using a simulation of the full static Hamiltonian for the troilite magnetic sextet. ●—H ordinary chondrites, ▲—L ordinary chondrites, ■—LL ordinary chondrites, ♦—main group pallasite, ◇—howardite. Data were taken from Refs. [35–39,41–43,50].

5.3. Chromite, Hercynite and Magnesiochromite

Chromite $FeCr_2O_4$ is a spinel with a cubic structure and two sites for metal atoms: tetrahedral (A) and octahedral [B]. Iron in chromite is usually located at eight (A) sites while chromium occupies sixteen [B] sites. Chromite has been found in various stony and stony-iron meteorites such as ordinary chondrites, howardite and the stony part of the main group pallasite. However, chemical analysis using EDS demonstrated the presence of some minor metals in chromite, with Al as the third metal and sometimes with Mg as the third metal. These metals can form (i) hercynite $FeAl_2O_4$ or mixed spinel like $FeAl_{1-x}Cr_xO_4$ with a small value of x and (ii) magnesiochromite $Fe_{1-x}Mg_xCr_2O_4$. Selected SEM images of chromite with the presence of hercynite and magnesiochromite determined by EDS are shown in Figure 31a–c. The XRD patterns shown in Figure 16c,d (Annama H5, Bursa L6), Figure 17d (Kemer L4), Figure 18a,b (Ozerki L5, Bjurböle L/LL4) and Figure 21c (Sariçiçek howardite) demonstrate the presence of chromite and hercynite while the XRD pattern shown in Figure 21d (Seymchan PMG) indicates the presence of chromite and magnesiochromite. Magnetization measurements also indicated the presence of chromite and hercynite in some ordinary chondrites (two examples are shown in Figure 31d,e).

The ferrimagnetic-paramagnetic phase transitions in chromite can be clearly seen in the temperature range of 40–80 K while the magnetic phase transition observed around 18 K can be assigned to hercynite the Curie temperature of which is in the range of 13–15 K (see [60] and references therein).

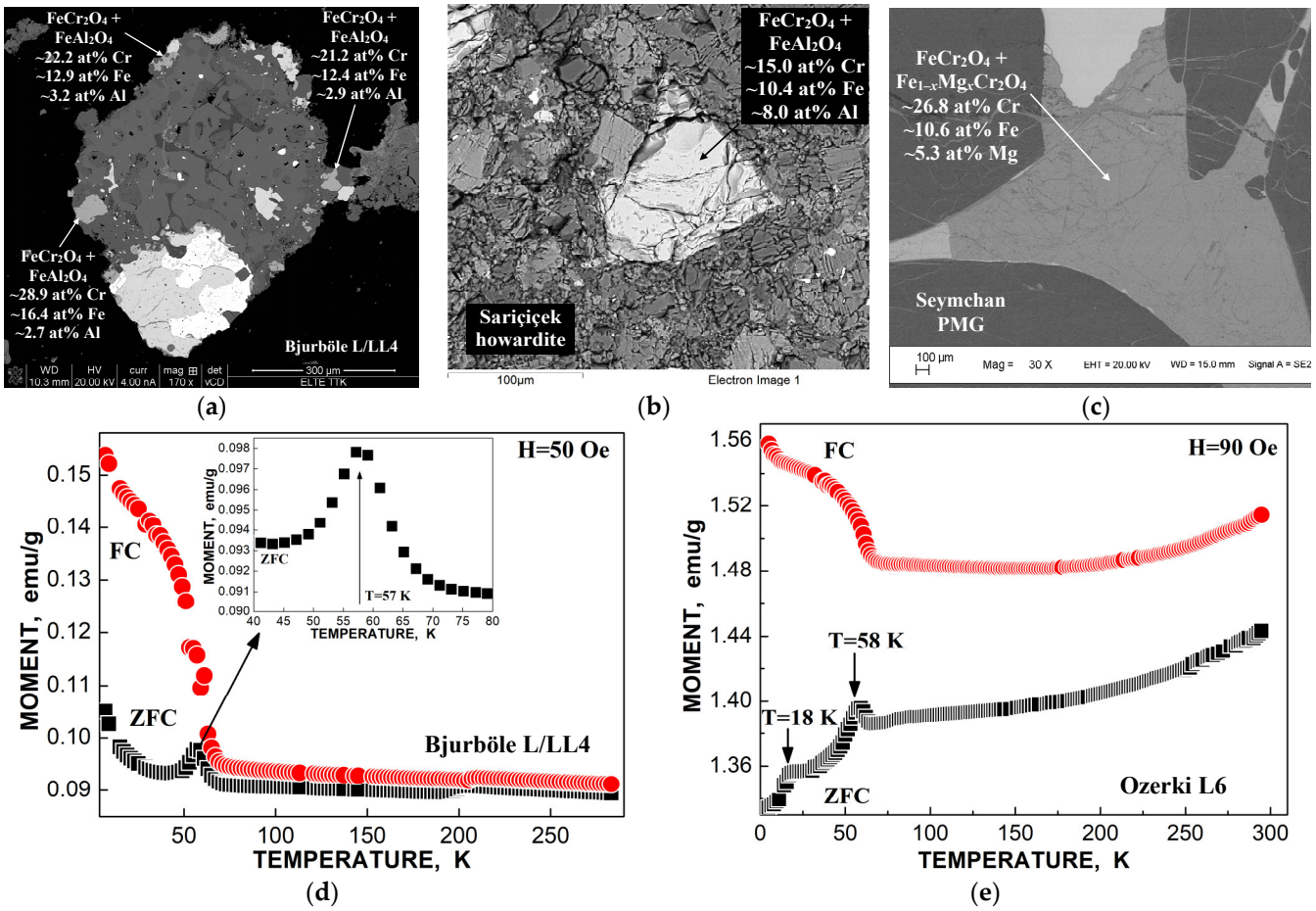

Figure 31. Selected SEM images with EDS results of chromite inclusions with hercynite and magnesiochromite in Bjurböle L/LL4 ordinary chondrite (**a**), Sariçiçek howardite (**b**) and Seymchan main group pallasite (**c**) and zero-field-cooled (ZFC) and field-cooled (FC) magnetization curves of Bjurböle L/LL4 (**d**) and Ozerki L6 (**e**) with the magnetic phase transitions indicated by arrows related to chromite (at ~57 K and ~58 K) and hercynite (at ~18 K). Adapted from Refs. [32,38,39,50].

Based on SEM with EDS, XRD and magnetization results confirming the presence of chromite and hercynite in the studied meteorites, the minor spectral components (broad single peak and quadrupole doublet) revealed in the Mössbauer spectra of ordinary chondrites Annama H5 (Figure 16c), Bursa L6 (Figure 16d), Kemer L4 (Figure 17d), Ozerki L6 (Figure 18a), Bjurböle L/LL4 (Figure 18b) as well as NWA 6286 LL6, NWA 7857 LL6 and Chelyabinsk LL5 fragments (Figure 32) were assigned to chromite and hercynite, respectively (some details can be also found in [61] and references therein). Components associated with chromite (broad single peak) and hercynite (quadrupole doublet) were also revealed in the Mössbauer spectrum of Sariçiçek howardite (Figure 21c). A chromite component was revealed in the Mössbauer spectrum of Seymchan PMG as well, while another single peak assigned to magnesiochromite was found instead of hercynite (Figure 21d). The values of δ for chromite components in these Mössbauer spectra were: (i) in the range of 0.589–0.855 ($\pm$0.022) mm/s for ordinary chondrites except Kemer L4 with $\delta = 1.361 \pm 0.227$ mm/s, (ii) 0.953 $\pm$ 0.022 mm/s for Sariçiçek howardite and (iii) 0.886 $\pm$ 0.009 mm/s for Seymchan PMG. The ^{57}Fe hyperfine parameters

for hercynite quadrupole doublets in these spectra were: (i) δ in the range of 0.625–1.137 (±0.017) mm/s, Δ in the range of 1.347–1.645 (±0.017) mm/s for ordinary chondrites and (ii) δ = 1.012 ± 0.016 mm/s, Δ = 1.363 ± 0.016 mm/s for Sariçiçek howardite. The value δ = 0.796 ± 0.021 mm/s was obtained for magnesiochromite in Seymchan PMG.

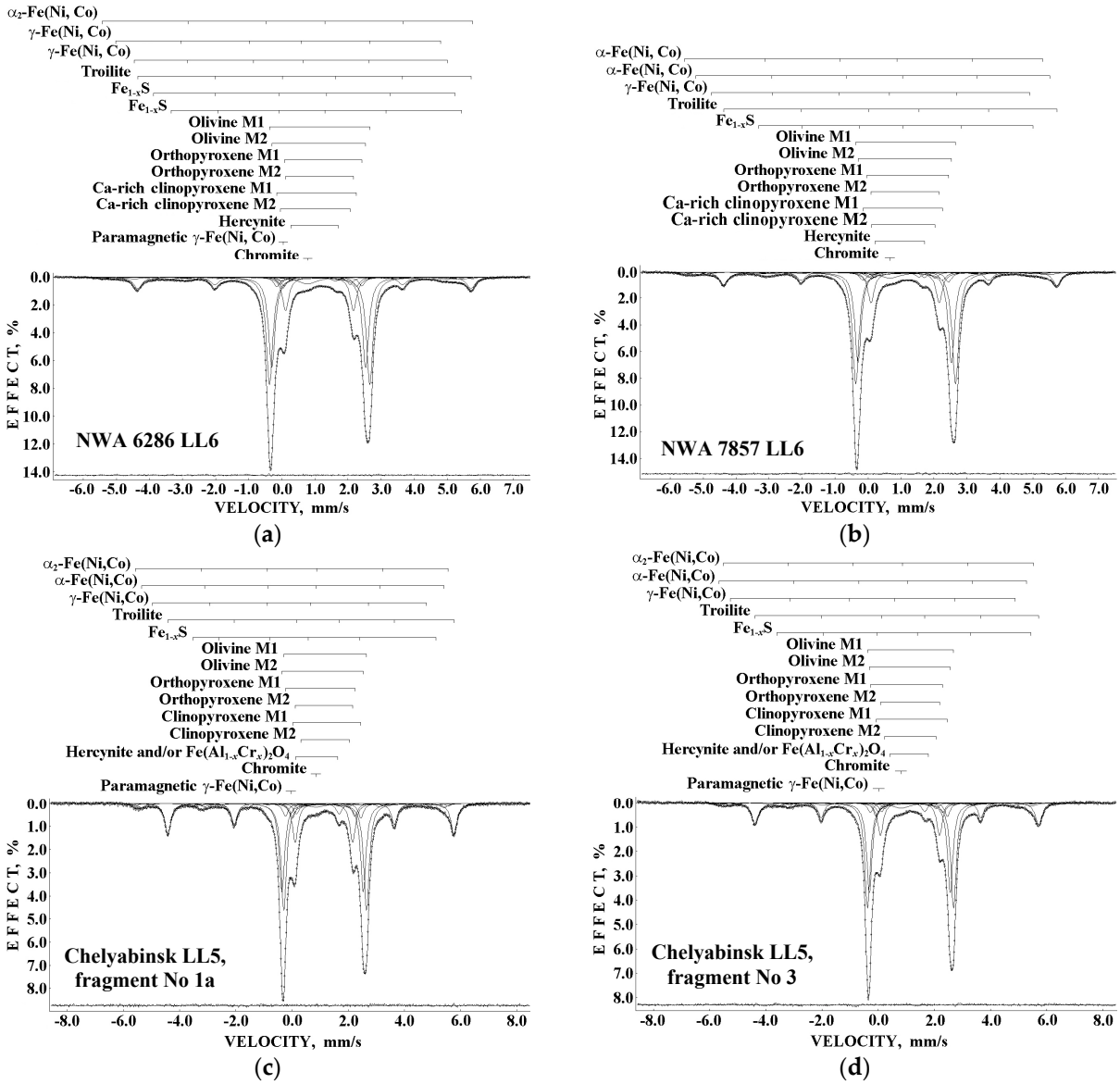

Figure 32. Room temperature Mössbauer spectra of ordinary chondrites: NWA 6286 LL6 (**a**), NWA 7857 LL6 (**b**), Chelyabinsk LL5, fragments No 1a (**c**) and No 3 (**d**). Indicated components are the results of the best fits. The differential spectra are shown at the bottom. Adapted from Refs. [38,39].

5.4. Ilmenite

Ilmenite $FeTiO_3$ is an accessory mineral in stony and stony-iron meteorites. These inclusions were observed by SEM with EDS in three meteorites: Chelyabinsk LL5, fragment No 2a and Bursa L6 ordinary chondrites and Sariçiçek howardite as shown in Figure 33a–c. XRD studies confirmed the presence of ilmenite in Bursa L6 and Sariçiçek as shown in Figures 16b and 21a, respectively, as well as in Chelyabinsk LL5, fragment No 2a (Figure 33d). The content of ilmenite was determined from XRD in these meteorites as follows: 0.1 wt.% in Bursa L6 [37], 1.0 wt.% in Sariçiçek [50] and 0.1 wt.% in Chelyabinsk LL5, No 2a [43]. The ilmenite component in the Mössbauer spectra of these meteorites can be seen in Figure 16d (Bursa L6), Figure 21c (Sariçiçek) and Figure 33e (Chelyabinsk LL5,

No 2a). It should be noted that ilmenite was found in one fragment of Chelyabinsk LL5 (No 2a) only, while in the other four fragments ilmenite was absent.

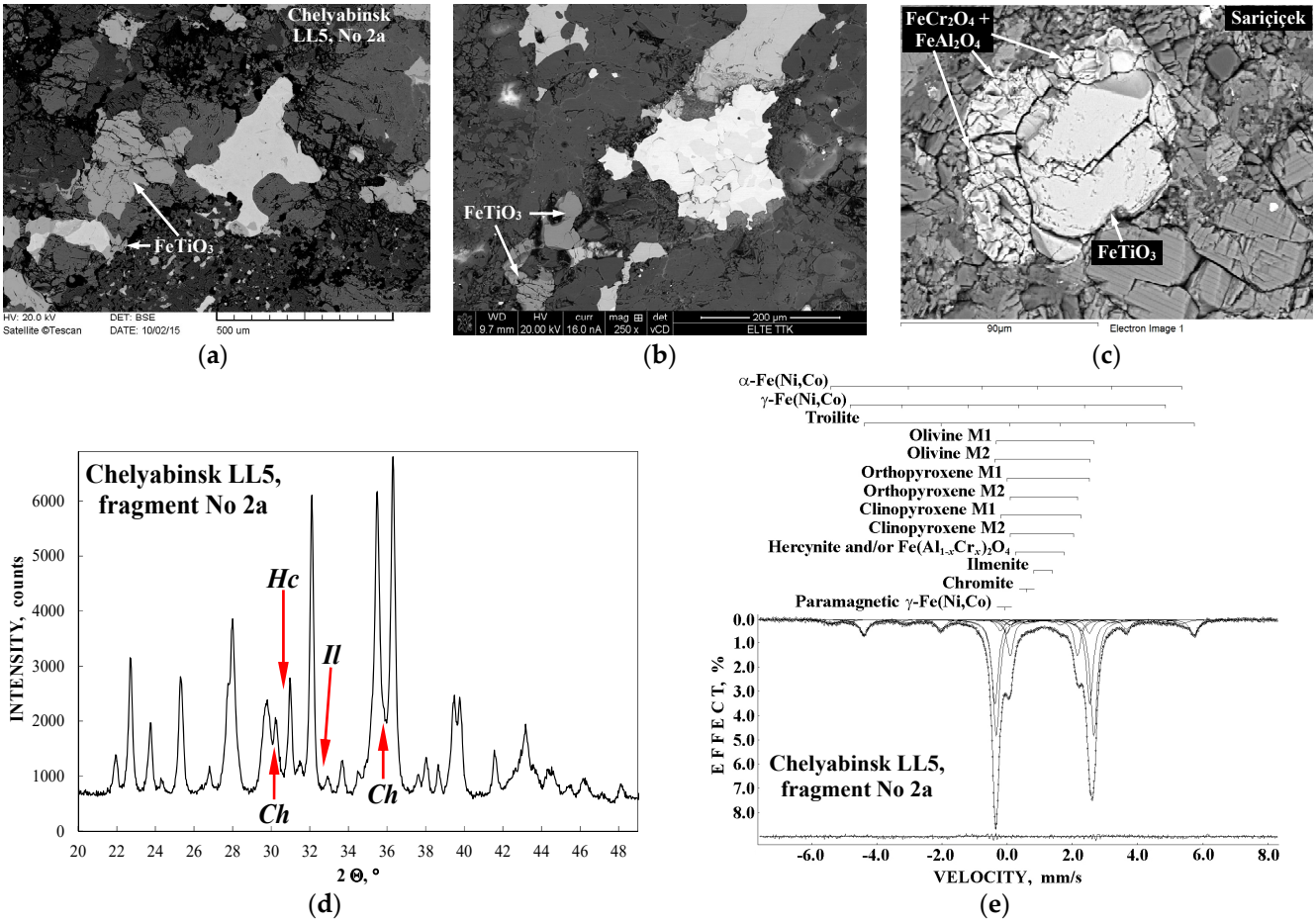

Figure 33. Selected SEM images with the results of EDS of ilmenite inclusions in Chelyabinsk LL5, fragment No 2a, ordinary chondrite (**a**), Bursa L6 ordinary chondrite (**b**) and Sariçiçek howardite (**c**), XRD pattern of Chelyabinsk LL5, fragment No 2a, with some selected phases indicated by arrows: ***Ch*** is chromite, ***Hc*** is hercynite and ***Il*** is ilmenite (**d**) and the room temperature Mössbauer spectrum of Chelyabinsk LL5, fragment No 2a, indicated components are the results of the best fit, the differential spectrum is shown at the bottom (**e**). Adapted from Refs. [36,43,50].

The ^{57}Fe hyperfine parameters and relative area for the ilmenite component deduced from the Mössbauer spectra are the following: (i) δ = 0.949 ± 0.015 mm/s, Δ = 0.654 ± 0.026 mm/s and A = ~0.5% for Bursa L6, (ii) δ = 1.099 ± 0.017 mm/s, Δ = 0.559 ± 0.029 mm/s and A = ~0.8% for Chelyabinsk LL5, No 2a and (iii) δ = 1.072 ± 0.016 mm/s, Δ = 0.701 ± 0.016 mm/s and A = ~1.8% (Fe^{2+} ilmenite) and δ = 0.210 ± 0.016 mm/s, Δ = 0.689 ± 0.020 mm/s and A = ~1.3% (Fe^{3+} ilmenite) for Sariçiçek. These ^{57}Fe hyperfine parameters are slightly different for the Fe^{2+} ilmenite found in these meteorites. Moreover, Sariçiçek howardite demonstrates the presence of Fe^{2+} and Fe^{3+} ilmenite. This is possible due to the inter-valence charge-transition mechanism Fe^{2+} Ti^{4+} → Fe^{3+} Ti^{3+} described in [62]. The total relative area of the ilmenite spectral components in the spectrum of Sariçiçek (~3.1%) is larger than the relative area for ilmenite component in the spectra of Chelyabinsk LL5, No 2a and Bursa L6 ordinary chondrites, which are in fact similar, that is in agreement with the XRD results.

5.5. Magnesioferrite

Magnesioferrite $MgFe_2O_4$ is also a spinel like chromite, hercynite and magnesiochromite which were considered above. However, in general, cation distribution among the tetrahedral (A) and octahedral [B] sites in magnesioferrite can be written as $(Mg_{1-x}Fe_x)_A[Mg_xFe_{2-x}]_BO_4$, where x is the inversion parameter (see, e.g., [63]). Magnesioferrite was not found in the bulk meteorite materials. This spinel was observed in the fusion crust of ordinary chondrites which formed by meteorite surface combustion while passing through the Earth atmosphere at a high speed. Firstly, magnesioferrite was found in the fusion crust in Saratov L4 ordinary chondrite using XRD [64]. The fusion crust extracted from Chelyabinsk LL5 fragments No 1a and No 2a, Kemer L4 and Ozerki L6 was studied by various techniques including Mössbauer spectroscopy with a high velocity resolution in [37,38,43]. XRD patterns of the fusion crust from Kemer L4 and Ozerki L6 ordinary chondrites are shown in Figure 34a,b. The room temperature Mössbauer spectra of the fusion crust from these meteorites are shown in Figure 34c,d.

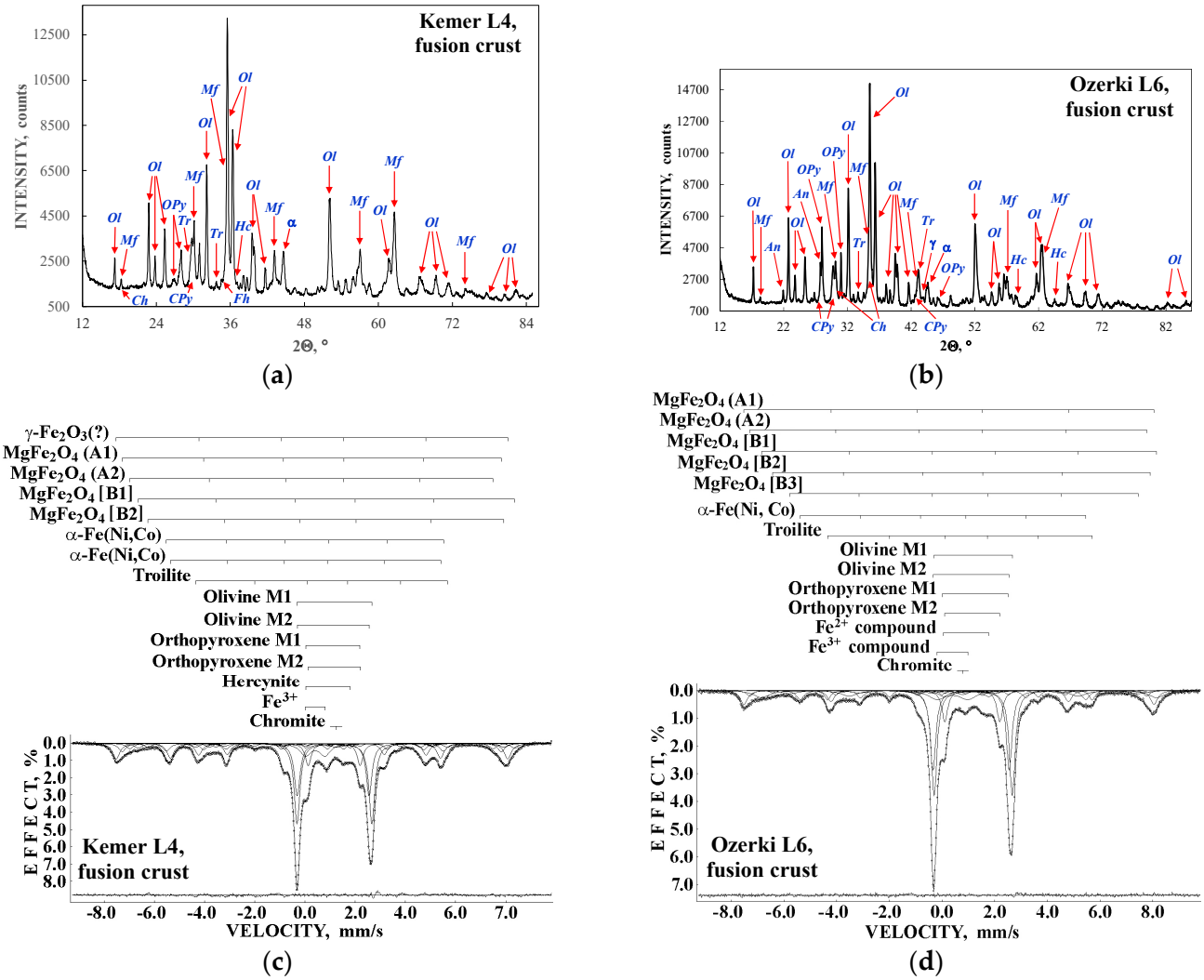

Figure 34. XRD patterns of the fusion crust extracted from Kemer L4 (**a**) and Ozerki L6 (**b**) ordinary chondrites: indicated phases are olivine (***Ol***), orthopyroxene (***OPy***), Ca-rich clinopyroxene (***CPy***), α-Fe(Ni, Co) phase (***α***), γ-Fe(Ni, Co) phase (***γ***), troilite (***Tr***), chromite (***Ch***), hercynite (***Hc***), ferrihydrite (***Fh***) and magnesioferrite (***Mf***); and the room temperature Mössbauer spectra of the fusion crust extracted from Kemer L4 (**c**) and Ozerki L6 (**d**) ordinary chondrites; indicated components are the results of the best fits, the differential spectra are shown at the bottom. Adapted from Refs. [37,38].

These Mössbauer spectra demonstrate the presence of additional magnetic sextets besides sextets related to the α-Fe(Ni, Co) phase and troilite. The spectrum of the fusion crust of Kemer L4 also had a magnetic sextet associated with maghemite γ-Fe_2O_3 which could be a result of terrestrial weathering. The other magnetic sextets were assigned to ^{57}Fe in the tetrahedral (A) and octahedral [B] sites in magnesioferrite. Similarly, magnetic sextets assigned to the (A) and [B] sites in magnesioferrite were revealed in the Mössbauer spectra of the fusion crust extracted from Chelyabinsk LL5 ordinary chondrite (fragments No 1a and No 2a) [43]. A comparison of the ^{57}Fe hyperfine and other Mössbauer parameters for magnesioferrite in the fusion crust extracted from these ordinary chondrites is shown in Table 12. Magnetic sextets with smaller values of δ were related to ^{57}Fe in the (A) sites while those with larger δ values were assigned to ^{57}Fe in the [B] sites. Several sextets attributed to (A) or [B] sites were considered as a result of differences in the iron local microenvironment and variations in the number of Mg^{2+} cations in the local microenvironments around the (A) and [B] sites (see [65]). Magnesioferrite formation in the fusion crust of meteorites may be a result of combustion of the Fe-Ni-Co alloy, troilite as well as olivine and orthopyroxene as the sources of Mg^{2+}. Therefore, variations in the chemical composition and the inversion parameter x in magnesioferrites in different fusion crusts may be a reason for the different number of magnetic sextets and their Mössbauer parameters. It was also interesting that the authors of [43] compared the total relative areas of magnesioferrite components for the fusion crusts in fragments No 1a and No 2a of Chelyabinsk LL5 and determined that A_{tot}^{Mf} = ~32.9% for No 1a and A_{tot}^{Mf} = ~21.5% for No 2a. This difference was considered to be a result of the different depths of these fragments in the 20-m sized Chelyabinsk meteoroid and, therefore, different time of their releasing during the meteoroid fragmentation and, consequently, these fragments had different time of fall with material combustion.

Table 12. Mössbauer parameters for magnesioferrite deduced from the Mössbauer spectra of the fusion crust extracted from ordinary chondrites (data were taken from [37,38,43]).

Meteorite	Γ, mm/s	δ, mm/s	2ε, mm/s	H_{eff}, kOe	*A*, %	Phase/Site
Chelyabinsk LL5, fragment No 1a	0.364 ± 0.040	0.232 ± 0.020	0.008 ± 0.020	481.9 ± 0.6	13.3	$MgFe_2O_4$ (A)
	0.290 ± 0.040	0.412 ± 0.020	0.027 ± 0.020	480.9 ± 0.6	5.2	$MgFe_2O_4$ [B1]
	0.405 ± 0.040	0.659 ± 0.020	0.058 ± 0.020	477.9 ± 0.6	5.4	$MgFe_2O_4$ [B2]
	0.476 ± 0.040	0.592 ± 0.020	−0.047 ± 0.020	445.0 ± 0.6	6.1	$MgFe_2O_4$ [B3]
	0.558 ± 0.057	0.659 ± 0.020	0.044 ± 0.027	416.0 ± 1.2	3.0	$MgFe_2O_4$ [B4]
Chelyabinsk LL5, fragment No 2a	0.414 ± 0.040	0.242 ± 0.020	−0.035 ± 0.020	480.4 ± 0.6	8.2	$MgFe_2O_4$ (A)
	0.516 ± 0.053	0.496 ± 0.022	0.054 ± 0.020	478.9 ± 0.9	7.2	$MgFe_2O_4$ [B1]
	0.534 ± 0.073	0.495 ± 0.020	−0.036 ± 0.028	444.3 ± 1.6	4.5	$MgFe_2O_4$ [B2]
	0.408 ± 0.092	0.614 ± 0.025	−0.017 ± 0.048	410.9 ± 1.8	1.6	$MgFe_2O_4$ [B3]
Kemer L4	0.340 ± 0.038	0.305 ± 0.019	−0.076 ± 0.019	469.2 ± 0.5	5.9	$MgFe_2O_4$ (A1)
	0.340 ± 0.038	0.318 ± 0.019	−0.127 ± 0.019	449.5 ± 0.5	3.8	$MgFe_2O_4$ (A2)
	0.340 ± 0.038	0.822 ± 0.019	0.056 ± 0.019	465.7 ± 0.5	3.5	$MgFe_2O_4$ [B1]
	0.340 ± 0.038	0.865 ± 0.019	−0.084 ± 0.019	440.2 ± 0.6	2.9	$MgFe_2O_4$ [B2]
Ozerki L6	0.329 ± 0.030	0.277 ± 0.015	−0.026 ± 0.015	484.0 ± 0.5	8.2	$MgFe_2O_4$ (A1)
	0.317 ± 0.043	0.271 ± 0.015	−0.078 ± 0.015	469.4 ± 1.0	3.6	$MgFe_2O_4$ (A2)
	0.747 ± 0.055	0.721 ± 0.016	−0.188 ± 0.023	467.0 ± 0.9	9.8	$MgFe_2O_4$ [B1]
	0.318 ± 0.067	0.538 ± 0.020	0.373 ± 0.036	447.7 ± 1.6	1.5	$MgFe_2O_4$ [B2]
	0.776 ± 0.078	0.781 ± 0.021	0.089 ± 0.045	413.4 ± 1.6	4.6	$MgFe_2O_4$ [B3]

5.6. Schreibersite and Rhabdite

Iron-nickel phosphides $(Fe, Ni)_3P$ were found in iron meteorites in the forms of (i) macro inclusions called schreibersite and (ii) prismatic idiomorphic microcrystals precipitated in the α-Fe(Ni, Co) matrix called rhabdites. The crystal structures of schreibersite and rhabdite are similar with tetragonal space group. These iron-nickel phosphides contain three nonequivalent M1, M2 and M3 sites for Fe and Ni. These sites are occupied by metals in different ways. Schreibersite and rhabdite were extracted from the Sikhote-Alin IIAB iron meteorite and studied using various techniques including Mössbauer spectroscopy with a

high velocity resolution in [66–69]. SEM images of the extracted schreibersite and rhabdite are shown in Figure 35a,b, respectively. EDS measurements showed that the average ratios of Fe and Ni contents in the two phosphides were different: 64%:36% in schreibersite and 52%:48% in rhabdite [68]. The XRD patterns of schreibersite and rhabdite are shown in Figure 35c and demonstrate similar peak positions. However, the unit cell parameters were slightly different: $a = b = 9.049(8)$ Å and $c = 4.461(8)$ Å for schreibersite and $a = b = 9.029(3)$ Å and $c = 4.461(5)$ Å for rhabdite. The unit cell of $(Fe, Ni)_3P$ with M1, M2 and M3 sites is shown in Figure 35d.

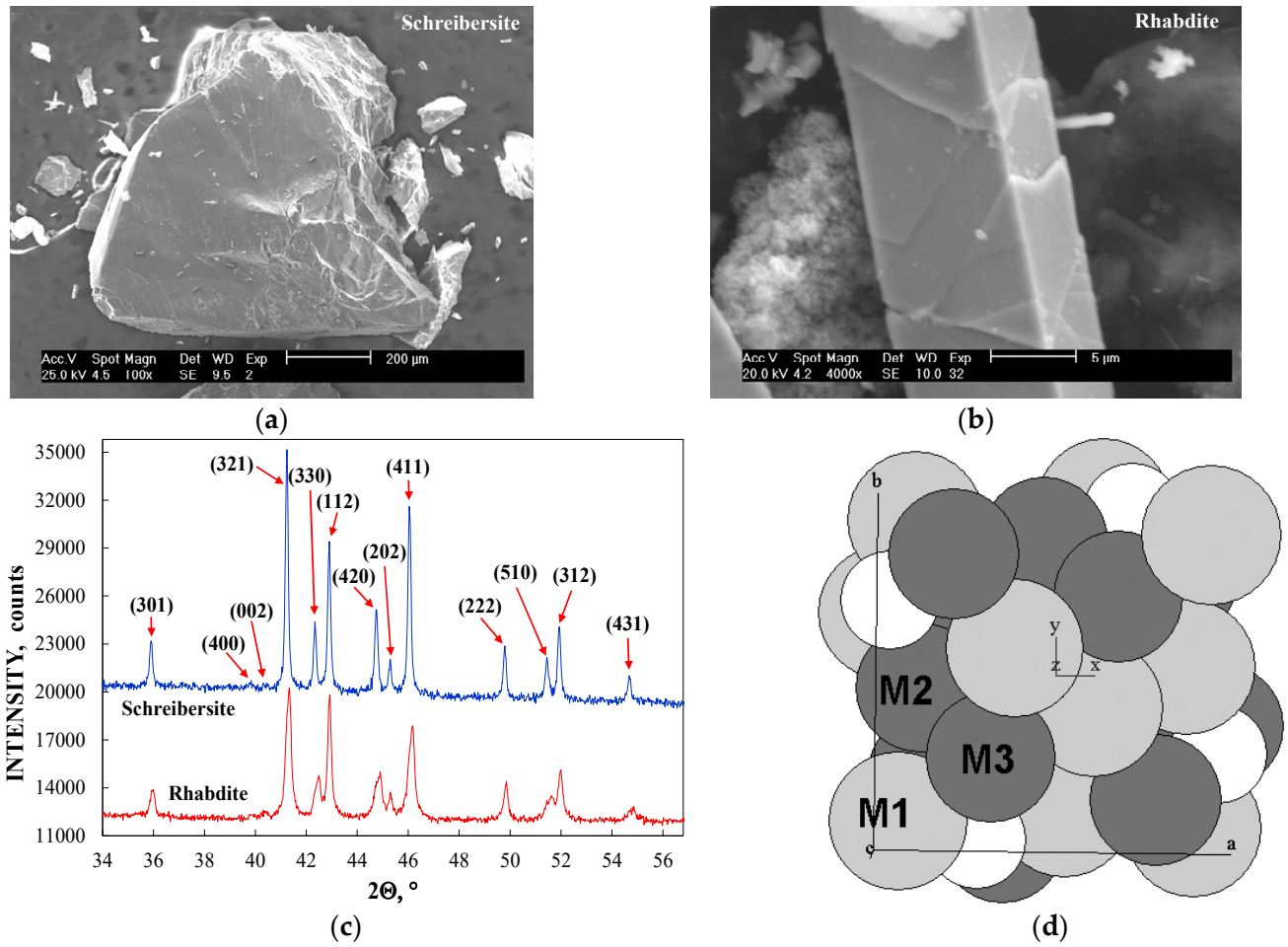

Figure 35. Iron-nickel phosphides extracted from the Sikhote-Alin IIAB iron meteorite: SEM images of schreibersite (**a**) and rhabdite (**b**), XRD patterns for schreibersite and rhabdites with indication of Miller indices (**c**) and crystallographically nonequivalent sites M1, M2 and M3 for metal atoms in $(Fe, Ni)_3P$, ○—P, ●—Fe, ●—Ni (**d**). Adapted from Refs. [66–68].

The Mössbauer spectra of schreibersite and rhabdite extracted from the Sikhote-Alin IIAB iron meteorite were measured at different temperatures: the schreibersite spectra were measured at 295 and 90 K while the rhabdite spectra were measured at 295, 220, 150 and 90 K. The Mössbauer spectra of both iron-nickel phosphides measured at 295 and 90 K are shown in Figure 36. The room temperature Mössbauer spectra demonstrate the difference between schreibersite and rhabdite which can be explained by the superparamagnetic state of the latter microcrystals. The magnetization measurements carried out in [66] determined that the Curie temperatures for the two phosphides were different: higher than 455 K for schreibersite and 345 K for rhabdite.

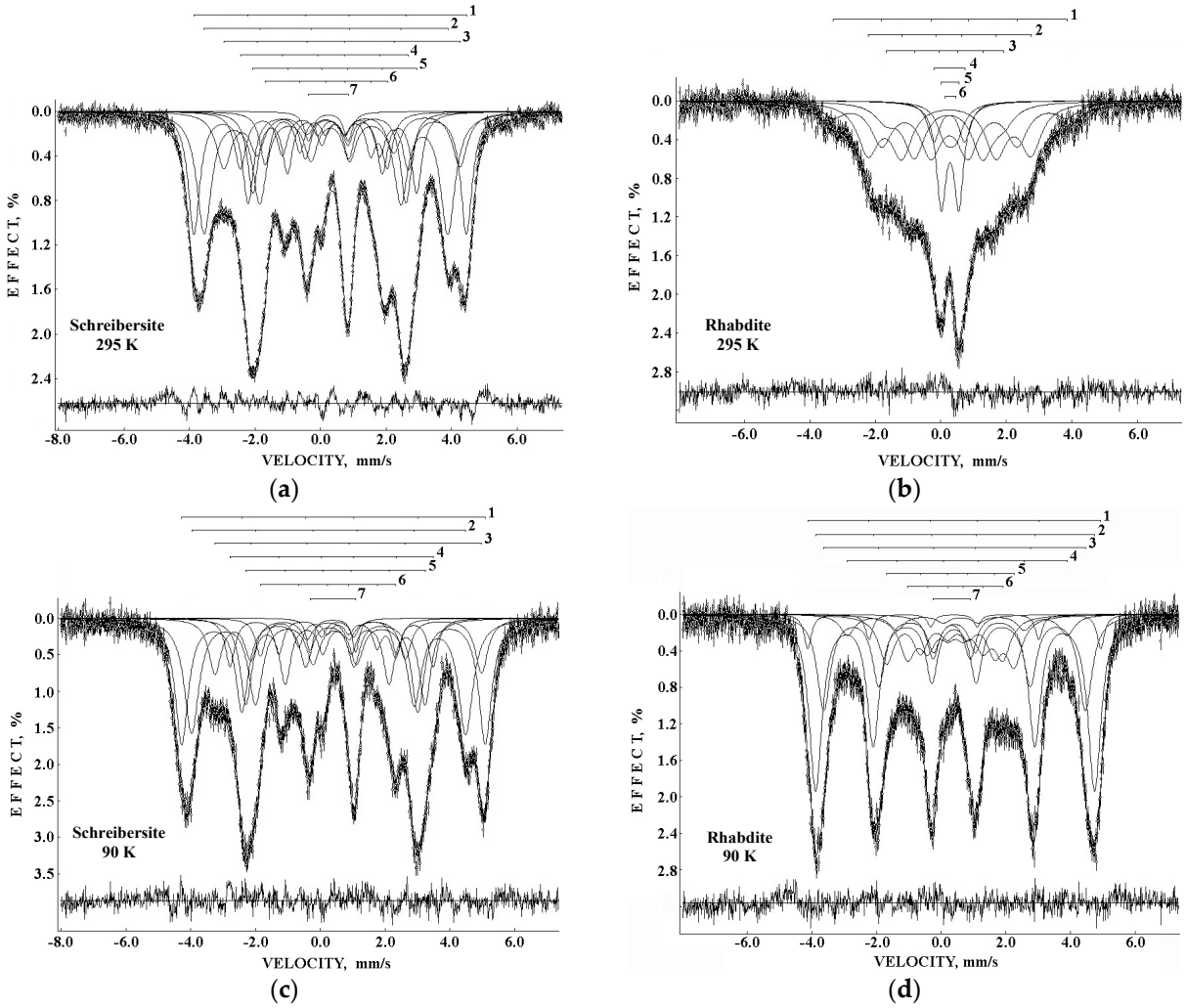

Figure 36. Mössbauer spectra of iron-nickel phosphides extracted from the Sikhote-Alin IIAB iron meteorite: schreibersite (**a**,**c**) and rhabdites (**b**,**d**) measured at 295 K (**a**,**b**) and 90 K (**c**,**d**). The indicated components are the results of the best fits. The differential spectra are shown at the bottom. Adapted from Ref. [68].

The Mössbauer spectra of rhabdites where additionally measured at 220 and 150 K to observe a decrease of the paramagnetic components in the spectra (these spectra are not shown here). The spectra of rhabdite measured at 220, 150 and 90 K were fitted in [66–69] using a model suggested in [70] and considered two magnetic sextets for each site in (Fe, Ni)$_3$P. Therefore, the Mössbauer spectra of schreibersite and rhabdite were fitted using six magnetic sextets and one paramagnetic quadrupole doublet (the room temperature spectrum of rhabdites was fitted using three magnetic sextets and three paramagnetic quadrupole doublets). The Mössbauer parameters for sextets deduced from the 90 K spectra are presented in Table 13 and assigned to the M1, M2 and M3 sites similar to [70].

The total relative areas of spectral components assigned to the M1, M2 and M3 sites were approximately constant at various temperatures: (i) 54%, 22% and 21% for schreibersite at 295 and 90 K and (ii) 44%, 28% and 28% for rhabdite at 220, 150 and 90 K. If the *f*-factors can be considered to be the same, these values can be taken as the relative iron fractions in the M1, M2 and M3 sites of schreibersite and rhabdite. An evaluation of the average concentration of Fe and Ni atoms in these two iron-nickel phosphides showed that the M1 sites were occupied by 8 Fe atoms, each of the M2 and M3 sites was occupied by 3.4 Fe and 4.6 Ni atoms in schreibersite while the M1 sites were occupied by 5.5 Fe and 2.5 Ni atoms, each of the M2 and M3 sites was occupied by 3.5 Fe and 4.5 Ni atoms in rhab-

dite [68]. This result demonstrates slightly different occupancies of these sites by Fe and Ni in two iron-nickel phosphides with different morphology resulting from their different formation (heterogeneous nucleation for schreibersite and homogeneous nucleation for rhabdites [71]) extracted from the Sikhote-Alin IIAB iron meteorite.

Table 13. Mössbauer parameters for magnetic sextets in the 90 K spectra of schreibersite and rhabdites extracted from the Sikhote-Alin IIAB iron meteorite (data were taken from Refs. [68,69]).

$(Fe, Ni)_3P$	No [1]	δ, mm/s	2ε, mm/s	H_{eff}, kOe	*A*, %	Site
Schreibersite	1	0.356 ± 0.015	0.110 ± 0.015	291.0 ± 0.5	27.7	M1
	2	0.359 ± 0.015	−0.192 ± 0.015	262.7 ± 0.5	28.1	M1
	3	0.556 ± 0.015	0.625 ± 0.016	255.5 ± 0.6	11.6	M2
	4	0.449 ± 0.015	−0.189 ± 0.015	194.8 ± 0.5	7.8	M2
	5	0.500 ± 0.015	−0.050 ± 0.015	171.8 ± 0.5	16.8	M3
	6	0.396 ± 0.015	−0.305 ± 0.015	129.7 ± 0.7	6.1	M3
Rhabdite	1	0.399 ± 0.015	0.399 ± 0.015	281.4 ± 0.5	4.4	M1
	2	0.414 ± 0.015	0.033 ± 0.015	267.9 ± 0.5	39.7	M1
	3	0.415 ± 0.015	0.002 ± 0.015	251.3 ± 0.5	22.4	M2
	4	0.549 ± 0.015	−0.106 ± 0.015	210.8 ± 0.5	5.4	M2
	5	0.397 ± 0.015	−0.219 ± 0.015	122.6 ± 0.5	12.8	M3
	6	0.434 ± 0.015	−0.005 ± 0.015	91.5 ± 0.5	11.0	M3

[1] The number of spectral components.

6. Conclusions

An increase in the sensitivity and accuracy of Mössbauer spectroscopy represents a way to deeply study various complex materials containing different iron-bearing phases and minerals. Meteorites are a kind of materials of extraterrestrial origin which were formed along with the Solar System formation and with further evolution of asteroid and planetary matter. Moreover, meteorites have undergone various extreme factors in space (a very slow cooling from the melt, shock metamorphism, reheating, thermal metamorphism, etc.). Therefore, meteorites contain phases (minerals) similar to those found on Earth but with some features related to the effect of extreme factors which cannot be reproduced in the terrestrial conditions. Thus, attempts to see deeper inside the iron-bearing phases (minerals) in meteorites may bring additional information about their structural features and thermal/shock history. Mössbauer spectroscopy with a high velocity resolution, i.e., with a high discretization of the velocity reference signal up to 2^{12}, in fact, is one of the ways to increase the sensitivity and precision of the technique. The application of Mössbauer spectroscopy with a high velocity resolution using SM-2201 spectrometers to study various meteorites and their separate phases (minerals) demonstrated the following results. The extraterrestrial Fe-Ni-Co alloy found in iron, stony-iron and stony meteorites contains various phases: α-Fe(Ni, Co) (kamacite), α_2-Fe(Ni, Co) (martensite), γ-Fe(Ni, Co) (taenite) and γ-FeNi(Co) (tetrataenite) as well as plessite structure α-Fe(Ni, Co)/α_2-Fe(Ni, Co) + γ-Fe(Ni, Co) which was confirmed by optical and scanning electron microscopy with energy dispersive spectroscopy and X-ray diffraction. Mössbauer spectroscopy revealed components for these metal phases which ^{57}Fe hyperfine parameters were assigned to these phases: H_{eff} > ~345 kOe for the α_2-Fe(Ni, Co) phase (martensite), ~327 kOe < H_{eff} ≤ ~345 kOe for the α-Fe(Ni, Co) phase (kamacite), ~283 kOe ≤ H_{eff} ≤ ~327 kOe for the γ-Fe(Ni, Co) phase (taenite), including the values of H_{eff} < ~290 kOe which may also be associated with the γ-FeNi(Co) phase (tetrataenite) and ~−0.20 mm/s < δ < ~0.15 mm/s for the paramagnetic γ-Fe(Ni, Co) phase (paramagnetic taenite). Moreover, it was shown that variation in Ni concentration within one phase as well as different probabilities of various Ni contents in the Fe local microenvironment may lead to revealing of several magnetic sextets associated with the same phase with slightly different ^{57}Fe hyperfine parameters. The study of stony and stony-iron meteorites containing silicate crystals (olivine, orthopyroxene and clinopyroxene) with two crystallographically nonequivalent M1 and M2 sites for Fe^{2+} and Mg^{2+} cations showed the possibility to excavate components in the Mössbauer spectra of the bulk meteorite samples which were related to the ^{57}Fe

in the M1 and M2 sites in these silicate minerals. Moreover, based on the Mössbauer results it was possible to compare the ^{57}Fe hyperfine parameters for the same sites in the same silicate crystals in different meteorites and to observe some similarities and some differences related to small variations in the iron local microenvironments. Additionally, it was possible to estimate the ratios of the Fe^{2+} occupancies of the M1 and M2 sites in these silicates which agreed with the same ratios deduced from X-ray diffraction. Using these occupancies, it was possible to estimate the distribution coefficient and the temperature of equilibrium cation distribution in olivine and orthopyroxene which are related to the thermal history of these minerals. It was also possible to excavate spectral components related to the minor phases in stony and stony-iron meteorites such as non-stoichiometric troilite (in fact the local ^{57}Fe microenvironments in troilite with iron deficiency $Fe_{1-x}S$ with $x \leq 0.05$), chromite, hercynite, magnesiochromite and ilmenite. The study of two extracted iron-nickel phosphides (schreibersite and rhabdite) with three nonequivalent M1, M2 and M3 sites for Fe and Ni demonstrated some differences in the ^{57}Fe hyperfine parameters for two phosphides and estimated different occupations of these sites by Fe and Ni in schreibersite and rhabdite. Thus, these examples of the applications of Mössbauer spectroscopy with a high velocity resolution demonstrate high potential of this technique for the study of extraterrestrial materials with a high sensitivity, precision, and accuracy.

Author Contributions: Conceptualization, supervision, writing—original draft preparation of this review, M.I.O.; validation, data curation, writing—review and editing of this work, A.A.M. and M.V.G. All authors have read and agreed to the published version of the manuscript.

Funding: This work was supported by the Ministry of Science and Higher Education of the Russian Federation, project № FEUZ-2023-0013. M.I.O., M.V.G. and A.A.M. gratefully acknowledge the Ural Federal University Program of Development within the Priority-2030 Program (research funding from the Ministry of Science and Higher Education of the Russian Federation). The Zavaritsky Institute of Geology and Geochemistry of the Ural Branch of the Russian Academy of Sciences is supported by the Ministry of Science and Higher Education of the Russian Federation, project № AAAA-A19-119071090011-6 (A.A.M.).

Data Availability Statement: All data can be found in the published papers or by request to the corresponding author.

Acknowledgments: The authors wish to thank their colleagues, who was involved in various studies of meteorites, for fruitful cooperation: V.I. Grokhovsky, V.A. Semionkin, A.V. Chukin, E.V. Petrova, M.S. Karabonalov, M.Yu. Larionov and G.A. Yakovlev (Ural Federal University, Ekaterinburg, Russian Federation), D.A. Zamyatin (The Zavaritsky Institute of Geology and Geochemistry of the Ural Branch of the Russian Academy of Sciences, Ekaterinburg, Russian Federation), E. Kuzmann, Z. Homonnay, Cs. Szabó, Z. Bendő, Á. Szabó, G. Varga and Z. Dankházi (Eötvös Loránd University, Budapest, Hungary), Z. Klencsár (Centre for Energy Research, Budapest, Hungary), I. Felner (The Hebrew University, Jerusalem, Israel), B.A. Nogueira and R. Fausto (University of Coimbra, Coimbra, Portugal), P. Jenniskens (SETI Institute, Mountain View, CA, USA), O. Unsalan (Ege University, Izmir, Turkey), M. Yesiltas (Kirklareli University, Kirklareli, Turkey), M. Gritsevich (Finnish Geospatial Research Institute, Masala, Finland) and T. Kohout (University of Helsinki, Helsinki, Finland).

Conflicts of Interest: The authors declare no conflict of interest.

References

1. Wasson, J.T. *Meteorites. Classification and Properties*; Springer: Berlin/Heidelberg, Germany; New York, NY, USA, 1974; pp. 1–320.
2. Maksimova, A.A.; Oshtrakh, M.I. Applications of Mössbauer spectroscopy in meteoritical and planetary science, Part I: Undifferentiated meteorites. *Minerals* **2021**, *11*, 612. [CrossRef]
3. Maksimova, A.A.; Goryunov, M.V.; Oshtrakh, M.I. Applications of Mössbauer spectroscopy in meteoritical and planetary science, Part II: Differentiated meteorites, Moon and Mars. *Minerals* **2021**, *11*, 614. [CrossRef]
4. Klingelhöfer, G. Extraterrestrial Mössbauer spectroscopy. In *The Rudolf Mössbauer Story*; Kalvius, M., Kienle, P., Eds.; Springer: Berlin/Heidelberg, Germany, 2012; pp. 293–316.
5. Stefanik, M.; Cesnek, M.; Sklenka, L.; Kmjec, T.; Miglierini, M. Neutron activation analysis of meteorites at the VR-1 training reactor. *Rad. Phys. Chem.* **2020**, *171*, 108675. [CrossRef]

6. Yan, L.; Zhao, J.; Toellner, T.S.; Divan, R.; Xu, S.; Cai, Z.; Boesenberg, J.S.; Friedrich, J.M.; Cramera, S.P.; Alp, E.E. Exploration of synchrotron Mössbauer microscopy with micrometer resolution: Forward and a new backscattering modality on natural samples. *J. Synchrotron Rad.* **2012**, *19*, 814–820. [CrossRef] [PubMed]
7. Blukis, R.; Rüffer, R.; Chumakov, A.I.; Harrison, R.J. A high spatial resolution synchrotron Mössbauer study of the Tazewell IIICD and Esquel pallasite meteorites. *Meteorit. Planet. Sci.* **2017**, *52*, 925–936. [CrossRef] [PubMed]
8. Oshtrakh, M.I.; Grokhovsky, V.I.; Petrova, E.V.; Larionov, M.Y.; Uymina, K.A.; Semionkin, V.A.; Abramova, N.V. Study of meteorites using Mössbauer spectroscopy with high velocity resolution. In *Proceedings of the International Conference "Mössbauer Spectroscopy in Materials Science 2008"*; Mashlan, M., Zboril, R., Eds.; AIP Conference Proceedings; AIP Publishing: Melville/New York, NY, USA, 2008; Volume 1070, pp. 131–139.
9. Grokhovsky, V.I.; Zhiganova, E.V.; Larionov, M.Y.; Uimina, K.A.; Oshtrakh, M.I. Mössbauer spectroscopy with high velocity resolution in the meteorites study. *Phys. Metals Metallogr.* **2008**, *105*, 177–187.
10. Grokhovsky, V.I.; Oshtrakh, M.I.; Petrova, E.V.; Larionov, M.Y.; Uymina, K.A.; Semionkin, V.A. Mössbauer spectroscopy with high velocity resolution in the study of iron-bearing minerals in meteorites. *Eur. J. Mineral.* **2009**, *21*, 51–63. [CrossRef]
11. Oshtrakh, M.I.; Grokhovsky, V.I.; Petrova, E.V.; Larionov, M.Y.; Goryunov, M.V.; Semionkin, V.A. Mössbauer spectroscopy with a high velocity resolution applied for the study of meteoritic iron-bearing minerals. *J. Mol. Struct.* **2013**, *1044*, 268–278. [CrossRef]
12. Oshtrakh, M.I.; Maksimova, A.A.; Goryunov, M.V.; Yakovlev, G.A.; Petrova, E.V.; Larionov, M.Y.; Grokhovsky, V.I.; Semionkin, V.A. Mössbauer spectroscopy with a high velocity resolution: Advances in the study of meteoritic iron-bearing minerals. In *Proceedings of the Workshop on The Modern Analytical Methods Applied to Earth and Planetary Sciences*; Gucsik, A., Ed.; The MicroMatLab Kft Hungary: Sopron, Hungary, 2015; pp. 43–86. ISBN 978-963-12-1410-9.
13. Oshtrakh, M.I.; Semionkin, V.A.; Milder, O.B.; Novikov, E.G. Mössbauer spectroscopy with high velocity resolution: An increase of analytical possibilities in biomedical research. *J. Radioanal. Nucl. Chem.* **2009**, *281*, 63–67. [CrossRef]
14. Semionkin, V.A.; Oshtrakh, M.I.; Milder, O.B.; Novikov, E.G. A High velocity resolution Mössbauer spectrometric system for biomedical research. *Bull. Rus. Acad. Sci. Phys.* **2010**, *74*, 416–420. [CrossRef]
15. Oshtrakh, M.I.; Semionkin, V.A. Mössbauer spectroscopy with a high velocity resolution: Advances in biomedical, pharmaceutical, cosmochemical and nanotechnological research. *Spectrochim. Acta, Part A Molec. and Biomolec. Spectroscopy* **2013**, *100*, 78–87. [CrossRef]
16. Oshtrakh, M.I.; Semionkin, V.A. Mössbauer spectroscopy with a high velocity resolution: Principles and applications. In *Proceedings of the International Conference "Mössbauer Spectroscopy in Materials Science 2016"*; Tuček, J., Miglierini, M., Eds.; AIP Conference Proceedings; AIP Publishing: Melville/New York, NY, USA, 2016; Volume 1781, p. 020019.
17. Rubin, A.E. Mineralogy of meteorite groups. *Meteorit. Planet. Sci.* **1997**, *32*, 231–247. [CrossRef]
18. Rubin, A.E.; Ma, C. Meteoritic minerals and their origins. *Chem. Erde* **2017**, *77*, 325–385. [CrossRef]
19. Weisberg, M.K.; McCoy, T.J.; Krot, A.N. Systematics and evaluation of meteorite classification. In *Meteorites and the Early Solar System II*; Lauretta, D.S., McSween, H.Y., Jr., Eds.; The University of Arizona Press: Tucson, AZ, USA, 2006; pp. 19–52.
20. Van Schmus, W.R.; Wood, J.A. A chemical-petrologic classification for the chondritic meteorites. *Geochim. Cosmochim. Acta* **1967**, *31*, 747–765. [CrossRef]
21. Dodd, R.T. *Meteorites: A Petrological-Chemical Synthesis*; Cambridge University Press: Cambridge, UK, 1981; pp. 1–368.
22. Mittlefehldt, D.W. Asteroid (4) Vesta: I. The howardite-eucrite-diogenite (HED) clan of meteorites. *Chem. Erde* **2015**, *75*, 155–183. [CrossRef]
23. Klencsar, Z.; Kuzmann, E.; Vertes, A. User-friendly software for Mossbauer spectrum analysis. *J. Radioanal. Nucl. Chem.* **1996**, *210*, 105–118. [CrossRef]
24. Oshtrakh, M.I.; Grokhovsky, V.I.; Abramova, N.V.; Semionkin, V.A.; Milder, O.B. Iron-nickel alloy from iron meteorite Chinga studied using Mössbauer spectroscopy with high velocity resolution. *Hyperfine Interact.* **2009**, *190*, 135–142. [CrossRef]
25. Oshtrakh, M.I.; Goryunov, M.V.; Grokhovsky, V.I.; Chukin, A.V.; Shtolz, A.K.; Semionkin, V.A. Study of visually different areas in the Chinga iron meteorite fragment using Mössbauer spectroscopy with a high velocity resolution. *Hyperfine Interact.* **2013**, *219*, 25–31. [CrossRef]
26. Goryunov, M.V.; Yakovlev, G.A.; Chukin, A.V.; Grokhovsky, V.I.; Semionkin, V.A.; Oshtrakh, M.I. Iron meteorites and their weathering products: Mössbauer spectroscopy with a high velocity resolution of the iron-bearing minerals. *Eur. J. Mineral.* **2016**, *28*, 601–610. [CrossRef]
27. Oshtrakh, M.I.; Yakovlev, G.A.; Grokhovsky, V.I.; Semionkin, V.A. Re-examination of Dronino iron meteorite and its weathering products using Mössbauer spectroscopy with a high velocity resolution. *Hyperfine Interact.* **2016**, *237*, 42. [CrossRef]
28. Grokhovsky, V.I.; Oshtrakh, M.I.; Milder, O.B.; Semionkin, V.A. Mössbauer spectroscopy of iron meteorite Dronino and products of its corrosion. *Hyperfine Interact.* **2005**, *166*, 671–677. [CrossRef]
29. Goryunov, M.V.; Oshtrakh, M.I.; Chukin, A.V.; Grokhovsky, V.I.; Semionkin, V.A. Comparative study of Aliskerovo, Anyujskij, Sikhote-Alin and Sterlitamak iron meteorites using Mössbauer spectroscopy. *Hyperfine Interact.* **2016**, *237*, 15. [CrossRef]
30. Goryunov, M.V.; Varga, G.; Dankházi, Z.; Felner, I.; Chukin, A.V.; Kuzmann, E.; Homonnay, Z.; Grokhovsky, V.I.; Oshtrakh, M.I. Characterization of iron meteorites by scanning electron microscopy, X-ray diffraction, magnetization measurements and Mössbauer spectroscopy: Gibeon IVA. *Meteorit. Planet. Sci.* **2023**, *58*, 875–884. [CrossRef]

31. Goryunov, M.V.; Varga, G.; Dankházi, Z.; Felner, I.; Chukin, A.V.; Kuzmann, E.; Grokhovsky, V.I.; Homonnay, Z.; Oshtrakh, M.I. Characterization of iron meteorites by scanning electron microscopy, X-ray diffraction, magnetization measurements and Mössbauer spectroscopy: Mundrabilla IAB-ung. *Meteorit. Planet. Sci.* **2023**, *in press*. [CrossRef]
32. Oshtrakh, M.I.; Maksimova, A.A.; Goryunov, M.V.; Petrova, E.V.; Felner, I.; Chukin, A.V.; Grokhovsky, V.I. Study of metallic Fe-Ni-Co alloy and stony part isolated from Seymchan meteorite using X-ray diffraction, magnetization measurement and Mössbauer spectroscopy. *J. Mol. Struct.* **2018**, *1174*, 112–121. [CrossRef]
33. Oshtrakh, M.I.; Grokhovsky, V.I.; Uymina, K.A.; Semionkin, V.A. Study of hyperfine interactions in carbonaceous chondrite Isheyevo (CH/CB) using Mössbauer spectroscopy with high velocity resolution. *Hyperfine Interact.* **2007**, *177*, 73–79. [CrossRef]
34. Ivanova, M.A.; Kononkova, N.N.; Krot, A.N.; Greenwood, R.C.; Franchi, I.A.; Verchovsky, A.B.; Trieloff, M.; Korochantseva, E.V.; Brandstätter, F. The Isheyevo meteorite: Mineralogy, petrology, bulk chemistry, oxygen, nitrogen, carbon isotopic compositions, and ^{40}Ar-^{39}Ar ages. *Meteorit. Planet. Sci.* **2008**, *43*, 915–940. [CrossRef]
35. Kohout, T.; Haloda, J.; Halodová, P.; Meier, M.M.M.; Maden, C.; Busemann, H.; Laubenstein, M.; Caffee, M.W.; Welten, K.C.; Hopp, J.; et al. Annama H chondrite—Mineralogy, physical properties, cosmic ray exposure, and parent body history. *Meteorit. Planet. Sci.* **2017**, *52*, 1525–1541. [CrossRef]
36. Maksimova, A.A.; Petrova, E.V.; Chukin, A.V.; Unsalan, O.; Szabó, Á.; Dankházi, Z.; Felner, I.; Zamyatin, D.A.; Kuzmann, E.; Homonnay, Z.; et al. Study of Bursa L6 ordinary chondrite by X-ray diffraction, magnetization measurements and Mössbauer spectroscopy. *Meteorit. Planet. Sci.* **2020**, *55*, 2780–2793. [CrossRef]
37. Maksimova, A.A.; Petrova, E.V.; Chukin, A.V.; Karabanalov, M.S.; Nogueira, B.A.; Fausto, R.; Yesiltas, M.; Felner, I.; Oshtrakh, M.I. Characterization of Kemer L4 meteorite using Raman spectroscopy, X-ray diffraction, magnetization measurements and Mössbauer spectroscopy. *Spectrochim. Acta Part A Mol. Biomol. Spectrosc.* **2020**, *242*, 118723. [CrossRef]
38. Maksimova, A.A.; Petrova, E.V.; Chukin, A.V.; Karabanalov, M.S.; Felner, I.; Gritsevich, M.; Oshtrakh, M.I. Characterization of the matrix and fusion crust of the recent meteorite fall Ozerki L6. *Meteorit. Planet. Sci.* **2020**, *55*, 231–244. [CrossRef]
39. Maksimova, A.A.; Petrova, E.V.; Chukin, A.V.; Nogueira, B.A.; Fausto, R.; Szabó, Á.; Dankházi, Z.; Felner, I.; Gritsevich, M.; Kohout, T.; et al. Bjurböle L/LL4 ordinary chondrite properties studied by Raman spectroscopy, X-ray diffraction, magnetization measurements and Mössbauer spectroscopy. *Spectrochim. Acta Part A Mol. Biomol. Spectrosc.* **2021**, *248*, 119196. [CrossRef] [PubMed]
40. Maksimova, A.A.; Oshtrakh, M.I.; Petrova, E.V.; Grokhovsky, V.I.; Semionkin, V.A. Comparison of iron-bearing minerals in ordinary chondrites from H, L and LL groups using Mössbauer spectroscopy with a high velocity resolution. *Spectrochim. Acta Part A Mol. Biomol. Spectrosc.* **2017**, *172*, 65–76. [CrossRef]
41. Maksimova, A.A.; Kamalov, R.V.; Chukin, A.V.; Felner, I.; Oshtrakh, M.I. An analysis of orthopyroxene from Tsarev L5 meteorite using X-ray diffraction, magnetization measurement and Mössbauer spectroscopy. *J. Mol. Struct.* **2018**, *1174*, 6–11. [CrossRef]
42. Maksimova, A.A.; Oshtrakh, M.I.; Chukin, A.V.; Felner, I.; Yakovlev, G.A.; Semionkin, V.A. Characterization of Northwest Africa 6286 and 7857 ordinary chondrites using X-ray diffraction, magnetization measurements and Mössbauer spectroscopy. *Spectrochim. Acta Part A Mol. Biomol. Spectrosc.* **2018**, *192*, 275–284. [CrossRef]
43. Oshtrakh, M.I.; Maksimova, A.A.; Chukin, A.V.; Petrova, E.V.; Jenniskens, P.; Kuzmann, E.; Grokhovsky, V.I.; Homonnay, Z.; Semionkin, V.A. Variability of Chelyabinsk meteoroid stones studied by Mössbauer spectroscopy and X-ray diffraction. *Spectrochim. Acta Part A Mol. Biomol. Spectrosc.* **2019**, *219*, 206–224. [CrossRef] [PubMed]
44. Petrova, E.V.; Oshtrakh, M.I.; Grokhovsky, V.I.; Semionkin, V.A. Study of metal grains extracted from chondrite Tzarev L5 using Mössbauer spectroscopy with high velocity resolution. *Hyperfine Interact.* **2007**, *177*, 81–87. [CrossRef]
45. Petrova, E.V.; Oshtrakh, M.I.; Grokhovsky, V.I. Hyperfine interactions in metal extracted from ordinary chondrite Tsarev L5: A study using Mössbauer spectroscopy with high velocity resolution. *J. Phys. Chem. Solids* **2008**, *69*, 1790–1795. [CrossRef]
46. Dos Santos, E.; Gattacceca, J.; Rochette, P.; Scorzelli, R.B.; Fillion, G. Magnetic hysteresis properties and ^{57}Fe Mössbauer spectroscopy of iron and stony-iron meteorites: Implications for mineralogy and thermal history. *Phys. Earth Planet. Inter.* **2015**, *242*, 50–64. [CrossRef]
47. Morozov, M.; Brinkmann, C.; Lottermoser, W.; Tippelt, G.; Amthauer, G.; Kroll, H. Octahedral cation partitioning in Mg,Fe^{2+}-olivine. Mössbauer spectroscopic study of synthetic $(Mg_{0.5}\ Fe^{2+}{}_{0.5})_2SiO_4$ (Fa_{50}). *Eur. J. Mineral.* **2005**, *17*, 495–500. [CrossRef]
48. Van Alboom, A.; De Grave, E.; Vandenberghe, R.E. Study of the temperature dependence of the hyperfine parameters in two orthopyroxenes by ^{57}Fe Mössbauer spectroscopy. *Phys. Chem. Minerals* **1993**, *20*, 263–275. [CrossRef]
49. Dyar, M.D.; Klima, R.L.; Fleagle, A.; Peel, S.E. Fundamental Mössbauer parameters of synthetic Ca-Mg-Fe pyroxenes. *Am. Mineral.* **2013**, *98*, 1172–1186. [CrossRef]
50. Maksimova, A.A.; Unsalan, O.; Chukin, A.V.; Karabanalov, M.S.; Jenniskens, P.; Felner, I.; Semionkin, V.A.; Oshtrakh, M.I. The interior and the fusion crust in Sariçiçek howardite: Study using X-ray diffraction, magnetization measurements and Mössbauer spectroscopy. *Spectrochim. Acta Part A Mol. Biomol. Spectrosc.* **2020**, *228*, 117819. [CrossRef] [PubMed]
51. Maksimova, A.A.; Petrova, E.V.; Chukin, A.V.; Oshtrakh, M.I. Fe^{2+} partitioning between the M1 and M2 sites in silicate crystals in some stony and stony-iron meteorites studied using X-ray diffraction and Mössbauer spectroscopy. *J. Mol. Struct.* **2020**, *1216*, 128391. [CrossRef]
52. Kruse, O.; Ericsson, T. A Mössbauer investigation of natural troilite from the Agpalilik meteorite. *Phys. Chem. Miner.* **1988**, *15*, 509–513. [CrossRef]

53. Oshtrakh, M.I.; Klencsár, Z.; Petrova, E.V.; Grokhovsky, V.I.; Chukin, A.V.; Shtoltz, A.K.; Maksimova, A.A.; Felner, I.; Kuzmann, E.; Homonnay, Z.; et al. Iron sulfide (troilite) inclusion extracted from Sikhote-Alin iron meteorite: Composition, structure and magnetic properties. *Mat. Chem. Phys.* **2016**, *174*, 100–111. [CrossRef]
54. Kruse, O. Phase transitions and kinetics in natural FeS measured by X-ray diffraction and Mössbauer spectroscopy at elevated temperatures. *Am. Mineral.* **1992**, *77*, 391–398.
55. Park, J.Y.; Kim, K.J. Magnetotransport and magnetic properties of sulfospinels $Zn_xFe_{1-x}Cr_2S_4$. *Hyperfine Interact.* **2006**, *169*, 1267–1272. [CrossRef]
56. Maksimova, A.A.; Oshtrakh, M.I.; Klencsár, Z.; Petrova, E.V.; Grokhovsky, V.I.; Kuzmann, E.; Homonnay, Z.; Semionkin, V.A. A Comparative study of troilite in bulk ordinary chondrites Farmington L5, Tsarev L5 and Chelyabinsk LL5 using Mössbauer spectroscopy with a high velocity resolution. *J. Mol. Struct.* **2014**, *1073*, 196–201. [CrossRef]
57. Maksimova, A.A.; Klencsár, Z.; Oshtrakh, M.I.; Petrova, E.V.; Grokhovsky, V.I.; Kuzmann, E.; Homonnay, Z.; Semionkin, V.A. Mössbauer parameters of ordinary chondrites influenced by the fit accuracy of the troilite component: An example of Chelyabinsk LL5 meteorite. *Hyperfine Interact.* **2016**, *237*, 33. [CrossRef]
58. Oshtrakh, M.I.; Maksimova, A.A.; Klencsár, Z.; Petrova, E.V.; Grokhovsky, V.I.; Kuzmann, E.; Homonnay, Z.; Semionkin, V.A. Study of Chelyabinsk LL5 meteorite fragments with different lithology using Mössbauer spectroscopy with a high velocity resolution. *J. Radioanal. Nucl. Chem.* **2016**, *308*, 1103–1111. [CrossRef]
59. Kruse, O. Mössbauer and X-ray study of the effects of vacancy concentration in synthetic hexagonal pyrrhotites. *Am. Mineral.* **1990**, *75*, 755–763.
60. Gattacceca, J.; Rochette, P.; Lagroix, F.; Mathé, P.-E.; Zanda, B. Low temperature magnetic transition of chromite in ordinary chondrites. *Geophys. Res. Lett.* **2011**, *38*, L10203. [CrossRef]
61. Maksimova, A.A.; Chukin, A.V.; Felner, I.; Oshtrakh, M.I. Spinels in meteorites: Observation using Mössbauer spectroscopy. *Minerals* **2019**, *9*, 42. [CrossRef]
62. Burns, R.G. Intervalence transitions in mixed valence minerals of iron and titanium. *Ann. Rev. Earth Planet. Sci.* **1981**, *9*, 345–383. [CrossRef]
63. Antic, B.; Jovic, N.; Pavlovic, M.B.; Kremenovic, A.; Manojlović, D.; Vucinic-Vasic, M.; Nikolić, A.S. Magnetization enhancement in nanostructured random type $MgFe_2O_4$ spinel prepared by soft mechanochemical route. *J. App. Phys.* **2010**, *107*, 043525. [CrossRef]
64. Yudin, I.A.; Kozmanov, Y.D.; Remennikova, I.M. Investigation of minerals in the fusion crust of Saratov meteorite. *Meteorit. (Mosc.)* **1968**, *28*, 156–157. (in Russian).
65. Ushakov, M.V.; Nithya, V.D.; Rajeesh Kumar, N.; Arunkumar, S.; Chukin, A.V.; Kalai Selvan, R.; Oshtrakh, M.I. X-ray diffraction, magnetic measurements and Mössbauer spectroscopy of $MgFe_2O_4$ nanoparticles. *J. Alloys Comp.* **2022**, *912*, 165125. [CrossRef]
66. Oshtrakh, M.I.; Larionov, M.Y.; Grokhovsky, V.I.; Semionkin, V.A. Study of iron meteorite Sikhote-Alin and extracted iron-nickel phosphides using Mössbauer spectroscopy with high velocity resolution. *Hyperfine Interact.* **2008**, *186*, 53–59. [CrossRef]
67. Oshtrakh, M.I.; Larionov, M.Y.; Grokhovsky, V.I.; Semionkin, V.A. Temperature dependent high velocity resolution Mössbauer spectroscopic study of iron nickel phosphide microcrystals (rhabdites) extracted from Sikhote-Alin iron meteorite. *J. Alloys Comp.* **2011**, *509*, 1781–1784. [CrossRef]
68. Oshtrakh, M.I.; Larionov, M.Y.; Grokhovsky, V.I.; Semionkin, V.A. An analysis of Fe and Ni distribution in M1, M2 and M3 sites of iron nickel phosphides extracted from Sikhote-Alin meteorite using Mössbauer spectroscopy with a high velocity resolution. *J. Mol. Struct.* **2011**, *993*, 38–42. [CrossRef]
69. Oshtrakh, M.I.; Larionov, M.Y.; Grokhovsky, V.I.; Semionkin, V.A. Study of rhabdite (iron nickel phosphide) microcrystals extracted from Sikhote-Alin iron meteorite by magnetization measurements and Mössbauer spectroscopy. *Mat. Chem. Phys.* **2011**, *130*, 373–380. [CrossRef]
70. Scorzelli, R.B.; Danon, J. Mössbauer study of schreibersite from Bocaiuva iron meteorite. *Meteoritics* **1986**, *21*, 509, (abstract).
71. Geist, V.; Wagner, G.; Nolze, G.; Moretzki, O. Investigations of the meteoritic mineral $(Fe, Ni)_3P$. *Cryst. Res. Technol.* **2005**, *40*, 52–64. [CrossRef]